University of Alberta

Investigating the catalytic combustion of methane and BTEX in a counter-diffusive radiant heater

by

Naeimeh Jodeiri Naghashkar

A thesis submitted to the Faculty of Graduate Studies and Research
in partial fulfillment of the requirements for the degree of

Doctor of Philosophy
in
Chemical Engineering

Department of Chemical and Materials Engineering

Spring 2011
Edmonton, Alberta

Examining Committee

Dr. R. E. Hayes, Department of Chemical and Materials Engineering

Dr. S. E. Wanke, Department of Chemical and Materials Engineering

Dr. L. W. Kostiuk, Department of Mechanical Engineering

Dr. W. C. McCaffrey, Department of Chemical and Materials Engineering

Dr. P. K. Plucinski, Department of Chemical Engineering, University of Bath

To my parents

and

To Hassan and Ayda

Abstract

This research was aimed at investigating a counter-diffusive catalytic reactor for mitigation of methane and BTEX emissions from the natural gas dehydration process. A commercial radiant heater unit was used in the experiments and the effect of methane flow rate on its conversion was studied. Methane conversion decreased with increasing methane feed rate. It was found that the external diffusion of oxygen through the boundary layer was the limiting factor in the system. Complete methane conversion was achieved when the oxygen diffusion limitation was overcome by inducing convective air flux in the boundary layer in front of the catalyst pad.

To simulate natural gas dehydration emissions, which contain excess amount of water, the effect of addition of liquid water and water vapor on methane combustion was also studied. Small volumes of liquid water did not affect the methane combustion, however, at 2 g/min liquid water, which is comparable to the amount of water produced during the reaction, combustion was inhibited. Added water vapor did not show any influence on combustion efficiency. The presence of pentane and toluene, representing the non-aromatic hydrocarbons and BTEX substances in the emissions, inhibited methane conversion due to the competition for oxygen since pentane and toluene are easier to oxidize compared to methane.

Two-dimensional modeling of the radiant heater system was conducted using the COMSOL Multiphysics software package. Comparing the model data

for methane conversion with experimental results revealed similar decreasing trend in conversion with increasing the methane flow rate; however, the model under-predicted the conversion. Increasing the mass transfer coefficient, resulted in improved methane conversion, confirming the dominance of mass diffusion limitation in the system. In fact, the real mass transfer coefficient was 1.5-2 times higher than the values originally used in the model. Changing the kinetic parameters did not significantly improve the conversion leading to the conclusion that the catalytic radiant heater system is not kinetically controlled. Developing the three-dimensional model of the system in Fluent revealed that the fuel distribution in the system is not a significant factor, in agreement with experimental observation.

Acknowledgement

The completion of this thesis would not have been possible without the help and support of a number of people around me. First and foremost I owe my deepest gratitude to my supervisors, Professor Robert E. Hayes and Professor Sieghard E. Wanke, who supported me throughout this thesis with their immense knowledge and constructive discussions. I deeply appreciate the time they dedicated for our regular meetings and also for off schedule chats whenever I needed. Their ethical conduct, patience, enthusiasm and encouragement are inspirational to me. One simply could not wish for better supervisors.

I would like to thank Dr. Tariq M. Mannan who helped me when I first came to the lab to familiarize myself with lab instruments and by patiently answering my questions. I also would like to sincerely thank Dr. Long Wu for his constant help during my experiments. He helped me to set up the experimental apparatus in the lab and made a lot of complicated tasks much easier for me. Without his assistance and great discussions, this journey would have been a difficult one for me. I wish to extend my thanks to Dr. Joseph Mmbaga who made me understand the modeling software when I first started and was the first one to talk to when I couldn't make sense of my results.

I appreciate the instrument shop staff at the University of Alberta, Walter Boddez and Richard Cooper, who were always willing to help with any problems that I had in the lab with the instruments and generously lent me their equipment to use. The support and friendliness of these individuals is exemplary. I also have

to thank the computer support staff in the Chemical Engineering department, Bob Barton and Jack Gibeau, for the assistance with computer and software problems that I had once in a while. Their hands seem to do magic with the computer.

I am forever indebted to my parents. Their continuous support and love throughout my life and especially during my PhD studies far from home has made me who I am today. They had to sacrifice so much so that I can pursue my education. I am proud to have them as my parents.

I would like to thank my husband, Dr. Hassan Abbasnezhad, for his unconditional love and encouragement in this journey. He has always been there for me, supporting me when I was overwhelmed with frustration. He has been a great mentor since my bachelors program in Iran until now.

My lovely daughter, Ayda, is the best thing that has happened to me. Her life started at the same time that I started my PhD and she is the one who endured long hours of studying in the office or experimenting in the lab. She has been my motivation every single day. Her big smile and sweet words keeps me going. I thank her for her patience and understanding.

Table of Content

List of Tables

List of Figures

List of symbols

Latin Symbols	Description	Unit
C_p	heat capacity	(J/kgK)
D_{i-j}	binary diffusion coefficient	(m^2/s)
D_{i_m}	diffusion coefficient of species 'i' in the mixture	(m^2/s)
E	activation energy	(J/mol)
g	gravitational acceleration	(m/s^2)
Gr	Grashof number	
h	heat transfer coefficient	(W/m^2K)
k	thermal conductivity	(W/mK)
k'	reaction rate constant	(mol/m^3s)
k_m	mass transfer coefficient	(m/s)
k_{mix}	gas mixture thermal conductivity	(W/mK)
k_p	permeability	(m^2)
K_{tr}	monoatomic thermal conductivity	($K^{0.17}kg^{0.5}/mol^{0.5}P^{0.67}$)
K_{0LT}	pre-exponntial factor at low temperature	(kg/m^3s)
K_{0HT}	pre-expnential factor at high temperature	(kg/m^3s)
M	molecular weight	(kg/mol)
M_{ave}	average species molecular weight	(kg/mol)
Nu	Nusselt number	
P	static pressure	(Pa)
Pr	Prandtl number	

P_c	critical pressure	(Pa)
q	Heat flux	(W/m^2)
R	universal gas constant	(J/molK)
R_{rxn}	reaction rate	(kg/m^3s)
Ra	Rayleigh number	
Sh	Sherwood number	
T	temperature	(^oC or K)
T'	mean temperature	(K)
T_c	critical temperature	(K)
T_s	wall temperature	(K)
T_∞	ambient temperature	(K)
T_r	reduced temperature	
u	x-velocity	(m/s)
w	mass fraction	
Greek symbols	**Description**	**Units**
α	thermal diffusivity	(m^2/s)
β	thermal expansion coefficient	(1/K)
ΔH_{rxn}	enthalpy change	(kJ/mol)
ε	emissivity	
μ	dynamic viscosity	(Ns/m^2)
ν	kinematic viscosity	(m^2/s)
v'	atomic diffusion volume	
ρ	fluid density	(kg/m^3)
σ	Stefan-Boltzman constant	(W/m^2K^4)

List of Abbreviations

Symbol	description
BTEX	benzene, toluene, ethylbenzen, xylene
CEPA	Canadian Environmental Protection Act
CFCs	chloroflurocarbons
CFD	computational fluid dynamics
EUB	energy and utilities board
GC	gas chromatograph
GHG	greenhouse gas
GWP	global warming potential
HAP	hazardous air pollutants
HPLC	high performance liquid chromatography
IPCC	Intergovernmental Panel on Climate Change
Mtoe	million tones of oil equivalent
OEL	Occupational Exposure Limit
RF	response factor
TCD	thermal conductivity detector
TEG	triethylen glycol
TOF	turn over frequency
UNFCC	United Nations Framework on Climate Change
VOC	volatile organic compound

Chapter 1

Introduction

1.1 Background

Canada, with its significant natural resources, is considered to be one of the world leaders in energy production and export. Western Canada, and particularly the province of Alberta, has abundant resources of energy, including fossil fuels, and is the energy centre of the country. About three quarters of Canada's total primary energy supply comes from fossil fuels (International Energy Agency 2004). Canada's total energy production grew substantially from 274 Mtoe[1] (million tonnes of oil equivalent) in 1990 to 392 Mtoe in 2002, and net energy export increased from 61 Mtoe in 1990 to 138 Mtoe in 2002, with oil and gas representing 30% and 61%, respectively. The United States of America is the main market for Canada's energy products and services, accounting for 98% of Canada's export in 2004 (Foreign Affairs and International Trade Canada 2010).

Alberta's economy relies heavily on the production, sale and combustion of fossil fuels. Its rich economy has brought wealth and prosperity to the region; however, the increased rates of oil and gas production and processing activities has led to many environmental issues, including greenhouse gases (GHG) emissions. This region has the highest GHG emissions among all the provinces in Canada. In 2008, about 42% of the facility reported GHG emissions belonged to

[1] The tonne of oil equivalent is the amount of energy released by burning one tonne of crude oil.

Alberta with energy related activities being the major emission source (Government of Canada, Environment Canada 2010).

Recently, the climate change and the potential impacts associated with it have been a major concern and a hotly debated issue in Canada and around the world. The average temperature of the earth's surface has risen by 0.74^{o}C since the late 1800s and it is predicted to increase by another 1.8^{o}C to 4^{o}C by the year 2100 (United Nations Framework Convention on Climate Change (UNFCC) 2010). Many speculate that the main reason behind the increasing temperature is industrialization which is associated with burning oil, gas and coal, the cutting of forests, and the practice of certain farming methods. These activities have increased the amount of GHG in the atmosphere, especially methane, carbon dioxide and nitrogen oxides. Such gases occur naturally and they are critical for life on earth because they keep some of the sun's warmth from reflecting back into space, without which the planet would be a cold and unlivable place. However, in increasing quantities they push the global temperatures to high levels, altering the climate. The consequences of increasing the temperature are expected to include rising sea levels, melting of glaciers, changes in precipitation patterns with increased risk of flooding and draught, and changes in frequency and intensity of extreme weather events (Khilyuk, Chilingar 2004, Jaccard M. 2007). Although many impacts of climate change are expected to be felt most strongly in developing countries, Canada is not immune from direct impacts. A 4^{o}C average global warming, the estimate for 2100, would be expected to warm northern Canada by roughly 8^{o}C. This change would have dramatic effects on

natural systems and human inhabitants in northern Canada. Other parts of Canada would probably suffer from water shortages and extreme weather events.

To address this global challenge, over a decade ago, most countries joined the United Nations Framework on Climate Change (UNFCC) to consider what can be done to overcome the climate change issue. In 1994, UNFCC entered into force with the objective of "stabilization of GHG concentrations in the atmosphere at a level that would prevent dangerous anthropogenic interference with the climate system" (United Nations Framework Convention on Climate Change (UNFCC) 2010). The role of convention was to encourage the industrialized countries to stabilize GHG emissions while the Kyoto Protocol is an international agreement linked to UNFCC which commits these countries to do so. Kyoto Protocol was adopted in Kyoto, Japan on 1997 and came into force in 2006. The protocol set targets for 37 industrialized countries, including Canada and the European community for reducing GHG emissions by an average of 5% against 1990 level over the period of 2008-2012. Canada ratified the UNFCC on December 1992 and its Kyoto Protocol on December 2002.

Other than GHG, some volatile organic compounds (VOC) are among harmful and toxic materials that are being emitted from different industrial processes. Compounds such as benzene, toluene, ethylbenzene and xylene (BTEX) are among the VOC that need to be mitigated before being released into the atmosphere. Therefore practical solutions are required to influence the increasing trend of global warming and climate change.

1.2 Motivation and research objectives

An increasing number of climatologists, researchers and environmental groups believe that the higher concentrations of GHG will induce global warming sufficiently to cause extensive disruption in climatic patterns. According to the reports by United Nation's Intergovernmental Panel on Climate Change (IPCC), global GHG emissions due to human activities have grown dramatically in recent decades and are very likely to be the primary cause of the observed increase in global average temperatures (IPCC, 2nd assessment report, the science of climate change). The influence of different GHG on global warming is usually compared using the global warming potential (GWP). The GWP is defined as the time-integrated change in radiative forcing due to the release of 1 kg of the gas relative to the radiative forcing from the release of 1 kg CO_2 (Government of Canada, Environment Canada 2010, Brühl 1993). Radiative forcing is a "measure of the influence a factor has in altering the balance of incoming and outgoing energy in the earth-atmosphere system and is an index of the importance of the factor as a potential climate change mechanism". GWP is a relative measure of the warming effect that the emission of a GHG might have on the surface troposphere with carbon dioxide taken as the reference. Methane is the second largest contributor to global warming however its GWP is 23 times higher than that for carbon dioxide over a 100-year time span (Su, Agnew 2006, Salomons et al. 2003).

The energy sector is responsible for the largest growth in GHG emissions (Forster et al. 2007). The primary GHG are carbon dioxide, methane, nitrous oxide and halocarbons (Government of Canada, Environment Canada 2010,

Danny Harvey 1993). In 2004, Canadians released about 758 megatonnes of carbon dioxide equivalent of GHG into the atmosphere (Government of Canada, Environment Canada 2010). Energy related activities are the largest source of GHG emissions in Canada. Alberta is the first jurisdiction in North America to impose comprehensive regulations requiring large facilities in various sectors to reduce their GHG emissions. As part of its efforts to address climate change, the province of Alberta has introduced legislation to address GHG emissions in the province: The Climate Change and Emissions Management Act. There are currently three regulations in effect under this Act. The Alberta Specified Gas Reporting Regulation indicates reporting requirements for large emitters; Specified Gas Emitters Regulation sets the targets for regulated entities and guidelines for compliance achievement; and Administrative Penalty Regulation indicating the penalty for not complying with the Climate Change and Emissions Management Act. As of July 1, 2006, the Specified Gas Emitters Regulation requires Alberta facilities that emit more than 100,000 tonnes of GHG per year, to reduce emission intensity by 12%. These facilities have four options to comply with the regulations:

- Reduce their emission by improving their operation system
- Purchase Alberta based offset credits
- Contribute to Climate Change and Emissions Management Fund
- Purchase or use Emission Performance Credits
- Offsets must be Alberta-based and originate from a voluntary action in a non-regulated sector.

A significant source of methane emissions in Alberta is the natural gas glycol dehydration process. Produced natural gas contains excess water that needs to be removed before being transported and delivered to the consumer. In addition to methane, the effluent of glycol dehydrator unit contains a mixture of BTEX, water and other hydrocarbons (Jodeiri et al. 2010). In fact, emissions from natural gas dehydration (glycol dehydration) facility are the primary source of benzene emissions in the oil and gas industry. Benzene is a hazardous air pollutant (HAP) and classified as toxic substance under the Canadian Environmental Protection Act (Canadian Environmental Protection Act 1993). It is carcinogenic to humans and studies have shown the correlation between exposure to benzene and onset of certain forms of leukemia.

To reduce benzene emissions from glycol dehydrators, on July 2006, the Alberta Energy and Utilities Board (EUB) and Alberta Environment have jointly issued Directive 039, entitles: Revised Program to Reduce Benzene Emissions from Glycol Dehydrators and licensees are required to comply with the defined benzene emission limits. Benzene emission limits were set depending on the date of installation or relocation of the glycol dehydrator. Also licensees are required to submit an annual dehydrator benzene inventory list by July 1 of each year (Canadian Association of Petroleum Producers June 2006).

These regulations and mandates for the GHG reduction and benzene emission control is the major motivation for conducting this research. The main objective of this research is to investigate the application of a catalytic reactor system for mitigation of methane and BTEX substances emitted in the oil and gas

industry operations particularly from glycol dehydrator effluents. This research includes the experimentation using a commercial reactor and computer modeling. By conducting this research through experiments, a better understanding of the physical phenomena involved in operation of the catalytic reactor system is achieved. Modeling is a useful approach for predicting the system behavior at different conditions. In fact using the model, the effect of different operating parameters on the system performance can be predicted without doing the real experiment which could be costly, dangerous and/or time consuming.

1.3 Thesis overview

This research was initiated to evaluate the performance of a catalytic reactor for treatment of methane and BTEX substances. Before reporting the experimental and modeling results some background information is needed to understand the problem in hand. Chapter 2 is devoted to introducing and defining the GHG and BTEX substances and their sources and sinks. The Natural gas dehydration process is described in detail and the emission sources are identified. In this chapter also the regulations for emission control and available emission control technologies are introduced. The conventional method of treatment of these compounds, along with the disadvantages and concerns related to these methods is discussed and reviewed. Then the proposed catalytic combustion method of treatment is introduced and discussed to gain an understanding of the characteristics of this system.

In Chapter 3, which is the literature review, previous works done in the area of catalytic combustion of methane and BTEX substances including kinetics and reaction mechanism and the factors influencing the catalytic system performance are covered. In Chapter 4, the results of the experiments with commercial counter-diffusive radiant heater unit are reported including parametric study of methane flow rate and its effect on reactor performance in terms of conversion, effect of mass transfer on system operation and the influence of addition of liquid and vapor compounds, representing the natural gas dehydration effluent, on the system.

The procedure and the generated data from a two-dimensional model of the counter-diffusive radiant heater are presented in Chapter 5 along with the comparison of the model and experimental results. Also the results of the three-dimensional model are presented in this chapter. The last chapter includes conclusions drawn from the results of this research and the recommendations for optimum performance of these systems.

Chapter 2

Methane and volatile organic compounds (VOC) emissions and common treatment methods

2.1 Introduction

The transition from a worker-based industry to machine-based economy, with the growth of factories and mass production, is traditionally known as the industrial revolution, which began in England and introduced the most fundamental changes to society (Silverstein, Silverstein & Nunn 2009). This revolution was accompanied by massive growth in energy consumption, met by the burning of coal. In fact, the industrial revolution marked the beginning of the period during which mankind began substantially altering the composition of the atmosphere. Nowadays, uncontrolled release of VOC to the atmosphere from different industrial processes has become a challenge for all the nations around the world. VOC are a class of substances in which carbon is bound to hydrogen or other elements. VOC may be defined as organic liquids or solids whose room temperature vapor pressures are greater than 0.01 psi and atmospheric boiling points are up to about 533 K (Hunter, Oyama 2000).

Two major categories of these compounds are methane, which is a strong GHG, and BTEX substances. Now there is scientific evidence that GHG alter the global climate and BTEX substances such as benzene, which are among hazardous air pollutants (HAP), pose health risk to human beings. In the following sections of this chapter, these two categories of VOC are discussed and their sources will be introduced.

2.2 What is the greenhouse effect?

The earth receives radiant energy from the sun, but it must re-radiate much of that energy back into space or our world would become progressively hotter. This radiation from the sun may be reflected back into space by the earth, or absorbed by naturally occurring trace gases in the atmosphere including water vapor, carbon dioxide and methane. This absorption occurs primarily in the troposphere, the region from the earth's surface up to an altitude of 10 to 15 km. When these molecules absorb energy, they cause general atmospheric warming, a phenomenon commonly called the greenhouse effect. In fact, the trace gases act like a thermal blanket to keep the earth warm enough to be a livable place. If no atmosphere would exist, the temperature would be low and no life would be possible (Danny Harvey 1993, Florides, Christodoulides 2009, Metz 2010). Because these trace gases can absorb heat and contribute to the earth warming, they are called GHG.

2.2.1 Radiative forcing

The influence of a GHG in causing the climate change is often evaluated in terms of its radiative forcing. It is "a measure of the influence of a factor in altering the balance of incoming and outgoing energy in the earth-atmosphere system and is an index of the importance of the factor as a potential climate change mechanism". The word radiative arises because these factors change the balance between incoming solar radiation and outgoing infrared radiation within the earth's atmosphere. This radiative balance controls the earth's surface

temperature. The term forcing is used to indicate that earth's radiative balance is being pushed away from its normal state.

Radiative forcing is usually quantified as the 'rate of energy change per unit area of the globe as measured at the top of the atmosphere' and is expressed in units of 'Watts per square metre'. When radiative forcing from a factor is evaluated as positive, the energy of the earth-atmosphere system will ultimately increase, leading to a warming of the system. In contrast, for a negative radiative forcing, the energy will ultimately decrease, leading to a cooling of the system (Forster et al. 2007).

2.2.2 Global warming potential

Human activities have caused the increase of GHG in the atmosphere and changed their balance. These additional gases are responsible for the additional warming of the earth. Carbon dioxide, methane, nitrous oxide and halocarbons are the most important GHG. Global GHG emissions due to human activities have grown since pre-industrial times, with an increase of 70% between 1970 and 2004 (Bernstein et al. 2007).

GHG differ in their warming influence on the global climate system due to their different radiative properties and lifetimes in the atmosphere. The ability and potential of a GHG to cause global warming is defined as GWP. The GWP may be expressed through a common metric based on the radiative forcing of CO_2. GWP is the time-integrated change in radiative forcing due to the instantaneous release of 1 kg of the gas expressed relative to the radiative forcing from the

release of 1 kg of CO_2. The GWP of CO_2 is set to one. Often GHG emission is expressed in terms of CO_2-equivalent which is defined as the amount of CO_2 required to produce a similar warming effect. The equivalent CO_2 emission is obtained by multiplying the emission of a GHG by its GWP for the given time horizon. For a mix of GHG, it is obtained by summing the equivalent CO_2 emissions of each gas. Equivalent CO_2 emission is a standard and useful parameter for comparing emissions of different GHG.

Assigning the GWP value for GHG allows policy makers to compare the impacts of emissions and reductions of different gases. For instance, methane is a significant contributor to the greenhouse effect and has a GWP of 23. This means methane is approximately 23 times more heat-absorptive than carbon dioxide per unit of weight. Therefore methane is most important GHG to be considered for mitigation.

2.3 Methane

Methane is a colorless, odorless, flammable gas that is the simplest hydrocarbon and is the major constituent of natural gas. Once emitted, methane remains in the atmosphere for about 12 years. It is mainly destroyed by oxidation reactions initiated by hydroxyl radicals. The reaction finally leads to formation of CO_2 and H_2O (Lelieveld, Crutzen & Brühl 1993, Wahlen 1993). Increasing emissions of methane and also reaction of hydroxyl radicals with other VOC, lead to lower hydroxyl radials concentrations which may increase methane lifetime in

the atmosphere. A small amount of methane is also absorbed directly by soils and oxidized by bacteria (Wahlen 1993).

In the atmosphere, methane is an infrared absorber contributing to global warming. When methane reaches the stratosphere, it undergoes photochemical dissociation and the released hydrogen oxides form water leading to formation of stratospheric ice clouds (MacDonald 1990). These clouds provide the substrate for the reaction involving derivation of chlorine from chloroflurocarbons (CFCs) and cause the stratospheric ozone depletion. Ozone depletion can lead to increased skin cancer, eye damage and harm to biological species due to the increased levels of ultra violet radiation reaching the earth surface (Dincer, Rosen 1999). Therefore methane not only contributes to global warming, it also is partly responsible for ozone depletion. Methane, usually in the form of natural gas, is used as feedstock in the chemical industry and as fuel for different applications such as heating homes and operating vehicles (Government of Canada, Environment Canada 2010).

2.3.1 Methane emission sources

Several sources contribute to methane emissions. The major difference between these emissions is the role of human in initiating these emissions. Levels of methane emission could vary significantly between different countries depending on the climate, human lifestyle, energy production and demand and waste management practices. However the climate change issue is not specific to industrialized countries only, since no boundary can be assumed between different regions in terms of climate and environment.

2.3.1.1 Natural methane emissions

Methane emissions are divided in two categories: natural and man-made (anthropogenic) sources. Methane is emitted from a variety of sources including wetlands, gas hydrates, permafrost, termites, oceans, freshwater bodies, non-wetland soils and other sources such as wildfire (Wuebbles, Hayhoe 2002, Silverstein, Silverstein & Nunn 2009). Wetlands are the main natural source for global methane emissions. In this ecosystem methane is produced by methane-producing bacteria from decomposition of organic material. The bacteria require an environment with large amount of organic material and no oxygen and this condition is available in wetlands. Termites are the second largest natural source of methane emissions. Methane is produced by the digestive system of insects and the amount depends on the type of species.

Methane emission in oceans and rivers is due to anaerobic digestion in zooplankton and fish and also methanogenisis in sediments and drainage areas along coastal regions. Methane is also emitted from methane hydrates. These hydrates are ice-like crystals formed between water and gas at high pressure and ambient temperature. These solid deposits with trapped methane in the structure can be found deep underground in polar regions and in ocean sediments. Changes in factors such as temperature, pressure and salt concentrations can trigger the methane release from hydrates.

Geologic emissions are another source of methane release. Mud volcanoes are one of the main sources of geologic methane emissions which release methane from within the earth (Etiope et al. 2007, Etiope, Favali 2004). Other geological

sources are geothermal seepage and submarine seepage. Wildfire also contributes to natural methane emissions as a result of incomplete combustion of organic material. Another source of methane which is due to wildfire, is release of methane trapped in the soil by melting the permafrost.

2.3.1.2 Anthropogenic methane emissions

Any GHG emission caused by human activity is called an anthropogenic emission. Canada is one of the highest per capita emitters of GHG mainly due to its size, climate and higher energy demand and resource-based economy (Government of Canada, Environment Canada 2010). In 1990, Canadians released 21.4 tonnes of GHG per capita which increased to 22.0 tonnes per capita by 2008.

Methane emission sources by sector can be categorized into energy, agriculture, waste and land use, land use change and forestry. In 2008, energy sector in Canada had the highest contribution to methane emissions. In the next section, emissions in this sector will be discussed in more details.

2.4 Energy sector

Energy related activities are the main source of methane emissions in Canada (Government of Canada, Environment Canada 2010). The emissions in the energy sector come from stationary combustion sources, transport and fugitive emissions. Fugitive emissions are defined as intentional or unintentional (e.g. leaks, accidents) GHG releases from the production, processing, transmission, storage and delivery of fossil fuels. Methane emissions from the energy sector in

2008 are presented in Table 2.1. From Table 2.1 it can be seen that fugitive emissions has the largest contribution to methane emissions in energy sector.

Table 2.1. Methane emission trend for energy sector (Government of Canada, Environment Canada 2010).

CH_4 sources/sinks	CH_4 emissions (kt CO_2) eq)
Total energy	53000
A. stationary combustion sources	4000
Electricity and heat generation	96
Fossil fuel industries	2000
Mining and oil and gas extraction	10
Manufacturing industries	60
Construction	0.5
Commercial and institutional	10
Residential	2000
Agriculture and forestry	0.8
B. Transport	600
Civil aviation	9
Road transportation	190
Railways	7
Navigation (domestic marine)	9
Other transportation	300
C. Fugitive sources	48000
Coal mining	800
Oil and natural gas	46800

2.4.1 Fugitive emissions

As mentioned previously, fugitive emissions are intentional or unintentional releases of GHG from production, processing, transmission, storage and delivery of fossil fuels. Also emissions from combustion of released gases before disposal, like flaring of natural gas in oil and gas production and processing units are considered fugitive emission (Government of Canada,

Environment Canada 2010). Coal mining and handling, and oil and natural gas production activities are the two sources of fugitive emissions. Overall the fugitive emission have increased from 1990 to 2008 with emission from oil and natural gas contributing to more than 99% of total fugitive emissions in 2008. Although the fugitive emissions from coal mining have decreased from 1990 to 2008, emissions from oil and natural gas sub-sector has increased 55% in this period due to increased production of heavy oil and natural gas mainly for export to the United States.

2.4.1.1 Coal mining

Coal in its natural form contains methane gas. Methane in coal deposits is either trapped under pressure in the open pores or adsorbed to the coal. Methane is released during coal mining due to lowering the pressure and exposure of coal surface to the atmosphere. Activities such as coal handling, storage, processing before combustion and transportations also contribute to methane emissions.

2.4.1.2 Oil and natural gas

This category includes the fugitive emissions from oil and gas production, processing, oil sands mining, bitumen extraction, heavy oil/bitumen upgrading, natural gas transmission and natural gas distribution. The oil and natural gas source category has three main components: conventional oil and gas production, unconventional oil production, and natural gas distribution.

2.4.1.2.1 Unconventional oil production

Emissions in this category come from oil sand open pit mining operations, *in situ* bitumen extraction, and heavy oil/bitumen upgrading to produce bitumen, synthetic crude oil and other derived products for sale. Fugitive methane emissions result from the open mine surfaces and from methanogenic bacteria in the mine tailings settling ponds.

2.4.1.2.2 Natural gas distribution

High pressure natural gas from the gate of transmission system is received by gas distribution system and distributed to the consumer through local pipelines. The major emission sources are fugitive emissions from main and service pipelines and meter/regulator stations.

2.4.1.2.3 Conventional oil and gas production

Emissions in this category include all fugitive emissions from exploration, production, processing and transmission of oil and natural gas. Emissions are usually the result of equipment leakage (bleed valves, fuel gas-operated pneumatic equipment), incomplete seals on equipment (flanges and valves), accidents, spills and intentional vents.

Natural gas that is produced needs some processing before being ready for use. This process is one of the major sources of fugitive methane emissions in the oil and gas industry. In addition to methane, VOC and BTEX substances are also released, which are known to have potential health risks for humans. In the next section the dehydration process and sources of methane and BTEX emissions will

be discussed in detail. Typical natural gas dehydrator emissions are shown in Table 2.2.

Table 2.2. Composition of emissions from natural gas dehydrator (personal communications, Elizabeth Dupuis, 2008)

Component	Amount (vol%)
H_2O	40.4
CH_4	40.1
C_2H_6	6.37
C_3H_8	4.6
i-C_4H_{10}	0.685
n-C_4H_{10}	1.84
i-C_5H_{12}	0.521
n-C_5H_{12}	0.607
Benzene	0.541
Toluene	0.762
Xylenes	0.435
CO_2	0.541
N_2	0.208
Methylcyclohexane	0.399
Ethylbenzene	0.197
hexanes	1.794

2.4.2 Natural gas dehydration

Natural gas is saturated with water at the wellhead; the water has to be removed before being delivered to the end user. This process is called natural gas dehydration. Presence of water in the gas can cause solid hydrate formation and pipeline corrosion (Braek et al. 2001). Typical water specification in many jurisdictions in Canada is 64 mg/Sm^3; however type of the process determines the water content (Carroll 2003). There are several methods for natural gas

dehydration. The most common method is using a liquid desiccant contactor-regeneration process. Wet gas is brought to contact with lean solvent. The water is absorbed by the solvent and the rich solvent containing water is regenerated. Dry gas is produced with this method.

2.4.2.1 Appropriate liquid desiccant

There are some criteria for the liquid desiccant in order to be suitable for gas dehydration. Some of the specifications for commercial application are:

- high affinity of the absorbing liquid for water (hygroscopic)
- low solubility of hydrocarbon components of natural gas in the solvent
- easy regeneration of rich liquid using heat
- very low vapor pressure to minimize the solvent loss due to vaporization and high thermal stability
- non-corrosive to the dehydration equipment
- non-reactive toward any components of natural gas including CO_2 and sulfur compounds

Different absorbing material could be used for gas dehydration such as monoethylene glycol, diethylene glycol, triethylene glycol and tetra ethylene glycol. The best water absorber which meets most of the above mentioned criteria is triethylene glycol (TEG) (Braek et al. 2001, Greenhouse Gas Technology Center, Southern Research Institute 2003).

2.4.2.2 Process description

A schematic of natural gas dehydration process is shown in Figure 2.1. Overall the process can be divided into two parts: water absorption and glycol regeneration. Wet natural gas enters a gas/liquid scrubber in counter current mode where free water in the stream is removed. The scrubber should have a high efficiency wire mesh mist extractor in the top portion to remove any liquid entrainment and particulates from the gas stream before moving into absorber. In the absorber, gas and liquid are mixed and actual water removal takes place. In this stage not only water is absorbed, some methane, BTEX and VOC are also absorbed by glycol (Braek et al. 2001). Gas enters from the bottom while solvent enters from the top and flows to the bottom of the unit absorbing water as it travels downward. The separator contains several equilibrium stages to ensure mass transfer from gas phase to liquid, so that the outlet gas contains desired water. Structured packing could be used for this purpose. The temperature in the separator is uniform and the pressure is in the range of 4000 to 8500 kPa.

The rich glycol containing water, methane, VOC and BTEX, is withdrawn from the bottom of the absorber. The rich glycol is usually preheated and then flashed at low pressure in flash tank where most of the volatile components are vaporized. Pressure in the flash tank is in the range of 300 to 700 kPa. The typical operating temperature is 100 to 160^{o}C (Fisher et al. 1995). The regeneration unit is composed of a reboiler, a still (distillation) column and a surge tank. The temperature of the reboiler is around 175^{o}C. The rich glycol flows into the still

column, where water and glycol are separated by fractional distillation. Water and glycol are separated based on the wide difference in their boiling points.

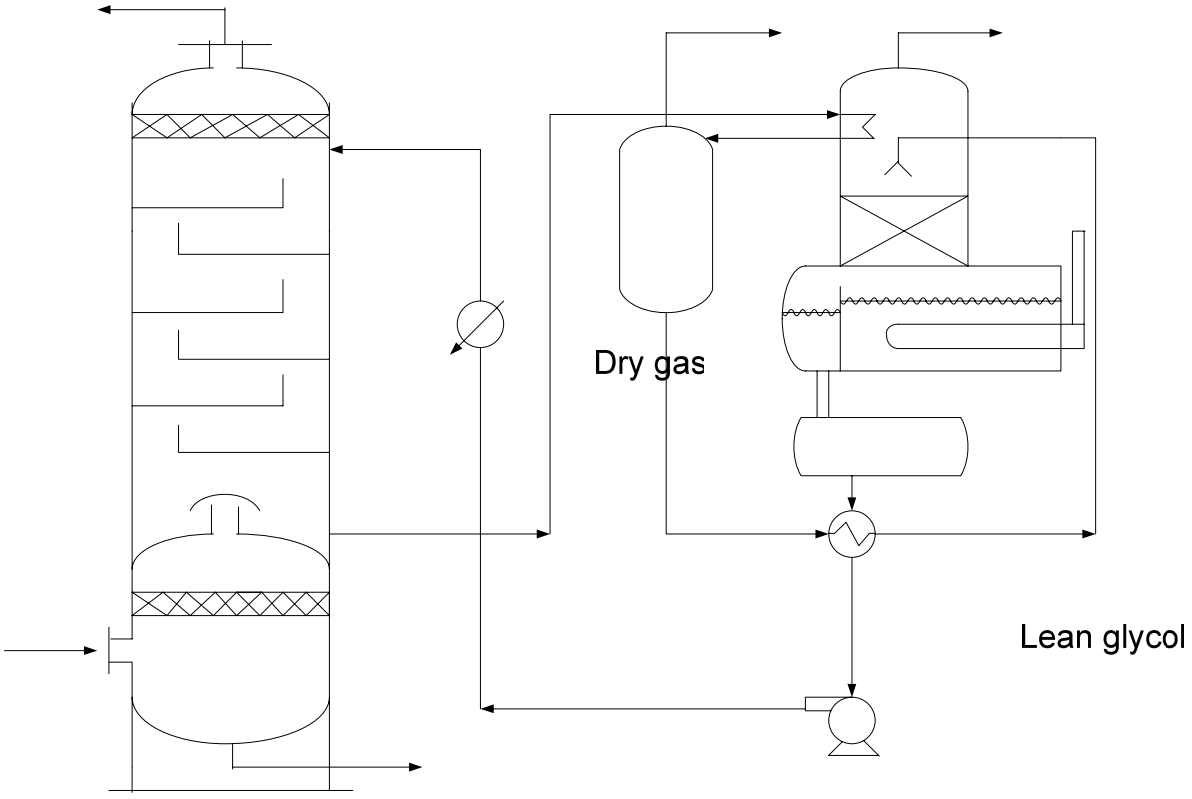

Figure 2.1. Schematic of glycol dehydration process (Carroll 2003)

In the still column, water-rich vapor rises in close contact with descending glycol-rich liquid. Between two phases, continuous exchange of heat and material takes place. The main purpose of still column is final separation between absorbed water and glycol, venting the separated water to atmosphere and recovering the glycol vaporized by reboiler. The hot and rich glycol, which is becoming lean, enters the surge tank and passes to the lean-rich heat exchanger where it is cooled. Then it is returned to the absorber and the cycle is repeated.

absorber

Rich glycol

Wet gas

scrubber

2.4.3 BTEX and other VOC emissions

The regeneration unit is the main source of emissions in natural gas dehydration process. The flash tank and still column vent are two major emission sources which contain water, methane, CO_2, VOC and BTEX (Braek et al. 2001, Greenhouse Gas Technology Center, Southern Research Institute 2003, Kirchgessner et al. 1997, Darwish, Al-Mehaideb & Break 2004, True 1995). BTEX substances are monocyclic aromatics that can be found in gasoline and other petroleum products (Braek et al. 2001). They are volatile and relatively soluble in water. Strong odor and high flammability are the other characteristics of these substances.

Exposure to BTEX compounds is associated with potential health risks. Toluene, ethylbenzene and xylene are irritants with narcotic effects, and benzene is also a human carcinogen. Benzene among these substances has higher solubility in TEG, higher solubility in water and greater volatility. These properties of benzene explain the high quantities of benzene emission in natural gas dehydration process.

2.4.3.1 Health risks of benzene

Benzene is a simple cyclic organic compound with aromatic odor. It is volatile, flammable and colorless liquid at room temperature. Benzene is used extensively in industry as a volatile solvent and as an intermediate in the production of many chemicals including ethylbenzene/styrene, cumene, and maleic anhydride (Environment Canada 1990). Benzene is also a natural component of petroleum (Kirk et al. 1983). In gasoline, benzene acts as an octane-

enhancer. Benzene has been demonstrated to cause cancer in human and experimental animals (Canadian Environmental Protection Act 1993). Therefore it is considered "non-threshold toxicant" meaning that exposure to benzene at any concentration would cause adverse health effects. Workers may become exposed by inhalation or by direct contact with the skin. This can occur during changing the pumps and when handling rich glycol at dehydrators. The main route of exposure to benzene is by inhalation. Once inhaled, it is either exhaled or absorbed by the blood. The absorbed benzene is distributed in the body and processed to an easily excreted form. The by-products can be toxic to bone marrow and cause blood disorder such as leukemia and anemia. This is the influence of long term (chronic) exposure to benzene. In Alberta, the Occupational Exposure Limit (OEL) to benzene is 1 ppm. Short term exposure to high concentrations (greater than 1 ppm over 8 hour period) is unlikely to occur when workers are operating the glycol dehydration.

2.4.3.2 Government regulations for benzene emissions

The Canadian upstream oil and gas industry has committed to minimize the health risks associated with benzene emissions from glycol dehydrator operations with a continuous reduction program. Their target was to reduce emissions by 90% from the 1995 national emissions baseline, which was about 9000 tonnes/year by January 2005 (Canadian Association of Petroleum Producers June 2006). Alberta Environment and Alberta EUB have jointly issued the Directive 039 named "revised program to reduce benzene emissions from glycol dehydrators" which came into effect on July 2006. Licensees are required to

comply with benzene emission limits. For dehydration facilities that are installed or relocated prior to January 1999, if its distance to permanent resident or public facility is less than 750 m, the benzene emission limit is 3 tonnes/year. This limit is 5 tonnes/year for facilities located more than 750 m away from a public facility. The emission limit from all dehydrators starting from January 1999 was set to 3 tonnes/year and after January 2007 this limit was set to be 1 tonnes/year. According to 2004 industrial survey, there are 3863 dehydrators in service in Canada.

2.5 Methane and VOC treatment methods

Production of energy has been increased due to the increase in global population and per capita consumption of energy. However high energy production rates in terms of oil and natural gas is associated with environmental challenges including global warming. Also adverse health effects on human are associated with these activities. In fact these negative effects on human and environment is the main motivation for development of treatment technologies for mitigation of these air pollutants. In the next sections of this chapter, different treatment methods for methane and other VOC will be explained.

2.5.1 Homogeneous combustion

Homogeneous combustion is the conventional method used for treatment of methane and other VOC emissions from glycol dehydrator vent stream (Fisher et al. 1995, Kirchgessner et al. 2004). Typical combustion devices include flares and thermal incinerators. Condensers are also used to separate condensables from

the vent stream while non-condensable gases are released into the atmosphere or combusted in flare or incinerator (Greenhouse Gas Technology Center, Southern Research Institute 2003). Condensers could be used prior to flares or incinerators.

2.5.1.1 Flaring

Flares are one of the devices used for treatment and control and methane and VOC including BTEX substances. In a flare, organic compounds are combusted in an open flame in open air using supplementary fuel to maintain the flare operation. Parameters affecting the efficiency of flare combustion are gas flammability, auto-ignition temperature, heating value (Btu/Scf), density and combustion zone mixing of the reaction components (U.S.EPA 2002, Stone et al. 1991). The flammability limit is defined as the minimum and maximum stoichiometric composition of fuel-oxygen mixture that will burn continuously at a given temperature and pressure without further ignition. Gases such as hydrogen with wide flammability limits will be combusted easier. The flammability limits affect the ignition stability and extinction. Heating value also can affect the flame structure and stability since low heating value gases produce cooler flames, weaker buoyant forces and non-complete mixing that could lead to extinction of flame.

In flares the velocity is usually very low and most of the flame structure is developed due to buoyancy forces induced by combustion. Therefore lighter gases will burn better. Mixing has an important role in flare combustion. Mixing can be achieved by injecting steam in the combustion zone to promote turbulent mixing and to induce air into the flame. Poor mixing can lead to smoking, which is more

likely to happen in case of fuels with high carbon to hydrogen molar ratio. Fuels with carbon to hydrogen molar ratio greater than 0.35 require more steam injection to prevent smoking. Mixing and temperature are the most critical factors in flare operation since there is no residence chamber to continue combustion reaction (Tyler 1995). The operating temperature in the flare is 1370-1920 K (Hunter, Oyama 2000).

2.5.1.1.1 Disadvantages of flares

There are several concerns regarding the operation of flares including noise, NO_x formation, energy consumption and safety problems (Hunter, Oyama 2000, Tyler 1995). Mixing at the flare tip can cause excess noise in nearby neighborhoods. Formation of harmful combustion by-products such as NO_x cannot be avoided in flares due to high operating temperatures (Seo, Kang & Shin 1999, Seo et al. 2002). Another disadvantage of flares is the need for supplemental fuel in case of less concentrated stream to maintain the flare operation. Flares are not safe control devices due to the presence of open flames and they are not accepted by the public as a VOC control option. In fact, fire hazard is the reason for elevating the flare to above ground levels (Vatavuk 1991). Another disadvantage of flaring in case of natural gas dehydration emission treatment, is the possibility of water and hydrocarbons condensing in the flare which can lead to smoking (Fisher et al. 1995, Kirchgessner et al. 2004).

2.5.1.2 Thermal incineration

Thermal incineration is another type of homogeneous combustion system for control of VOC. The heart of a thermal incinerator is the combustion chamber

where VOC are being combusted. It consists of a nozzle-stabilized flame maintained by a combination of supplementary fuel, organic waste gas and supplementary air if needed. Since the inlet temperature of organic gases is usually low, supplementary fuel is commonly supplied in order to raise the inlet gas temperature to sustain the combustion. Significant saving in supplementary fuel can be achieved by exchanging the heat between the hot combusted gas stream and the cold inlet gas flows. Upon passing through the flame, the waste gas is heated from its inlet temperature to its ignition temperature. Ignition temperature is defined as the temperature at which the combustion reaction rate and the energy production rate exceed the rate of heat loss that results in high gas temperatures (U.S.EPA 2002). Therefore any mixture of organic waste and air will ignite if its temperature is high enough and reaches the ignition temperature. Ignition occurs at some point during the heating of gas as it passes through the flame regardless of its concentration. The mixture will continue to react as it flows through the combustion chamber. Removal efficiency depends on residence time, temperature and proper mixing. There is flexibility between time and temperature such that the residence time can be shortened by elevating the temperature. Thermal incinerators usually operate in the range of 973-1073 K (Hunter, Oyama 2000).

2.5.1.2.1 Disadvantages of thermal incineration systems

Thermal incinerators also suffer from the formation of toxic NO_x compounds at high temperatures. These devices are susceptible to damage caused by severe temperature changes, and large fluctuations in temperature can induce

thermal stress (Hunter, Oyama 2000). Therefore they are better suited for treatment of constant flow streams. The operating costs of thermal incinerators are also relatively high since no hydrocarbon is recovered for sale (Fisher et al. 1995). This emission control method is not economically feasible due to the cost of additional fuel supplemented to sustain the incineration of VOC (Gearhart 1998).

2.5.1.3 Condensation

Condensation is a separation technique in which one or more components of a vapor mixture are separated as liquid from other volatiles by either cooling or pressurizing the gas stream (Hunter, Oyama 2000, U.S.EPA 2002). The efficiency of condensation depends on vapor pressure of the component to be separated, pressure and temperature that can be achieved during this process and the concentration of that component in the gas stream. Water-cooled condensers are common in the industry although a refrigerant can be used for this purpose instead of water. The choice of a refrigerant is important in order to ensure that potential leakage of the coolant is not more hazardous than the original gas stream. Condensation systems are more efficient when the gas stream compounds have low vapor pressures. Typically, condensation works best for higher molecular weight compounds.

There are two primary types of condensers: contact and non-contact (surface). Surface condensers are the most common type in which, heat is transferred across a barrier that separates gas stream from coolant. Shell and tube heat exchanger is an example of non-contact condensers. In contact condensation system, the coolant is directly sprayed into the gas stream to achieve the

maximum heat transfer. These systems are less complicated and less expensive however, the separation of coolant from condensate is required if either one is to be reused. Coolant in surface condensers is not in contact with the gas stream and can be reused without the need for additional processing.

2.5.1.3.1 Disadvantages of condensation

There are some drawbacks associated with condensation. First of all it does not completely eliminate the VOC from waste gas and the non-condensable stream still contains VOC. Another problem is related to recovery of liquid stream. If the condensate is not reused, the liquid stream needs to be discarded usually through a wastewater treatment plant. Thus, a wastewater problem is created from an air pollution problem (Hunter, Oyama 2000).

2.5.2 Catalytic combustion

The combustion system in which a catalyst is used to change and promote the rate of combustion reactions is called catalytic combustion system. Catalyst is a substance that increases the rate of reaction toward equilibrium (Thomas, Thomas 1967, Satterfield 1991, Thomson, Webb 1968, Bond 1987). It works by providing an alternative reaction pathway with lower activation energy, without being consumed during the reaction. The overall change in free energy for catalytic reaction equals that of the uncatalyzed reaction. Therefore the catalyst does not affect the equilibrium constant. In other words, catalyst changes the kinetics but not the thermodynamics (Chorkendrorff, Niemantsverdriet 2003). Catalyst was first discovered more than 190 years ago by Humphry Davy who realized that platinum wires could promote the combustion reactions in flammable

mixtures while he was investigating the development of a miner's safety lamp and the resulting reactions appeared to take place on the wire surface without flame (Weinberg 1986, Moulijn, van Leeuwen & van Santen 1993). Today platinum is used in many different catalyst formulations such as catalytic converters used for control of vehicle exhaust emissions (Hayes, Kolaczkowski 1997). In catalytic combustion systems, the catalyst is usually in solid phase while the reactants are in gas or liquid phase. Therefore catalytic combustion is alternately called heterogeneous combustion. Heterogeneous catalysis describes the enhancement in the rate of reaction by presence of an interface between two phases (Thomas, Thomas 1967).

2.5.2.1 Advantages of catalytic combustion

Compared to homogeneous combustion, catalytic combustion occurs at lower temperatures, which greatly reduces the chance of formation of NO_x (Jodeiri et al. 2010, Seo, Kang & Shin 1999, Pfefferle, Pfefferle 1987). Thermal and prompt NO_x are the two sources of NO_x formation in catalytic combustion. Thermal NO_x originate from direct combination of oxygen and nitrogen at temperatures higher than 1650^{o}C while prompt NO_x is generated due to the combustion of nitrogen containing fuel (Trimm 1983, Thevenin, Menon & Jaras 2003). Example applications of catalytic combustion are treatment of car exhaust, heaters and gas turbines. The operating temperatures in all three areas are less than 1200 K and the formation of NO_x is greatly reduced.

Using catalytic combustion, lean fuel:air mixtures can be oxidized without any limitation of flammability, which is not the case in homogeneous combustion.

Flammability limit is the composition limits outside which, the mixture will not permit the flame to propagate indefinitely however powerful the source of ignition that is applied (Ghigier 1981). The flammability limits depend on the type of fuel. For example for methane in air, the limits are between 5% and 16% methane by volume and the flame can only occur between these two compositions while in catalytic combustion there is no flammability limit to be considered (Hayes, Kolaczkowski 1997, Goralski, Schmidt 1999). If the fuel concentration is too low to maintain catalyst temperature heat needs to be supplied to the catalyst so that the oxidation is initiated. Since fugitive methane and BTEX emissions are usually at low concentrations, catalytic combustion can be applied for treatment of these lean fugitive emissions. Another advantage of catalytic combustion systems is that there is no visible flame involved which gives higher safety standard against fire (Seo et al. 2002).

Chapter 3

Literature review on methane and VOC catalytic combustion

3.1 Introduction

Fossil fuels have been used as the main source of energy for a long time, and currently more than 90% of the world energy demand comes from fossil fuels (Litto 2008). Natural gas, which has low amounts of nitrogen and sulfur, and the highest H:C ratio, is considered to be a clean fuel among fossil fuels (Burch, Loader 1994). The supply of natural gas is predicted to last through the foreseeable future, and therefore natural gas should be a very significant source of energy in the future (Ciuparu et al. 2002, Lyubovsky et al. 2003). The world population is expected to double by the middle of the 21st century, and economic development will continue to grow. Global demand for energy is expected to increase by as much as an order of magnitude by 2050, while primary energy demands are expected to increase by 1.5-3 times (Dincer, Rosen 1999). Increase in energy production is associated with environmental issues such as GHG and BTEX emissions, which is currently a large concern around the world. Therefore collaborative efforts are required to tackle the VOC emissions associated with excessive production and consumption of fossil fuels, especially natural gas.

Gas phase combustion has been the conventional method for mitigation of fugitive VOC emissions. However, with increasing awareness on the magnitude of environmental damage caused by these emissions and subsequent stringent regulations on the acceptable levels of these compounds, the shortcomings of this method cannot be overlooked. Catalytic combustion is an alternative to homogeneous combustion that offers zero NO_x emissions due to low operating

temperatures, flexible operating condition in terms of VOC concentration and flammability limits and safe operation. Catalytic combustion currently has several commercial applications including radiant heaters for paint drying and surface curing (Seo, Kang & Shin 1999, Seo et al. 2002) and space heating for well site buildings, compressor sites and oil batteries; sensors for detecting flammable gases in the air by measuring the heat liberated from its combustion; domestic catalytic burners such as stove for outdoor use that is not sensitive to wind and furnace burners (Saint-Just, der Kinderen 1996).

Catalytic combustion of methane which is the main component of natural gas, and BTEX substances has been extensively studied in the past in terms of kinetics and mechanism, reactor design and catalyst preparation in order to understand the process and to improve the performance of the system. To gain an insight into the work done in this area, relevant literature will be reviewed and compared in this chapter.

3.2 Methane catalytic combustion

Methane combustion produces the lowest CO_2 per unit of energy produced among all hydrocarbons (Ciuparu et al. 2002). It is the most stable and the most difficult hydrocarbon to oxidize. The overall complete methane combustion reaction is:

$$CH_4 + 2O_2 \rightleftharpoons CO_2 + 2H_2O \qquad \Delta H_{298} = -802.9\ \text{kJ/mol} \qquad (3.1)$$

The strength of C—H bond in methane molecule is 435 kJ/mol, indicating high activation energy for homogeneous combustion while the activation energy for dissociative adsorption of methane on the surface of transition metal catalyst is an order of magnitude lower implying the low temperature requirement for catalytic combustion of methane with negligible NO_x formation (Ciuparu et al. 2002). Catalytic combustion occurs according to the following steps:

1. Transport of reactants from bulk stream to the external surface of the catalyst (external or interphase diffusion)
2. Diffusion of reactants from catalyst surface into the catalyst pores (intraphase diffusion)
3. Adsorption of reactants on the active catalytic site
4. Reaction on the catalyst surface
5. Desorption of reaction products
6. Diffusion of products from catalyst pore to the catalyst surface
7. Transport of products into the bulk gas stream

Steps 1, 2, 6 and 7 are physical transport steps while steps 3, 4 and 5 are chemical kinetic steps (Moulijn, van Leeuwen & van Santen 1993). Combustion of all hydrocarbons is an exothermic reaction and the generated thermal energy within the catalyst is transported to the bulk gas phase by conduction and convection. The rate of surface reaction as a function of temperature is shown in Figure 3.1 (Lee, Trimm 1995). In section A-B which corresponds to lower temperatures, the reaction is controlled by kinetics. By increasing the temperature (B-C) rate of reaction is increasing exponentially and the system becomes mass

transfer controlled. In section C-D homogeneous gas phase reaction becomes significant and the effects of mass and heat transfer become important.

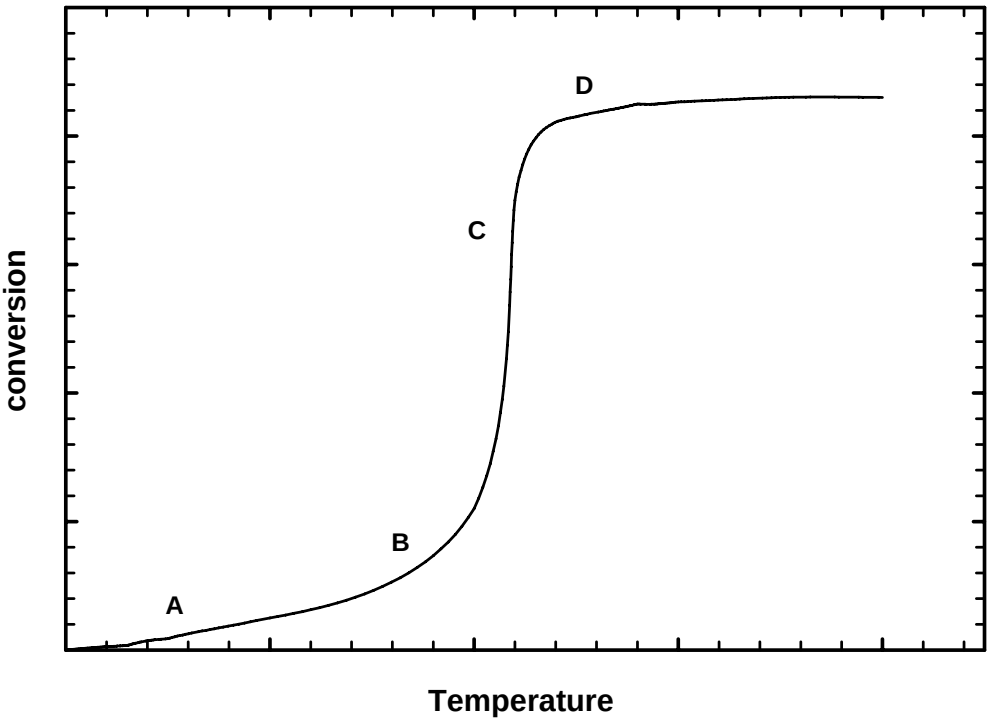

Figure 3.1. Hydrocarbon conversion in catalytic combustion vs. temperature (Lee, Trimm 1995)

3.3 Catalysts for methane combustion

The catalyst used for combustion generally consists of an active catalytic part and a support or substrate. There are a large number of combinations between different catalysts that makes the classification of catalysts complicated. On the other hand, some materials that are used as catalyst in a catalytic combustion system could be used as support in another system that adds to the complexity of catalyst systems classification. Examples of these materials are perovskites and

hexaaliminates (Choudhary, Banerjee & Choudhary 2002). Catalysts for methane combustion can be divided into two categories: noble metals and other transition metal oxides. They can be used with or without a support, however, supported catalysts are more common (Litto 2008, Guan et al. 2008).

The main role of the support is to maximize the surface area of the active metal catalysts by providing a large area over which it is dispersed (Moulijn, van Leeuwen & van Santen 1993, Escandón et al. 2005). Other positive effects of the support include increased thermal stability of the catalyst particles thus preventing agglomeration and sintering with subsequent loss of active sites, and greater resistance to poisoning (Thomson, Webb 1968). Catalysts for combustion may be supported on different types of materials such as pellets, honeycomb monoliths, parallel plates, fiber pads and gauze and sintered metals (Hayes, Kolaczkowski 1997, Kiwi-Minsker et al. 2000). Typical substances that are used as catalyst support are silica gel and γ-alumina that can be prepared with surface areas in the range of 100-800 m^2/g. The support could be catalytically inactive and undergoes little or no chemical interaction with metal or it can contribute to catalytic activity by modifying or reacting to some extent with other catalytic ingredients (Escandón et al. 2005).

In general a catalyst needs to possess several characteristics to be suitable for commercial applications (Trimm 1983, Hartley 1985):

- High selectivity toward the desired product, otherwise separation of products is needed which could be costly.

- High activity per unit volume of reactor, otherwise the cost of catalyst per unit of product would be high. In other words it should have high turn over frequency (TOF) which is defined as the number of molecules reacted per active site per unit of time.
- High mechanical strength and thermal stability at temperatures encountered in combustion.
- Adequate heat transfer properties to distribute the heat generated at the active site. Also a good catalyst should initiate the reaction at low temperatures.
- High attrition resistance (resistance to mechanical wear)

3.3.1 Noble metal based catalysts

For complete methane combustion, platinum and palladium are the most extensively studied and commonly used catalysts (Su, Agnew 2006, Sadamori 1999, Hayes 2004, Forzatti, Groppi 1999, Demoulin et al. 2008). Other noble metals are highly volatile and are not favored in catalytic combustion because of high temperatures achieved in combustion. The main advantage of noble metal catalysts over metal oxides is higher catalytic site activity and greater resistance to sulfur poisoning (Choudhary, Banerjee & Choudhary 2002). However noble metals are more expensive compared to metal oxides. Dispersing the noble metal on a support is an economic way of using these materials since lower amount of noble metal is needed when they are distributed on a support.

The most common catalyst for methane combustion is Pd supported on γ-alumina (Escandón et al. 2005). During catalytic combustion in oxygen-rich atmosphere, palladium oxide is the most active state compared to Pd (Choudhary, Banerjee & Choudhary 2002, Burch 1997). In fact during the combustion, Pd undergoes oxidation and the oxidized state plays an important role in catalyst activity. However, it is not stable due to sintering of PdO particles during combustion (Gao et al. 2008). Deactivation of Pd could also be due to formation of $Pd(OH)_2$. On the other hand, activity of platinum catalyst increases in going from oxygen-rich to fuel-rich condition. Although Pd is considered the most preferred catalyst for methane combustion, Pt supported on alumina is reported to be more effective than Pd/alumina in case of stoichiometric or rich mixtures (Choudhary, Banerjee & Choudhary 2002).

3.3.2 Metal oxide catalysts

Metal oxides are less expensive compared to noble metals and their use is more desirable from the economic stand point. However, they suffer from lower catalyst site activity and higher light-off temperatures (Choudhary, Banerjee & Choudhary 2002). Among different types of metal oxides including single metal oxides and mixed metal oxides, perovskite type metal oxides are more commonly investigated and used. These types of materials are represented by general formula of ABO_3 where larger cation A has a dodecahedral coordination and smaller B cation has a six-fold coordination. Among different perovskites, $LaMnO_3$ is considered a good candidate for methane combustion (Cimino, Pirone & Lisi 2002).

3.4 Mechanism and kinetics of methane catalytic combustion

There has been extensive research on the surface reaction mechanism and kinetics of methane combustion. All heterogeneous combustion processes follow the steps that involve transportation of reactants to the catalyst surface, diffusion into the catalyst site, adsorption and reaction, product desorption and transport to the external surface of the catalyst. In all heterogeneously catalyzed reactions at least one of the reactants must attach to the exterior surface of the catalyst. In case of reaction of two reactants A and B producing C two scenarios are possible. Either both species are attached to the surface and re-organization of atoms occurs in the resulting adsorbed layer or only one reactant is bound and converted to product:

$$1.\ A_{ads} + B_{ads} \rightarrow \text{product}$$
$$2.\ A_{ads} + B_{gas} \rightarrow \text{product}$$

Case 1 is called the Langmuir-Hinshelwood mechanism and Case 2 is called Eley-Rideal mechanism (Zhdanov 2002). Eley-Rideal mechanism suggest that the catalyst surface is covered with one species and reaction takes place between chemisorbed radical or atom and a molecule, the later impacting directly from gas phase (Chorkendrorff, Niemantsverdriet 2003). In Langmuir-Hinshelwood mechanism it is assumed that all species are adsorbed and accommodated in thermal equilibrium with the surface before they take part in reaction and species react in the chemisorbed form on the surface. Most reactions in heterogeneous catalysis follow this mechanism. However, in the Eley-Rideal

mechanism one of the reactants reacts directly out of the gas phase without being accommodated at the surface.

Most catalytic reactions include adsorption, desorption and Langmuir-Hinshelwood steps. Hougen and Watson have developed rate models based on Langmuir-Hinshelwood adsorption (Hayes, Kolaczkowski 1997). The procedure for developing the rate model is:

A) Proposing a mechanism based on Langmuir-Hinshelwood adsorption, surface reaction between adsorbed species and desorption.

B) Assuming one of the steps in mechanism is intrinsically slow (rate determining step) meaning that the value of rate constants in this step are small. Other steps are assumed to be in equilibrium.

C) Writing the overall rate of reaction in terms of the rate determining step which will contain concentration of adsorbed species, eliminating the adsorbed species concentration using the steps in equilibrium resulting in a rate expression in terms of gas phase concentrations.

The underlying assumptions of Langmuir-Hinshelwood adsorption is that each catalytic site can accommodate only one adsorbed species (monolayer) and the surface is completely uniform so that there is the same probability of adsorption on all sites. Attractive or repulsive forces between two adsorbed species are neglected so that the chance of adsorption to an empty site is independent of whether or not the adjacent site is occupied. Further, adsorption equilibrium is assumed to be established at all times (Satterfield 1991).

Based on previous numerical studies, Chou et al. (1999) proposed an improved multi-step surface reaction mechanism for methane combustion on Pt. The mechanism involves adsorption of O_2 and CH_4 and intermediates including CO, H_2 and OH on the active sites, surface reaction and desorption of CO_2 and H_2O. This mechanism is shown in Table 3.1. Note that Pt(s) represent the vacant Pt active site and species with label (s) are the adsorbed species on the active site. With the assumption of Langmuir-Hinshelwood surface reaction mechanism, the onset of surface ignition is determined by the competition between O_2 and CH_4 for surface sites. The dominant limiting process changes from O_2 desorption to CH_4 adsorption as the surface temperature increases. Through third reaction in Table 3.1, conversion of CH_4 may proceed on surfaces with high coverage of O(s). The heat generated by this reaction raises the surface temperature. Increasing the surface temperature leads to the drop in the surface O(s) coverage and increases the CH_4 adsorption process via the first reaction. When the surface temperature reaches a certain point, the CH_4 adsorption rate exceeds the O_2 adsorption rate such that the first reaction becomes dominant. Consequently, more CH_4 is adsorbed on the surface resulting in ignition on the catalyst surface.

Deutschmann et al. (2000) and Deshmukh and Vlachos (2007) also developed surface reaction mechanisms for methane combustion on Pt. These mechanisms are also shown in Table 3.1.

Table 3.1. Proposed surface reaction mechanism for methane combustion on Pt

Chou mechanism	Deutschmann mechanism	Deshmukh mechanism
Adsorption	Adsorption	Adsorption
$CH_4 + 2Pt(s) \rightarrow CH_3(s) + H(s)$	$H_2 + 2Pt(s) \rightarrow 2H(s)$	$O_2 + 2Pt(s) \rightarrow 2O(s)$
$O_2 + 2Pt(s) \rightarrow 2O(s)$	$H + Pt(s) \rightarrow H(s)$	$H_2O + Pt(s) \rightarrow H_2O(s)$
$CH_4 + O(s) + Pt(s) \rightarrow CH_3(s) + OH(s)$	$O_2 + 2Pt(s) \rightarrow 2O(s)$	$CH_4 + 2Pt(s) \rightarrow CH_3(s) + H(s)$
$CO + Pt(s) \rightarrow CO(s)$	[a] $O_2 + 2Pt(s) \rightarrow 2O(s)$	$CO_2 + Pt(s) \rightarrow CO_2(s)$
$H_2 + 2Pt(s) \rightarrow 2H(s)$	$O + Pt(s) \rightarrow O(s)$	Surface reaction
$OH + Pt(s) \rightarrow OH(s)$	$H_2O + Pt(s) \rightarrow H_2O(s)$	$H(s) + O(s) \rightarrow OH(s) + Pt(s)$
$H_2O + Pt(s) \rightarrow H_2O(s)$	$OH + Pt(s) \rightarrow OH(s)$	$OH(s) + Pt(s) \rightarrow H(s) + O(s)$
Surface reaction	$CO + Pt(s) \rightarrow CO(s)$	$H(s) + OH(s) \rightarrow H_2O(s) + Pt(s)$
$CH_3(s) + Pt(s) \rightarrow CH_2(s) + H(s)$	$CH_4 + 2Pt(s) \rightarrow CH_3(s) + H(s)$	$2OH(s) \rightarrow H_2O(s) + O(s)$
$CH_2(s) + Pt(s) \rightarrow CH(s) + H(s)$	Surface reaction	$CH_3(s) + O(s) \rightarrow CH_2(s) + OH(s)$
$CH(s) + Pt(s) \rightarrow C(s) + H(s)$	$O(s) + H(s) \Leftrightarrow OH(s) + Pt(s)$	$CH_2(s) + O(s) \rightarrow CH(s) + OH(s)$
$H(s) + O(s) \rightarrow OH(s) + Pt(s)$	$H(s) + OH(s) \Leftrightarrow H_2O(s) + Pt(s)$	$CH(s) + O(s) \rightarrow CO(s) + H(s)$
$OH(s) + Pt(s) \rightarrow H(s) + O(s)$	$OH(s) + OH(s) \Leftrightarrow H_2O(s) + O(s)$	$CO(s) + O(s) \rightarrow CO_2(s) + Pt(s)$
$H(s) + OH(s) \rightarrow H_2O(s) + Pt(s)$	$CO(s) + O(s) \rightarrow CO_2(s) + Pt(s)$	desorption
$2OH(s) \rightarrow H_2O(s) + O(s)$	$CH_3(s) + Pt(s) \rightarrow CH_2(s) + H(s)$	$2O(s) \rightarrow 2Pt(s) + O_2$
$H_2O(s) + Pt(s) \rightarrow OH(s) + H(s)$	$CH_2(s) + Pt(s) \rightarrow CH(s) + H(s)$	$H_2O(s) \rightarrow H_2O + Pt(s)$
$C(s) + O(s) \rightarrow CO(s) + Pt(s)$	$CH(s) + Pt(s) \rightarrow C(s) + H(s)$	$CO_2(s) \rightarrow CO_2 + Pt(s)$
$CO(s) + Pt(s) \rightarrow C(s) + O(s)$	$C(s) + O(s) \rightarrow CO(s) + Pt(s)$	

$CO(s) + O(s) \rightarrow CO_2 + 2Pt(s)$	$CO(s) + Pt(s) \rightarrow C(s) + O(s)$	
desorption	desorption	
$2O(s) \rightarrow 2Pt(s) + O_2$	$2H(s) \rightarrow 2Pt(s) + H_2$	
$CO(s) \rightarrow CO + Pt(s)$	$2O(s) \rightarrow 2Pt(s) + O_2$	
$2H(s) \rightarrow 2Pt(s) + H_2$	$H_2O(s) \rightarrow H_2O + Pt(s)$	
$OH(s) \rightarrow OH + Pt(s)$	$OH(s) \rightarrow OH + Pt(s)$	
$H_2O(s) \rightarrow H_2O + Pt(s)$	$CO(s) \rightarrow CO + Pt(s)$	
	$CO_2(s) \rightarrow CO_2 + Pt(s)$	

a) Reactions 4 and 5 in this mechanism represent alternative competing pathways.

In the former study the proposed mechanism consists of seven gas phase species and eleven surface species. The later study used a computer-assisted model reduction strategy and reduced the original 104 reactions to 15 reactions that can capture the predictions of the original detailed model. All these mechanisms take into account both homogeneous gas phase reactions and heterogeneous reactions on the catalyst surface.

After developing a mechanism for the reaction, rate expressions can be derived from these elementary reactions. Kinetics of methane combustion on Pt still is not well understood due to the special behavior of this reaction. For example under certain conditions reaction rate measured under steady state condition, exhibit step wise change with varying reactant pressure. Specially a two times increase of oxygen pressure can lead to five times decrease in reaction rate and then with further increase of oxygen pressure, reaction becomes independent of oxygen pressure (Firth, Holland 1969).

Another observation was that by increasing the surface coverage of oxygen, methane conversion increases rapidly and then decreases (Burch, Loader & Urbano 1996). Despite all this unusual behaviour, reaction rate can be represented in simple power law form:

$$-r_{CH_4} = k' P_{CH_4}{}^{\alpha} P_{O_2}{}^{\beta} \tag{3.2}$$

$$k' = k_0 exp\left(-\frac{E}{RT}\right) \tag{3.3}$$

k' is the rate constant and α and β are reaction order with respect to methane and oxygen, respectively. Kinetic studies of methane combustion have revealed non-monotonic dependence on oxygen pressure with both positive and negative order with respect to oxygen depending on its partial pressure (Ma, Trimm & Jiang 1996). In this study using Pt/γ-Al_2O_3 catalyst, the reaction rate increased by increasing the methane pressure and decreased by increasing oxygen pressure. In a study of combustion of C_1-C_4 hydrocarbons on Pt, Yao (1980) found the reaction order of 1 and -0.6 with respect to methane and oxygen in O_2/CH_4 of 1-4, respectively. In another study of methane combustion on Pt and Pd in a pulse flow microreactor, the orders of reaction with respect to methane and oxygen were found to be near 1 and zero at CH_4:O_2 in the ranging from 1:10 to 10:1 at temperature 580-710 K (Cullis, Willatt 1983). The same conclusion was made by Niwa et al. (1983) who investigated the methane combustion on Pt catalyst supported on Al_2O_3 at stoichiometric conditions.

The most common approach for developing the reaction rate is by applying the Langmuir-Hinshelwood model. The main advantage of this model is that the reaction order can be negative or positive depending on the reaction condition (Deshmukh, Vlachos 2007). Several Langmuir-Hinshelwood and Eley-Rideal type models have been developed for predicting the kinetics of methane oxidation and have been compared with experimental findings. The best expression is based on the reaction of adsorbed methane with atomic oxygen which can describe the reaction rate using the following equation:

$$-r_{CH_4} = \frac{k'_1 K'_1 (K'_2 P_{CH_4})^{0.5} (P_{O_2})^{0.5}}{\left(1 + K'_1 P_{CH_4} + (K'_2 P_{O_2})^{0.5}\right)} \tag{3.4}$$

where k'_1, K'_1 and K'_2 are rate constant, adsorption coefficient for methane and adsorption coefficient for oxygen, respectively. The activation energy using this model is 34.7 kJ/mol while this value in case of power law model is 88.5 kJ/mol (Ma, Trimm & Jiang 1996). In another study kinetics data was fitted with different possible Langmuir-Hinshelwood kinetic models and the following rate expression for low temperature combustion of methane (793 K) was obtained:

$$-r_{CH_4} = \frac{k'_1 (P_{CH_4})(P_{O_2})^{0.5}}{(1 + k'_2 (P_{O_2})^{0.5})} + \frac{k'_4 (P_{CH_4})(P_{O_2})}{(1 + k'_3 (P_{O_2}))} \tag{3.5}$$

where k'_1, k'_2, k'_3 and k'_4 are rate constants (Trimm, Lam 1980a). This expression is based on the reaction of gaseous or weakly adsorbed methane with surface oxygen adsorbed monatomically or diatomically on two different sites. Neglecting $k'_2 (P_{O_2})^{0.5}$ and $k'_3 (P_{O_2})^{0.5}$ in this rate expression compared to unity leads to the following expression:

$$-r_{CH_4} = k'_1 P_{CH_4} P_{O_2}{}^{0.5} + k'_4 P_{CH_4} P_{O_2} \tag{3.6}$$

The effect of temperature on order of reaction with respect to methane and oxygen was measured experimentally at constant CH_4:O_2 ratio over Pt supported porous and non-porous alumina fiber (Trimm, Lam 1980a). It was found that the reaction order with respect to methane is one while the order with respect to oxygen is 0.75 at T < 813 K and 1 at T > 813 K.

3.5 Important factors in catalytic activity

In catalytic combustion, catalytic material plays an important role and the system efficiency depends on the choice of the catalyst. Different types of catalysts, their synthesis and characterization and factors affecting their performance have been extensively studied in the past. There are several factors that can affect methane and VOC catalytic combustion efficiency including the feed ratio, type of catalyst, type and nature of support, catalyst loading, combustion products H_2O and CO_2, catalyst pre-treatment and temperature. Some of these factors will be discussed in the following section.

3.5.1 Type of catalyst and nature of active sites

Burch and Loader (1994) have investigated the activity of 4% Pt/Al_2O_3 and 4% Pd/Al_2O_3 at both fuel-lean and fuel-rich mixtures. In fuel-lean mixture (O_2:CH_4 was 5:1), Pd was more active compared to Pt in temperature range of 300-550^oC. In fuel-rich mixture, again Pd showed higher activity at low temperatures however above 350^oC Pt showed superior activity. The activity of Pt increased by moving from oxygen-rich to methane-rich conditions. In fact, in oxidizing environment, Pt is less active. Hicks et al. (1990) and Aryafar and Zaera (1997) also reported that the dispersed Pt in the form of PtO_2 catalyst is less active than large Pt crystals on which a layer of chemisorbed oxygen is formed which can be related to different activities of surface oxygen species. Measurement of the heat of adsorption of oxygen on reduced and oxidized Pt surfaces showed that oxygen is bound more weakly on Pt metal than on the oxide. Therefore, a less

oxidized form of Pt will be more active and Pt catalysts will be less active under oxygen-rich conditions. In case of Pd, oxygen bond on oxidized Pd is weaker compared to metal Pd and Pd is more active in oxidized form which is reflected in greater activity of Pd in fuel-lean conditions. Superior activity of Pt compared to Pd was also confirmed in another study at methane-rich conditions (Cullis, Willatt 1983).

3.5.2 Reaction products

The effect of combustion products, H_2O and CO_2 on catalyst activity has been studied. Cullis and Willat (1984) investigated the effect of CO_2 and H_2O addition on Pd/Al_2O_3 activity at 625 K and reactant mixture of 1.8×10^{-6} mole CH_4 and 3.6×10^{-6} mole O_2 and found that the addition of water in comparable amount to that formed during methane combustion has no effect on the catalyst activity. However large quantities of water inhibit the methane combustion. The same behavior was observed for CO_2. Ribeiro et al. (1994) studied the order of methane combustion with respect to H_2O at 550 K by maintaining the condition of excess CO_2 and changing the H_2O concentration. A similar procedure was repeated for finding the reaction order with respect to CO_2. They found the reaction order of -0.98 for H_2O suggesting the competition between methane and H_2O for active sites. Water reacts with PdO which is the stable form of Pd under fuel-lean condition (oxidizing), resulting in formation of $Pd(OH)_2$ (Cullis, Nevell & Trimm 1972). Therefore strong H_2O inhibition could be due to formation of Pd hydroxyls blocking the active sites preventing the CH_4 access to the sites. Inhibition by CO_2 was observed at concentrations greater than 0.5 vol% with reaction order of -2.

In an extensive study, Burch et al. (1995) measured methane conversion on Pd/Al_2O_3 at different temperatures with addition of either 20% CO_2 or 2.7% water to the reactant mixture. Both compounds showed inhibitory effect with effect of H_2O being much more significant. This effect was negligible at higher temperatures (conversions). The combined effect of CO_2 and H_2O on catalyst activity was studied indicating the independent inhibitory effect of the two compounds. When H_2O was first switched on, catalyst activity decreased rapidly such that later addition of CO_2 did not show significant effect on activity. Catalyst activity recovered by switching off the water but not to the original level. Switching off the CO_2 resulted in complete recovery of activity. When water was first switched on, it blocked the active sites and the effect of CO_2 was not pronounced. Negative effect of CO_2 was also observed at different metal support, loading and dispersion. The discrepancy between these results and findings of Ribeiro et al. (1994) regarding the stronger inhibitor could be due to the lower conversion levels (less than 2.5%) and low level of H_2O addition in the later study. In another study on methane combustion on Pd/Al_2O_3, zero reaction order with respect to CO_2 was reported while reaction order with respect to H_2O was close to unity in the temperature range of 563-773 K (van Giezen et al. 1999). It seems that the reported results for inhibitory effect of CO_2 on methane combustion are not consistent.

The activity of Pd/Al_2O_3 for methane combustion has been compared to that of bimetalic $Pd\text{-}Pt/Al_2O_3$. Pd/Al_2O_3 initially showed excellent activity toward methane combustion at 500^oC however the activity decreased dramatically during

the course of reaction possibly due to formation of $Pd(OH)_2$. Slight increase in activity with time for 2:1 Pd-Pt/Al_2O_3 was observed. To confirm the water inhibition effect on Pd/Al_2O_3, 5 vol% water was added periodically to the feed stream. In case of the bilemetalic catalyst, after water addition, activity decreased abruptly; however, it recovered when water flow was discontinued. The behaviour of Pd/Al_2O_3 was different since the catalyst activity decreased continuously and did not fully recover when water was removed (Persson et al. 2007).

3.5.3 Particle size and catalyst loading

The effect of catalyst particle size on activity was studied by measuring the specific rate of methane oxidation (Burch, Loader 1994). There was no correlation between the Pt particle size in the range of 1.4-3.7 nm on specific rate at temperature range of 425-500^oC, however, small increase in rate was observed at higher temperatures. Ribeiro et al. (1994) also reported small apparent activation energy and TOF change with Pd particle size in the range of 2-110 nm indicating structure insensitivity. In contrast, Hicks et al. (1990) observed the structure sensitivity of methane oxidation on Pt evident by higher TOF and lower apparent activation energy for small crystallites compared to large particles. For Pt, two types of Pt particles on the surface exist: completely dispersed Pt and Pt crystallites. In dispersed form, Pt is oxidized to PtO_2 while in the later form oxygen is adsorbed on crystallites providing highly active adsorbed oxygen. Therefore the large crystallites are more active than small dispersed Pt. Similar behavior was observed for Pd where the activity of dispersed PdO was lower than that for small Pd crystallites.

For a given support, increasing the precious metal loading leads to the increase in size of particles and higher catalyst loading does not necessarily guarantee the enhanced dispersion of metal. It instead leads to agglomeration of the particles. Increase in Pd particle size did not have any effect on its activity for methane oxidation (Cullis, Willatt 1983). However, Niwa et al. (1983) observed improved methane oxidation rate by increasing the Pt loading from 0.1% to 2% at temperature in the range of 300-500^{o}C. Burch and Loader (1994) also observed increase in methane oxidation in oxygen-rich environment by increasing the Pt loading from 0.5% to 4%. Sarbak and Andersson (2007) also found improved performance of Pt by increasing the metal loading from 3% to 9%. The rate of increase of activity from 3% to 9% loading was not very significant, indicating lower dispersion of Pt at 9% loading and limited availability of extra Pt particles.

3.5.4 Catalyst pre-treatment

Effect of pre-treatment of 2.7% Pd/Al_2O_3 on CO_2 production from methane oxidation was studied by conditioning the catalyst in H_2, He and O_2. Pre-treatment with H_2 increased the activity whereas pre-treatment in O_2 led to reduced activity (Cullis, Willatt 1983). Reactant gases were also used for catalyst pre-treatment. Baldwin and Burch (1990) studied the effect of Pd exposure to 1% methane/air mixture on methane conversion and observed higher conversions compared to the catalyst heated only in air although heat treatment in the reaction mixture leads to sintering and increase of Pd particle size. Briot et al. (1990) studied the effect of catalyst pre-treatment by preparing two samples: freshly reduced Pt/Al_2O_3 sample with H_2 (Catalyst I) and exposure of reduced sample to

reaction mixture (oxygen-rich) at 873 K for 14 hours and purging the sample with nitrogen at the same temperature and cooling to room temperature (Catalyst II). Catalyst II was more active in temperature range of 570-720 K. Above 720 K both catalysts showed the same activity. Also lower apparent activation energy was observed for Catalyst II.

3.6 Catalytic combustion of other VOC

Most of the work in the area of catalytic combustion involves methane. There are limited studies on the catalytic combustion of other VOC. One of the studies is devoted to catalytic combustion of benzene, toluene and n-hexane over $Pt/\gamma\text{-}Al_2O_3$ in a fixed bed reactor (Ordóñez et al. 2002). Total conversion of benzene and toluene was achieved at 155-160^oC and 180-190^oC, respectively while temperatures higher than 240^oC was needed for n-hexane combustion. Reactivity of each compound was studied by measuring the temperature at 10% and 50% conversion (T_{10} and T_{50}) at different concentrations. T_{50} was decreased by increasing the n-hexane concentration while slight increase in T_{50} was observed for toluene. In case of benzene first a decreasing trend was observed until 2000 ppm followed by increase in T_{50}. At concentrations less than 1000 ppm, n-hexane was the least reactive while at higher concentrations it had higher reactivity compared to benzene and toluene which was reflected in lower T_{50}. The same trend was observed at T_{10} with toluene having the highest T_{10} value at all concentrations.

Inhibitory effect of each compound on the conversion of others has also been investigated. Presence of hexane has negligible effect on combustion of benzene and toluene; however, hexane conversion decreased significantly when toluene and benzene were present which could be due to higher affinity of aromatics toward catalyst surface. Comparing the effect of benzene and toluene on each other showed higher inhibitory effect of toluene for benzene conversion. The inhibitory effect of n-hexane on toluene conversion on Pt/Al_2O_3 was also confirmed by Grabic et al. (2004).

The effect of mass transfer limitation on benzene combustion on Pd was studied at excess oxygen by evaluating the pore size and shape of the porous support. Catalysts with larger pore size showed better activity and steep increase in benzene conversion with increasing the temperature indicating efficient diffusion of benzene in larger pores (Ryoo et al. 2003). Takeguchi et al. (2003) investigated the toluene combustion over PdO supported on Al_2O_3, SnO_2, ZrO_2 and CeO_2 with 1.1 wt% catalyst loading in a fixed bed flow reactor and found that not only the catalyst activity is responsible for rate of toluene combustion, catalyst structure also plays an important role due to low toluene and oxygen concentrations at the end of catalyst bed, low diffusivity of toluene and weak interaction of toluene with PdO. PdO/SnO_2 showed the lowest light-off temperature while complete toluene conversion was achieved at lower temperature with PdO/Al_2O_3 with highest surface area. Therefore, pore structure plays an important role for effective diffusion of toluene to the active sites. The effect of pore structure was also confirmed by Xia and Kawi (2001) who

investigated catalytic combustion of toluene, benzene, ethylbenzene, cumene and mesitylene using different Pt supported catalysts. Higher activity was observed for catalysts with larger pore size which is due to lower resistance for diffusion of reactants and products in and out of pores. Toluene oxidation was more efficient in presence of catalyst with high loading and same dispersion due to availability of more active sites. They emphasized the role of hydrophobicity since the catalyst with higher surface hydrophobicity of support exhibited higher activity due to easy removal of water produced during the oxidation from active sites. Also addition of water to the reaction has the least effect on the most hydrophobic catalyst. They also confirmed the higher activity for catalysts with larger pore size.

Structure sensitivity of benzene combustion on Pt/Al_2O_3 has been investigated in a fixed bed tubular reactor by Garetto and Apesteguía (2001). By increasing Pt particle size, the light-off curves shift to lower temperatures and higher TOF can be achieved. Pre-treatment of catalyst in O_2, N_2 and reaction mixture (benzene, O_2 and N_2 mixture) revealed that only pre-treatment in reaction mixture shifted the light-off curve to lower temperatures. The reaction order of zero and one with respect to benzene and oxygen was found which is different from the order of reaction in case of methane combustion suggesting different reaction mechanisms. In fact assuming Langmuir-Hinshelwood mechanism, the rate constant for oxygen adsorption is very low compared to surface reaction. Hong et al. (2003) also reached to the same conclusion that the rate liming step is oxygen adsorption since catalyst activity increased by increasing oxygen from 10

to 30 mole % but remained unchanged with change in benzene concentration from 0.5 to 2 mole %. Order of reaction of one with respect to benzene has also been reported in other studies (Gangwal et al. 1988, Barresi, Baldi 1997).

3.7 Methane catalytic combustion in counter-diffusive mode

All the above reviewed works involve mixture of controlled amounts of reactants to the reactor. There is some research devoted to the catalytic combustion of methane and VOC in a counter-diffusive mode. A schematic of a counter-diffusive combustion system is show in Figure 3.2. It consists of inlet tubes for fuel, insulation layer, catalyst pad and electrical heating element. To start up the system, the heating element is used to warm up the reactor. The fuel is introduced using the fuel distributor while oxygen diffuses from the front face through the catalyst pad. Fuel and oxygen meet at the catalyst section and catalytic combustion takes place. The electrical heater is unplugged before fuel is fed. Trimm and Lam (1980b) used a convective-diffusive combustion system similar to Figure 3.2 for study of total oxidation of methane over Pt supported on alumina fiber pad both experimentally and numerically. They studied the effect of methane flow rate on temperature distribution across and through the catalyst pad and radiant energy from the catalyst surface.

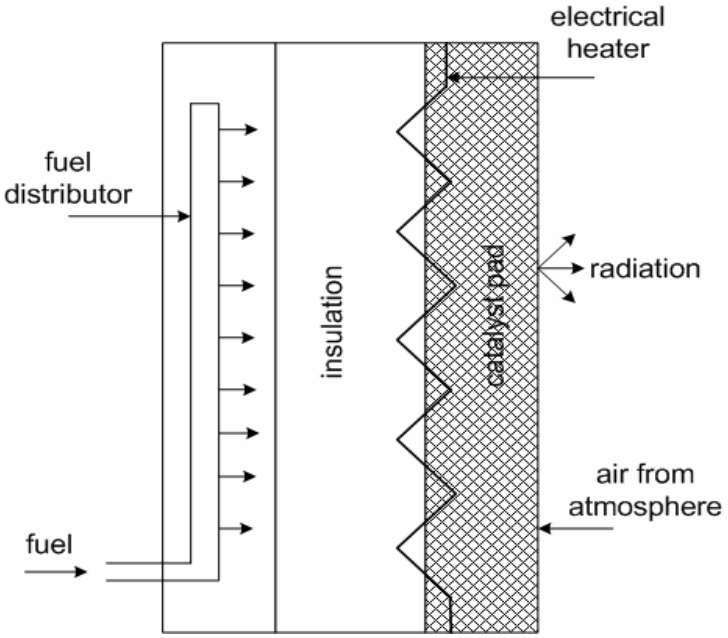

Figure 3.2. Schematic diagram of a counter-diffusive catalytic system

By increasing methane flow rate, the maximum temperature moved toward the front of the pad and its value decreased. The combustion efficiency also decreased at higher methane flow rate. The same results were obtained using a one-dimensional model except the predictions of temperature and combustion efficiency did not match the experimental observations in the edge of the pad.

The effect of fuel flow rate, pad thickness and pad packing density was investigated using the one-dimensional model. There is an optimum methane flow rate for the best performance of the system. The rate of heat generation is increased depending on the reaction rate which rises at higher methane flow rate. However, at the same time high methane flow rate prevent the diffusion of oxygen into the pad leading to detection of unburned methane in the exhaust gas. At lower flow rates oxygen diffusion becomes easier and with O_2:CH_4 > 2, complete methane conversion with no slippage can be achieved. It was found that

the catalyst pad thickness affects the temperature within the pad. Increasing the pad thickness could result in higher temperatures inside the pad while the temperature is the same in front of the pad. The combination of high temperature and low O_2:CH_4 could result in CO formation at higher pad thicknesses. The effect of increasing packing density was reflected on improved heat transfer and radiation efficiency (energy transmitted by radiation/energy released) and reduced combustion efficiency, maximum temperature and minimum O_2:CH_4 ratio.

In another study by Seo et al. (1999) a counter-diffusive catalytic system with propane and toluene as fuel was used. The objective was to alternatively use the toluene mixture evolved during the textile acrylic coating as fuel. Propane combustion was carried out in counter-diffusive mode with natural air diffusion while when switched the fuel to toluene, premixed toluene and air was used. The effect of system installation mode on combustion efficiency of propane was studied at vertical, upward and downward locations. In vertical and upward locations combustion efficiency was 99.5%; however, it started to decrease in case of downward installation suggesting that the hot combustion gases prevent the diffusion of combustion air. Since during the coating process, the materials are moved on a conveyer and the radiant heater is above these materials, air supply by force and premixing the fuel and air was examined. System performance was improved in both cases. The first method was preferred due to the high catalyst temperature associated with premixed feed causing the catalyst sintering. Catalytic combustion of toluene revealed that the amount of unburned toluene increases with increasing the hydrocarbon concentration and its space velocity. In

a later study, Seo et al. (2002) developed a catalytic burner with propane as fuel and Pt deposited on alumina fiber pad as catalyst for heating PVC tiles and tested the natural convection, forced convection and premixed feed flows at different installation modes. The installation mode significantly influenced the natural convection process which agrees with their previous study. The negative effect of higher space velocity on combustion efficiency was confirmed.

Radcliffe and Hickman (1975) used a diffusive catalytic heater for combustion of pure methane using different types of catalytic pads and the results indicated that fiber glass pad was the best in terms of methane combustion efficiency. The common feature in all the pads tested was that the efficiency decreased at low and high fuel flow rates. They also measured the fuel slippage and found that the flow rate at which the slippage is minimum does not exactly correspond to the maximum combustion efficiency. The temperature distribution across the pad was not uniform and the size of local hot and cold spots was changing. The range of temperature on the surface was 600-750 K depending of the pad, fuel flow rate and location on the pad. They explained the non-uniformity of temperature possibly by in-homogeneity in pad porosity or poor distribution of fuel behind the pad.

Heat that is released during the combustion is transferred to the surroundings by radiation from the front surface, by convection of hot combustion gases in the bulk flow through the pad and by conduction through the metal frame of the system. The contribution of each heat transfer mode was calculated and radiation was found to be the main mode. Substantial amount of nitrogen is

expected in the fuel side along with H_2O and CO_2 due to the diffusion of these components through the catalyst pad. Methane combustion efficiency was lower at the top of the pad and the O_2 concentration was lower. In fact the air at top parts of the pad is vitiated by combustion products preventing the effective diffusion of O_2 into the pad.

Sadamori (1999) investigated the counter-diffusive heater for methane combustion on Rh-alumina fiber pad and measured the gas composition and temperature through the pad. By increasing methane flow rate the position where O_2 and CH_4 are consumed moved closer to the surface which is in agreement with the results of Trimm et al. (1980a) indicating the role of O_2 diffusion from the front of the catalyst pad on heater performance. Kinetic studies at 400^oC in a microreactor in presence of H_2O and CO_2 revealed the reaction order of one and 0.5 with respect to methane and O_2, respectively.

There is very limited modeling work on counter-diffusive catalytic combustion and most of them are based on monolith channels (Mazumder, Sengupta 2002, Dupont et al. 2002, Hayes et al. 1996, Jahn et al. 1997, Veser, Frauhammer 2000, Groppi, Tronconi & Forzatti 1999). One of the few modeling works on counter-diffusive radiant system was conducted by Trimm and Lam (1980b) in which, a one-dimensional model was developed and the governing equations were solved using finite difference method. Model data were compared with experimental results form the counter-diffusive catalytic combustor. The model predicted wider reaction zone and the position of maximum temperature moved to the front of the catalyst pad by increasing fuel flow rate. However,

temperature prediction at the front and back of the pad was not accurate. Both model and experiments showed decreasing trend in combustion efficiency by increasing fuel inlet flow rate. It was discussed that at higher fuel flow rate the diffusion of oxygen to the catalyst pad becomes difficult and combustion efficiency decreases. At higher fuel flow rate the reaction zone moves to the front of the pad and the low contact time leads to methane slippage.

Specchia et al. (1981) proposed a model for methane catalytic combustion assuming very high reaction rate. They regarded the catalyst pad as an isothermal tubular reactor with constant longitudinal dispersion through the panel. The modeling data were compared with the experimental results obtained by Dongworth and Melvin (1977) in which they used a catalyst panel with 5% Pt deposited on γ/Al_2O_3. Two sets of data showed good agreement with each other in terms of components mole fraction. They report that the combustion takes place in a thin layer near the front surface of the catalyst pad. Both studies emphasize the oxygen diffusion into the catalyst pad to be the controlling factor in the diffusive catalytic combustion system.

Ablow and Sadamori (1987) investigated the methane combustion on porous alumina pad impregnated with rhodium in counter-diffusive catalytic heater experimentally and analytically. The model included temperature dependent transport coefficients however these coefficients were not considered to be concentration dependent. The reaction was assumed to be fast and controlled by reactants diffusion. They used constant species diffusion coefficient and studied the effect of changing the diffusion coefficient on temperature and species

distribution and found that the position of reaction zone and temperature distribution changes with diffusion coefficient. The experimental species distribution in the system agreed only roughly with model data.

Chapter 4

Experimental investigation of CH_4 and BTEX catalytic combustion in the counter-diffusive radiant heater

4.1 Introduction

Natural gas dehydration process emissions are one of the major sources of fugitive methane and BTEX emissions in the oil and gas industry. Methane is known as a strong GHG causing the global warming and climate change issues, while BTEX substances are proven to be carcinogenic and exposure to their emission impose serious health risks on human. Due to the governmental regulations on BTEX emission limits and inadequacy of homogeneous combustion, catalytic combustion is proposed to effectively mitigate these emissions. In addition to these hydrocarbons, natural gas dehydration emissions contain large amounts of water that makes the mitigation of the emissions even more challenging.

In this chapter, the experimental set up, procedure and results obtained using the small scale counter-diffusive radiant heater is discussed in detail. The preliminary experiments were conducted using methane to understand the basic physical phenomena involved during the operation of the counter-diffusive radiant heater and to evaluate the catalytic combustion efficiency. The effect of several parameters including methane flow rate on its conversion was studied. In addition, the effect of addition of water, n-pentane (C_5) and toluene (C_7) in both liquid and vapor phase, on the performance of the system was investigated.

4.2 Materials and methods

4.2.1 Chemicals

Methane combustion experiments were conducted using the municipal natural gas supply. For the experiments with water, reverse osmosis water was used. Anhydrous C_5 with a purity of 99 % from Sigma-Aldrich and C_7 of HPLC grade from Fisher Scientific were used in the catalytic combustion of other hydrocarbons, respectively. C_5 was used to represent all non-aromatic, non-methane hydrocarbons, while C_7 was selected to represent all BTEX substances.

4.2.2 Radiant heater structure and operation

Catalytic combustion of methane and BTEX substances were conducted in the counter-diffusive radiant heater system, provided by Scott Can. Industries Ltd. A diagram of the counter-diffusive radiant heater was shown in previous chapter in Figure 3.2. The dimensions of the unit are 0.3 m × 0.3 m × 0.05 m and the thickness of the commercial catalyst pad is 0.01 m. The unit consists of inlet tube for introducing the fuel, insulation layer, catalyst pad and electrical heating element. The fuel is introduced perpendicular to the catalyst pad. To start up the system, heating element is plugged in to warm up the catalyst pad. When the average temperature of the pad is about 150^{o}C, the electrical heater is unplugged and the fuel is introduced using the inlet tube. Oxygen from ambient air diffuses from the front face through the catalyst pad. Fuel and oxygen meet at the catalyst pad and the catalytic combustion takes place leading to high temperatures observed across the catalyst pad. The detailed structure of the commercial unit

and the complete experimental setup are shown in Figure 4.1 and 4.2, respectively. The role of insulation layer is to prevent the transfer of generated thermal energy during exothermic combustion to the back of the unit, where fuel is introduced. The wire mesh shown in Fig. 4.1.d protects the catalyst pad and the funneling hood at the top of the unit (Fig. 4.2) is used to capture the exhaust gas for analysis.

To study the effect of mass transfer to the catalyst pad, a 12 V fan was used to induce convective air flux in the boundary layer. The fan was mounted on top of the funneling hood. To improve the fuel combustion, in some of the experiments an aluminum plate with dimensions of 0.74 m × 0.45 m was used. The catalyst was Pt deposited on porous alumina fiber pad. The front face of the catalyst pad, which is exposed to air, was covered with a thin woven cloth to protect the pad and prevent the loss of active Pt particles from the surface. The cloth can be seen in Figure 4.1.a. The presence of Pt on the pad is identified by the color of the first layers of the pad near the surface.

4.2.3 GC calibration and methane conversion

The exhaust gas produced during the combustion along with unburned fuel is collected from the top of the funneling hood using Teflon tubes and is injected into the gas chromatograph (GC), 5890 model from HP for analysis with a thermal conductivity detector (TCD). The GC column was packed with Haysep Q from SUPELCO with helium from Praxair as the carrier gas. In addition to the exhaust gas, the incoming fuel could also be analyzed by the GC by taking a sample of the gas from the back space of the unit.

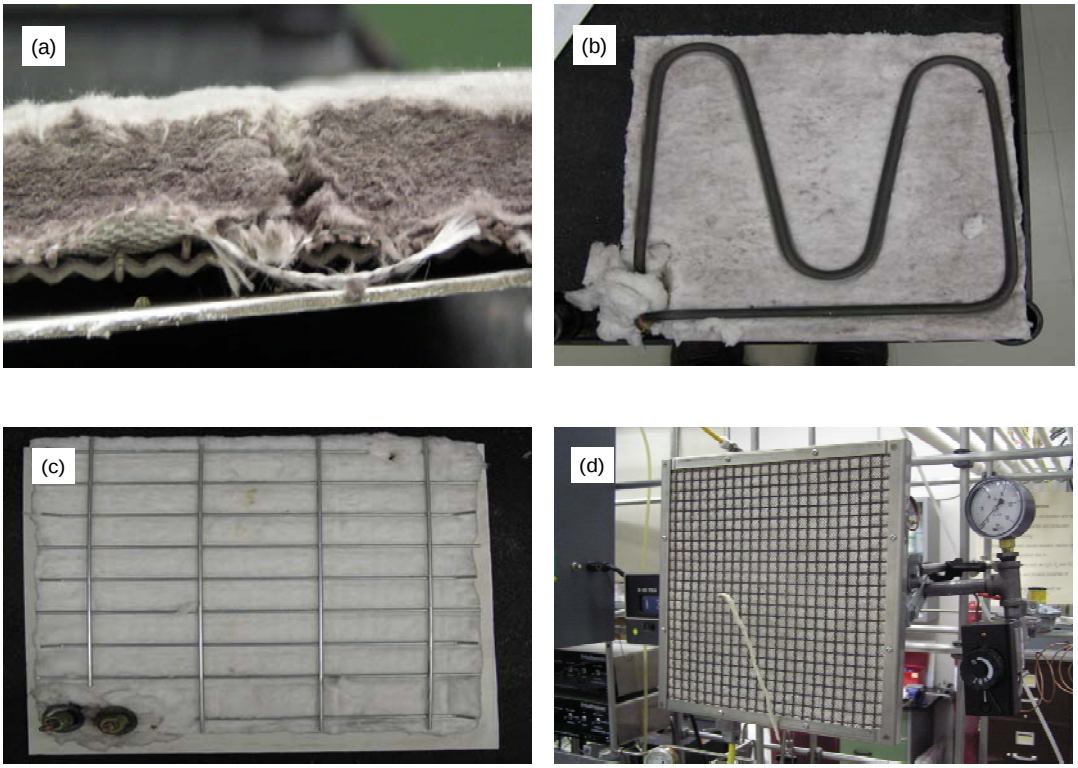

Figure 4.1. Views of the counter-diffusive radiant heater showing a) catalyst pad, b) electrical heater, c) insulation pad, d) catalyst pad protected by wire mesh

Figure 4.2. Experimental setup for catalytic combustion

To calculate the methane fractional conversion, calibration plots for methane and CO_2 were prepared, and response factors (RF) were calculated. RF is an indication of the sensitivity of the TCD to a compound that is analyzed. Figure 4.3 and 4.4 show the calibration and RF plots for CO_2 and methane, respectively. X_{CO2}, X_{CH4}, A_{CO2} and A_{CH4} represent the mole fraction of CO_2 and CH_4 and area under CO_2 and CH_4 peaks, respectively. Calibration mixtures were prepared by introducing known amounts of N_2 and CO_2 into a 2 L vessel and analyzing samples from the vessel by GC. Calibration mixtures of different compositions were prepared by diluting the gas mixture by addition of N_2 in several steps to obtain the lowest CO_2 concentration in the vessel in the last stage. The following equation was used to calculate the RF of CO_2:

$$RF_{CO_2} = \frac{CO_2 \text{ peak area}/N_2 \text{ peak area}}{CO_2 \text{ mole fraction}/N_2 \text{ mole fraction}} = \frac{A_{CO_2}/A_{N_2}}{X_{CO_2}/X_{N_2}} \tag{4.1}$$

A method, replacing CO_2 with CH_4, was used to obtain the RF of CH_4.

To evaluate the combustion efficiency, methane fractional conversion needs to be calculated. Methane flowing inside the heater is combusted producing CO_2 and H_2O. Also some unburned methane can be detected in the exhaust gas. The overall methane fractional conversion is defined as:

$$CH_4 \text{ conversion} = \frac{X_{CH_4(in)} - X_{CH_4(out)}}{X_{CH_4(in)}} \tag{4.2}$$

where $X_{CH4\ (in)}$ and $X_{CH4\ (out)}$ represent the mole fraction of CH_4 at the reactor inlet and exhaust gas, respectively.

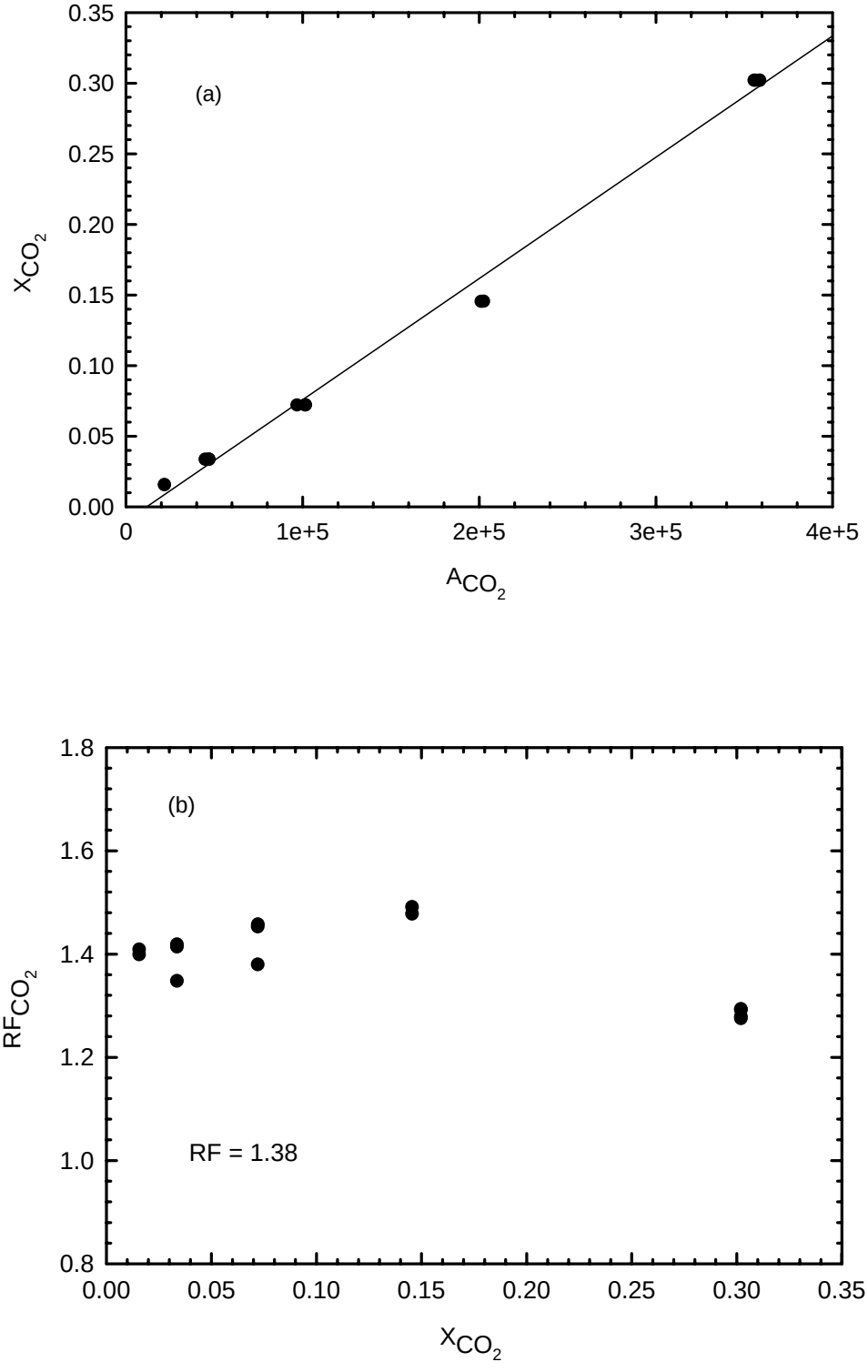

Figure 4.3. Calibration plot for CO_2 in nitrogen (a) and the GC RF (b)

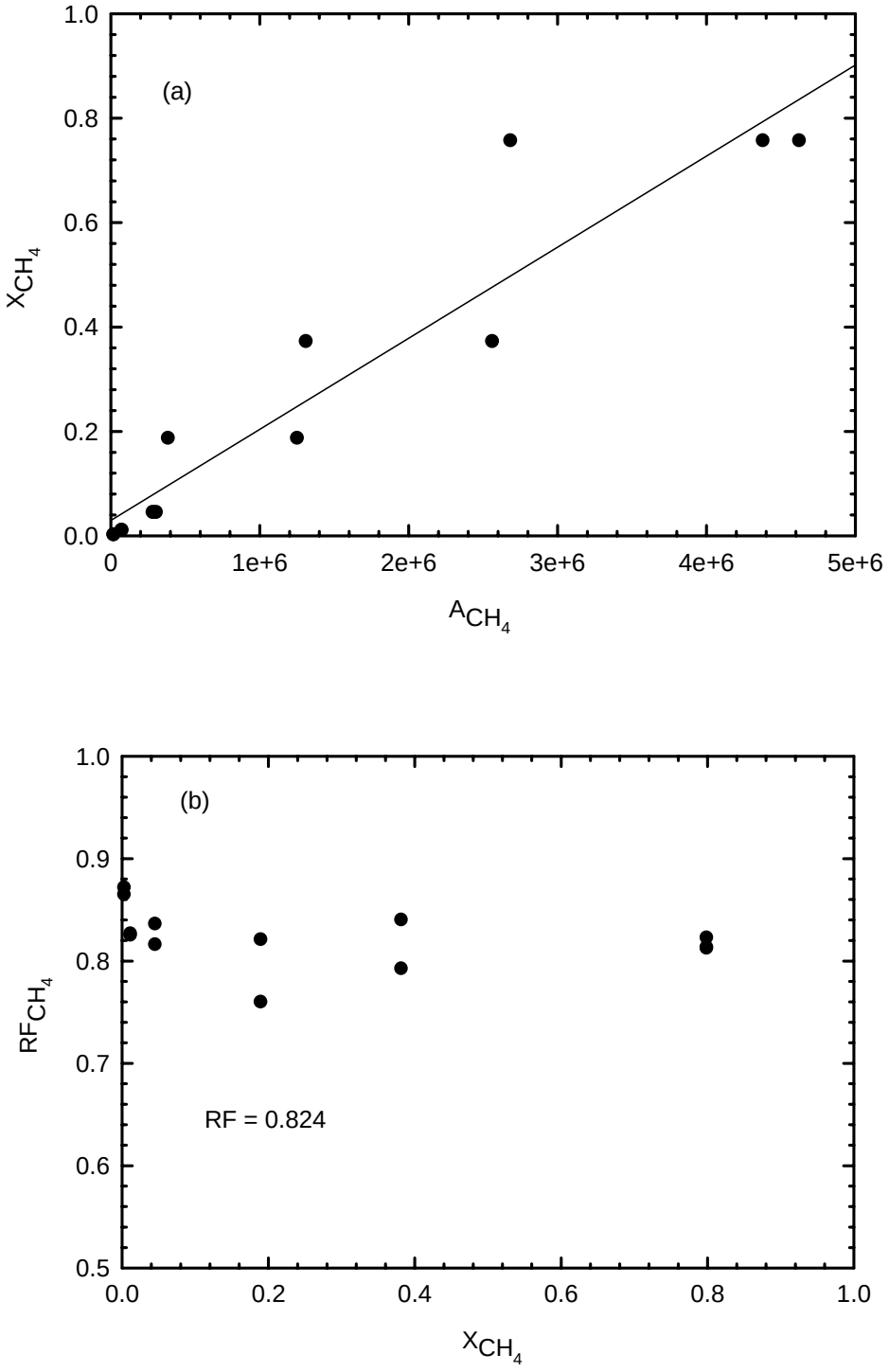

Figure 4.4. Calibration plot for CH_4 in nitrogen (a) and the GC RF (b)

Assuming CO_2 concentration in the air to be negligible, methane conversion can be calculated using only the outlet concentrations as:

$$CH_4\ conversion = \frac{X_{CO_2(out)}}{X_{CO_2(out)} + X_{CH_4(out)}} \tag{4.3}$$

Combining Equations 4.3 and 4.1, the methane conversion is given by:

$$CH_4\ conversion = \frac{A_{CO_2}/RF_{CO_2}}{A_{CO_2}/RF_{CO_2} + A_{CH_4}/RF_{CH_4}} \tag{4.4}$$

where all the areas refer to the areas in the product (exhaust) stream. Note, the methane fractional conversion can be calculated from the analysis of the exhaust stream; the composition of the feed does not have to be known.

4.2.4 Liquid and vapor components addition

The effluent of natural gas dehydrator contains excess water, BTEX and also hydrocarbons with high number of carbons. The amount of both methane and water according to the effluent composition (Table 2.2) is 40 vol%. The remaining 20 vol% comprise the BTEX and other hydrocarbons. In a series of experiments the effect of addition of water on the radiant heater performance was investigated. Instead of feeding the exact effluent, C_5 and C_7 were selected as representatives of the non-aromatic hydrocarbons and BTEX substances, and fed to the radiant heater. In the experiments related to addition of liquid water to the system, a water pump from LabAlliance was used in which the desired flow of water is selected and continuously fed to the system. A syringe pump from ISCO 500D model was used for delivering the C_5 and C_7 to the radiant heater. Water

and mixture of two hydrocarbons travelled through separate lines and were introduced to the heater from the back side to the heater. A cross sectional view of the system is shown in Figure 4.5.

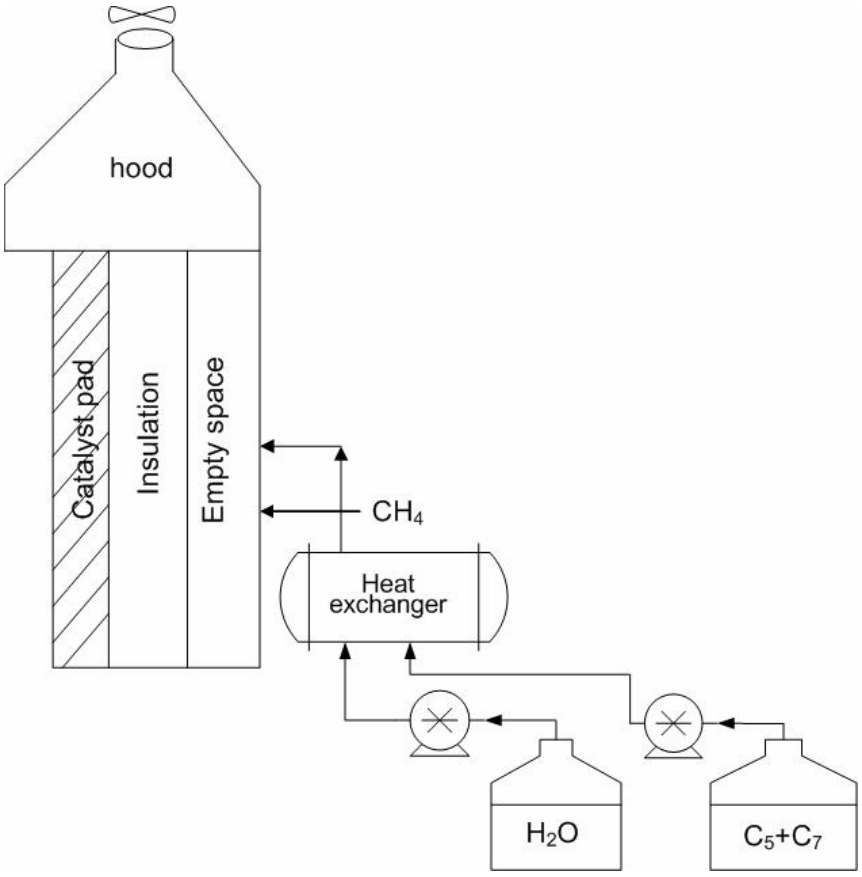

Figure 4.5. Cross sectional view of the counter-diffusive radiant heater

For experiments with addition of steam, and C_5 and C_7 vapor, the water, C_5 and/or C_7 were vaporized in a shell and tube heat exchanger prior to being introduced into the reactor. The heat exchanger used hot oil as the heat transfer fluid, which was heated in an oil bath. The bath temperature was set to 150^{o}C. The temperature of the catalyst pad and back space was monitored using type J thermocouples. Labview software package was used for data acquisition.

4.2.5 Methane conversion in presence of C_5 and C_7

Methane is known to be the most difficult hydrocarbon to oxidize. When C_5 and C_7 are injected into the radiant heater, it is expected that these hydrocarbons are primarily oxidized before methane combustion is initiated. To evaluate the methane conversion, it is assumed that complete combustion of C_5 and C_7 takes place. The ratio of molar flow rates of C_5 and C_7 in the feed is:

$$X_5 = \frac{N_{C_5(in)}}{N_{CH_4(in)}} \tag{4.5}$$

$$X_7 = \frac{N_{C_7(in)}}{N_{CH_4(in)}} \tag{4.6}$$

where $N_{C5(in)}$, $N_{C7(in)}$ and $N_{CH4(in)}$ represent the molar flow rates of C_5, C_7 and CH_4 at the inlet. The total carbon molar flow rate at the inlet would be:

$$N_c = N_{CH_4(in)}(1 + 5X_5 + 7X_7) \tag{4.7}$$

where N_c represent the total carbon molar flow rate at the heater inlet. Based on the dilution factor, $N_{CH4(in)}$ is not known at the heater inlet, however, $N_{CH4(out)}$ and $N_{CO2\,(out)}$ are known. The total carbon balance can be written as:

$$N_{CH_4(out)} + N_{CO_2(out)} = N_{CH_4(in)}(1 + 5X_5 + 7X_7) \tag{4.8}$$

or

$$N_{CH_4(in)} = \frac{N_{CH_4(out)} + N_{CO_2(out)}}{1 + 5X_5 + 7X_7} \tag{4.9}$$

the overall methane conversion equation is:

$$CH_4\ conversion = \frac{N_{CH_4(in)} - N_{CH_4(out)}}{N_{CH_4(in)}} \tag{4.10}$$

substituting the $N_{CH4(in)}$ from Equation 4.9 in 4.10 and multiplying by $(1+5X_5+7X_7)$ yields:

$$CH_4\ conversion = \frac{N_{CO_2(out)} - (5X_5+7X_7)N_{CH_4(out)}}{N_{CH_4(out)} + N_{CO_2(out)}} \tag{4.11}$$

This Equation reduces to Equation 4.3 when no C_5 or C_7 is present in the feed.

4.3 Results and discussion

4.3.1 Temperature distribution at different methane flow rates

To understand the fundamental phenomena involved in radiant heaters, some basic information is needed about its operation. In the first step, catalytic combustion of methane at different methane flow rates was studied. Temperature was monitored at four locations, which are shown in Figure 4.6. T_1, T_2 and T_3 represent the temperatures at three locations at 5 mm depth inside the catalyst pad, while T_4 is the temperature in the back space filled with fuel.

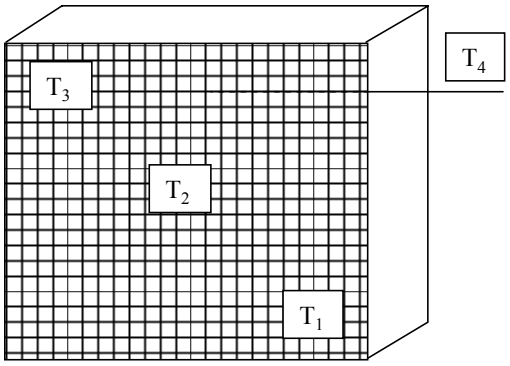

Figure 4.6. Location of thermocouples in the radiant heater

Figure 4.7-4.11 show the temperature at these locations at different methane flow rates. To check for the reproducibility of the results, the radiant heater operation was repeated regularly at each fuel flow rate. The two plots in Fig. 4.8 represent the temperature distribution from the radiant heater, operated on two different days. The temperature distributions across the catalyst pad were very similar indicating the high reproducibility of the experimental results.

It is observed from Figure 4.7 and 4.8 that the temperature is highest at the lower corner of the catalyst pad (T_1). It was initially hypothesized that the temperature distribution observed might result from variations in catalyst activity within the pad, or to the location of the feed pipe. The temperature distribution was subsequently measured at three different pad orientations.

In each new test, the heater was rotated 90 degrees to account for the effects of non-uniform catalyst distribution or feed point. The same temperature distribution was observed in all the different pad orientations indicating that the temperature distribution is related to the boundary layer development in front of the pad and mass transfer limitation of oxygen transport. At methane flow rate of 0.89 g/min, T_1 starts to decline after ignition, and at the same time T_2 and T_3 increase. At low methane flow rate, it seems that there is no combustion at the lower part of the pad; therefore more oxygen is available at the upper parts of the pad. When methane flow rate is decreased to 0.36 g/min, the heater could not be ignited. At around 75 min, the electrical heater was plugged in again to try to re-ignite the heater; however, there is no combustion taking place at this low fuel flow rate.

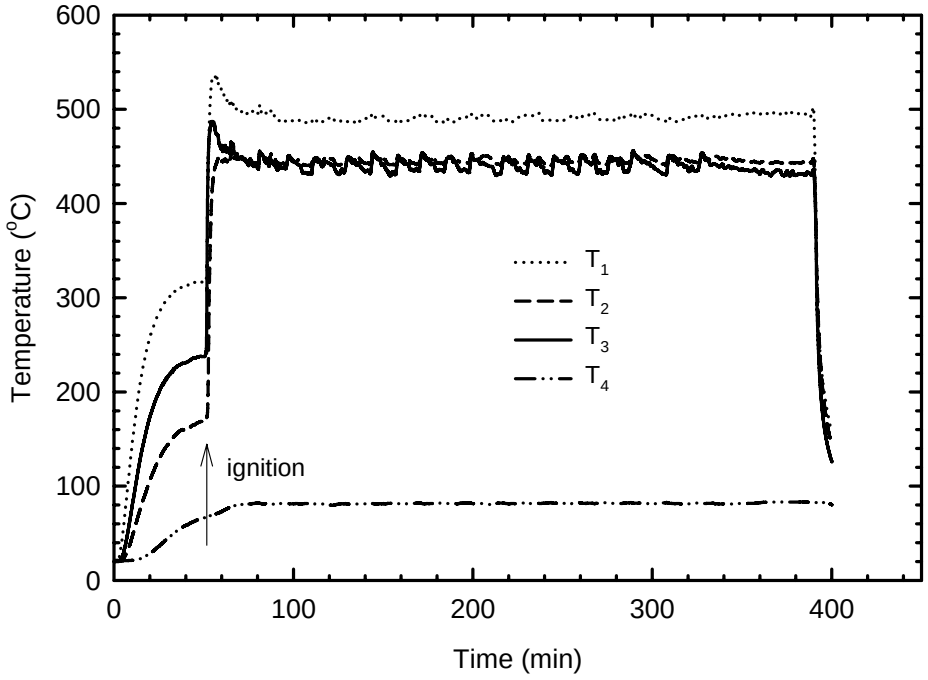

Figure 4.7. Temperature distribution at methane flow rate of 2.15 g/min

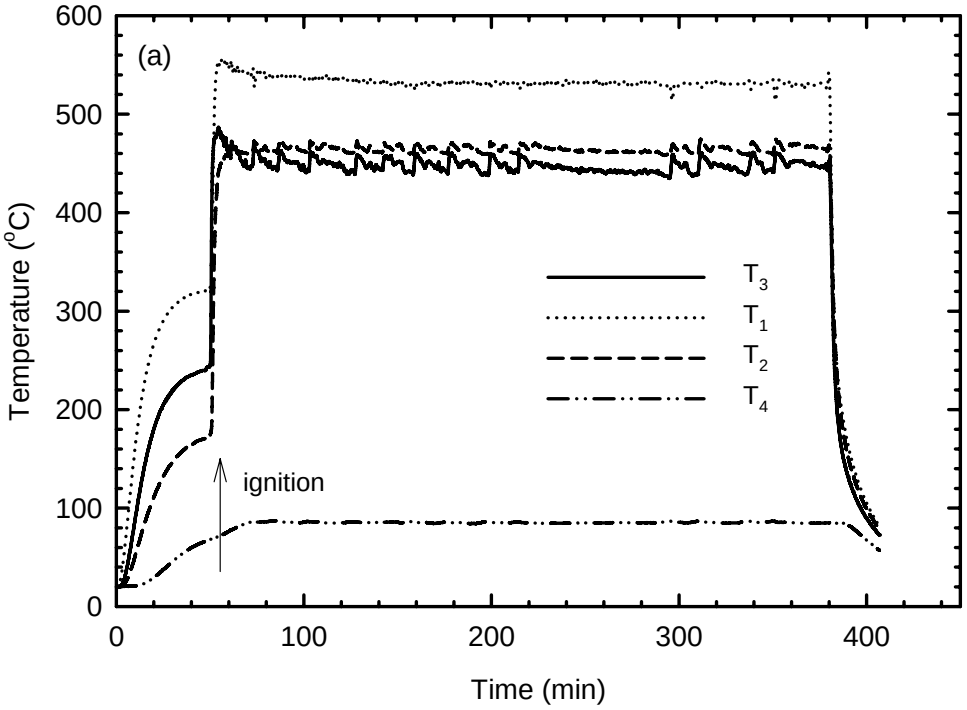

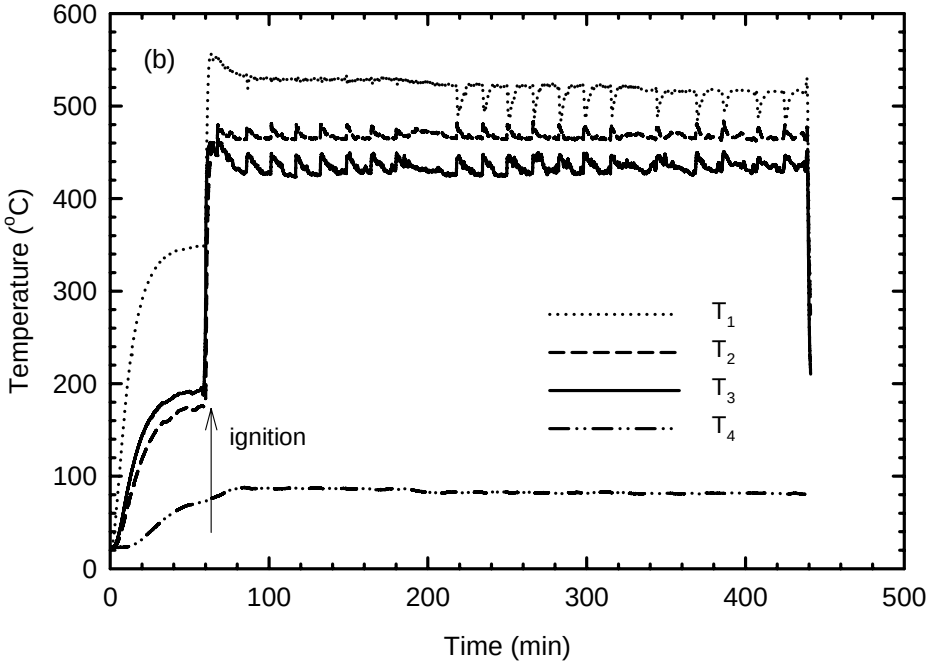

Figure 4.8. Temperature distribution at methane flow rate of 1.79 g/min on two different days

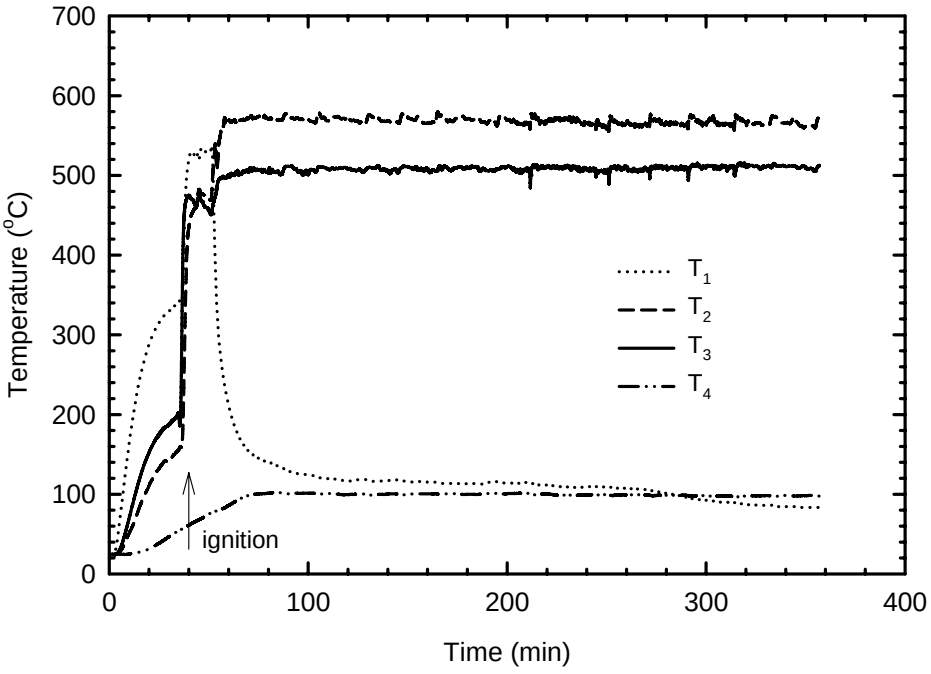

Figure 4.9. Temperature distribution at methane flow rate of 0.89 g/min

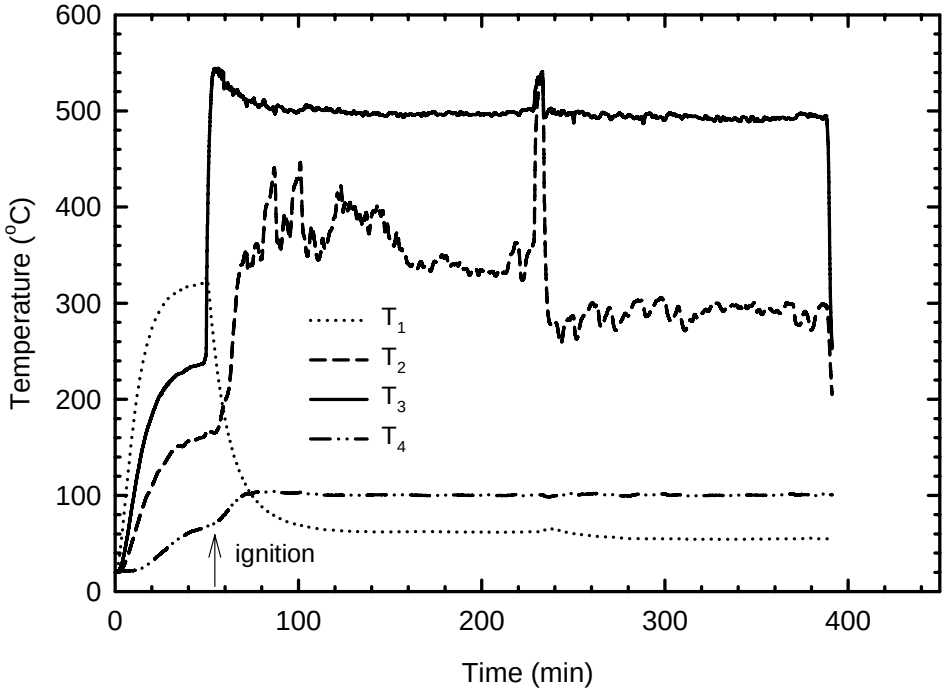

Figure 4.10. Temperature distribution at methane flow rate of 0.71 g/min

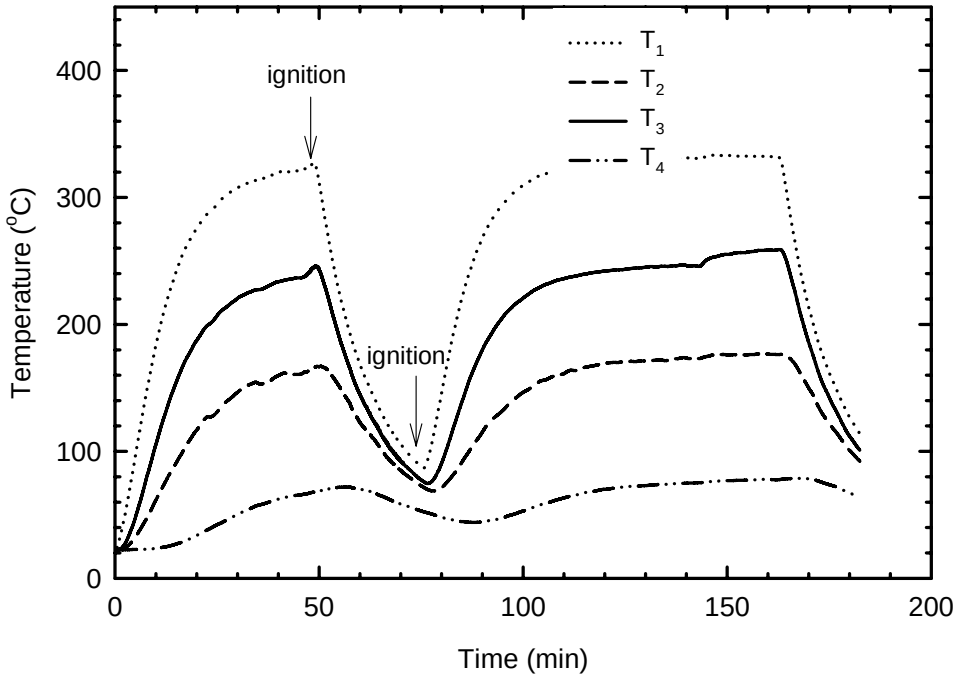

Figure 4.11. Temperature distribution at methane flow rate of 0.36 g/min

The flow rate of methane was changed during one experimental run and the results are shown in Figure 4.12. These runs also allow for the reproducibility check of previous experiments at each flow rate. It can be seen that, T_1 decreases by raising the flow rate from 1.79 g/min to 2.5 g/min. At high flow rates, methane pushes away the oxygen in front of the pad and prevents it from diffusing into the pad. This effect is less pronounced in the top parts of the pad. It seems that there is an optimum methane flow rate for radiant heater operation. This result was also observed in a previous study (Trimm, Lam 1980b).

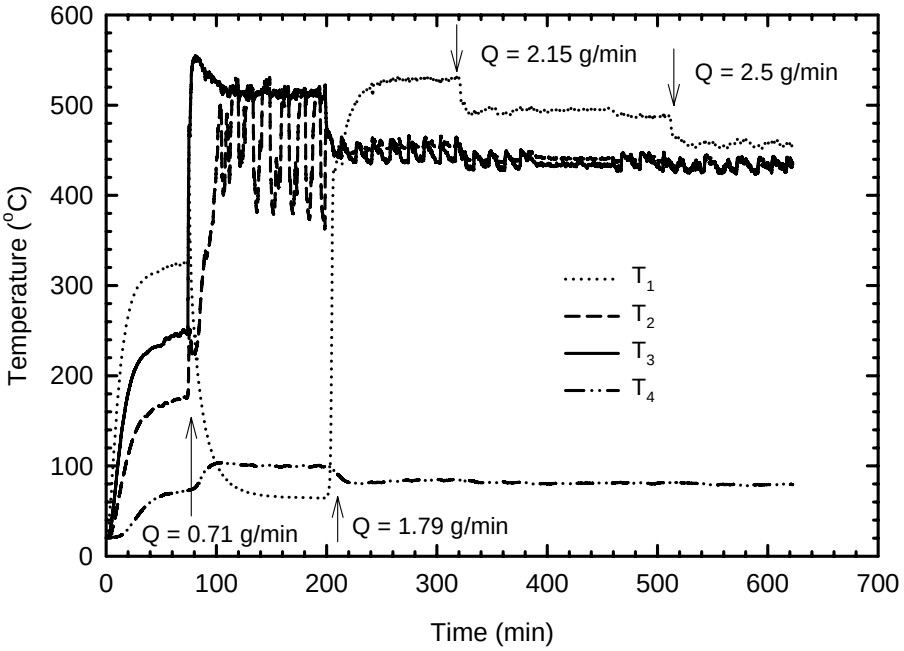

Figure 4.12. Temperature distribution at varying methane flow rates

4.3.2 Methane conversion at different flow rates

Methane fractional conversion indicates the radiant heater efficiency for methane combustion. The radiant heater was operated at several flow rates.

Methane conversion was calculated at each flow rates, using Equation 4.4 and the results are shown in Figure 4.13. It is seen that, by increasing the flow rate, methane conversion decreased, i.e. higher concentrations of methane were detected at the exhaust gas. This decreasing trend in methane conversion could be an indication of O_2 diffusion limitation through the boundary layer developed in front of the catalyst pad. The amount of methane combusted shows gradual rising trend in spite of decrease in conversion until it reaches a plateau.

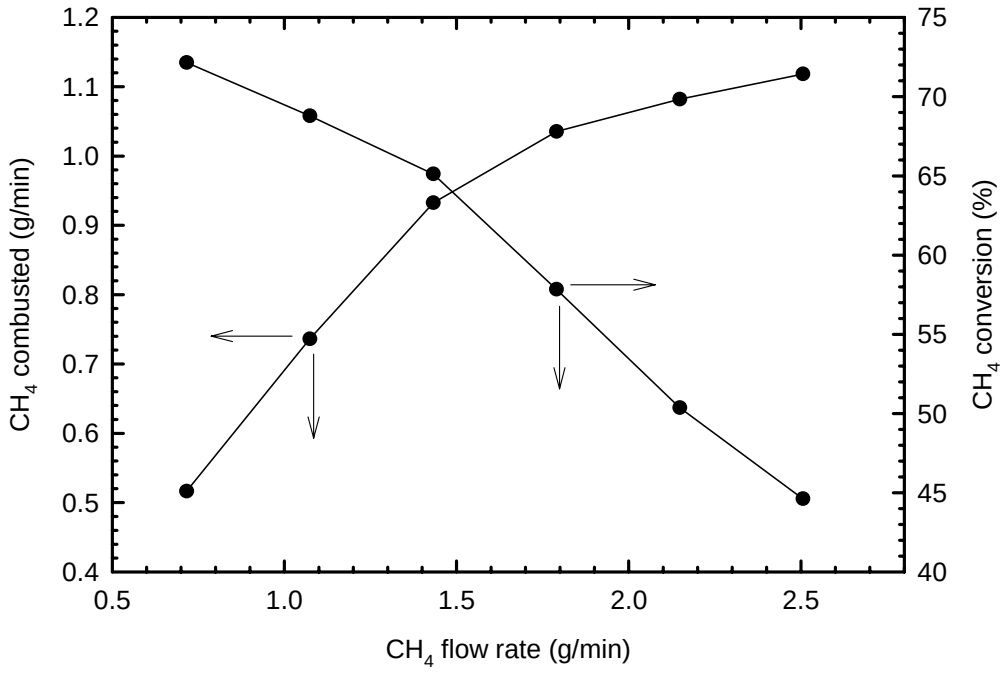

Figure 4.13. Methane conversion and O_2 consumption at different feed rates

4.3.3 Combustion of methane and C_5 with constant O_2 demand

In a series of experiments, different flow rates of methane and C_5 was added to the radiant heater, keeping the mixture O_2 demand, for complete conversion of hydrocarbons, constant. The amount of O_2 consumed at different combinations of methane and C_5 flow rates is shown in Figure 4.14.

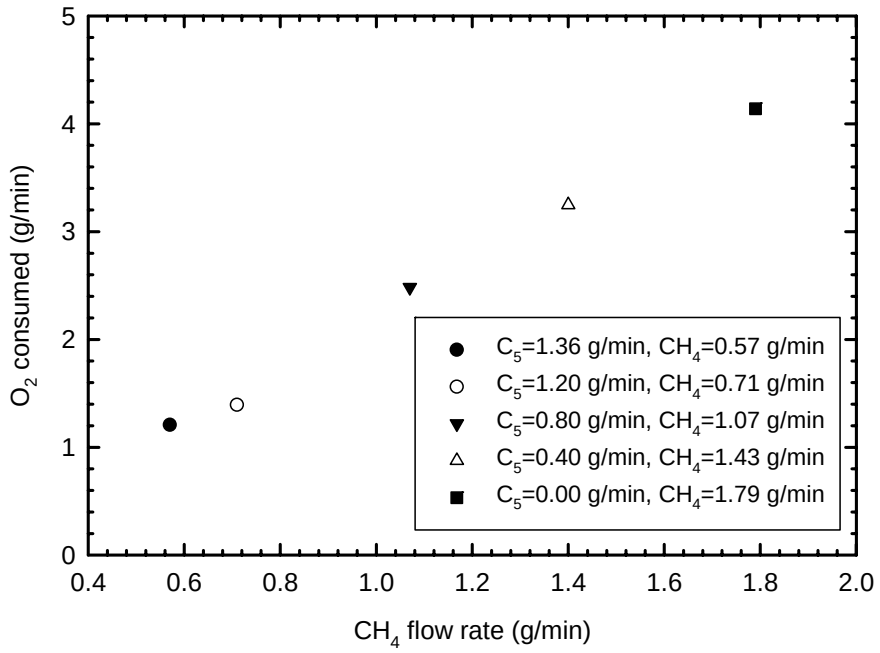

Figure 4.14. Oxygen consumption during methane and C_5 combustion with constant oxygen demand

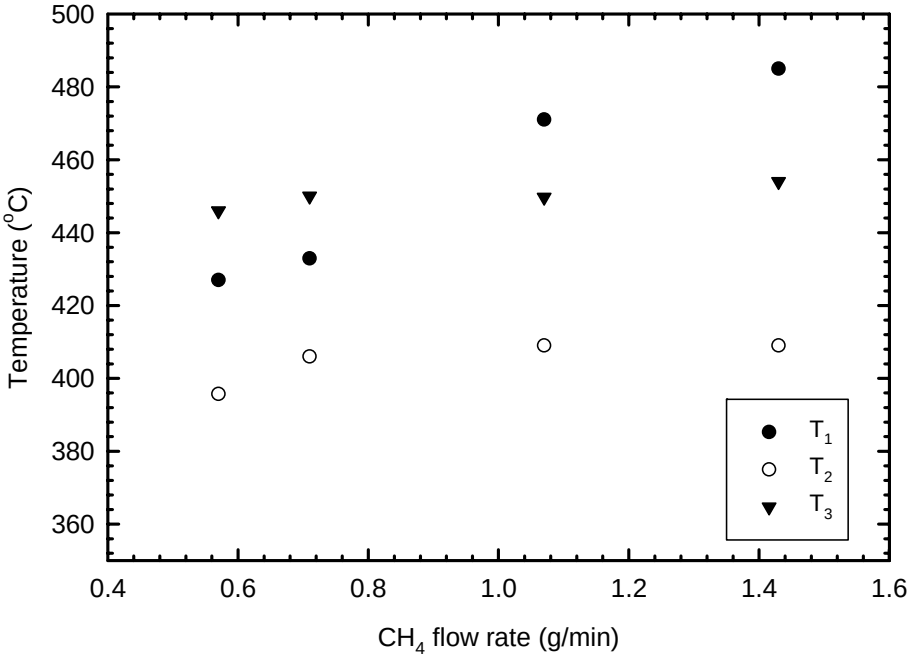

Figure 4.15. Temperature profile during methane and C_5 combustion with constant oxygen demand

It is seen that, O_2 consumption did not remain constant and it increased with higher methane and lower C_5 flow rates. These results are consistent with the results of methane conversion and the amount of methane combusted in Figure 4.13. It seems that high methane flow rate induces the convective air flow in the boundary layer leading to higher O_2 availability for combustion. Comparing the temperatures after addition of C_5 shows rising trend with increasing methane flow rate (Figure 4.15), which supports the effect of larger convective air flux at high methane flow rate and more O_2 availability for combustion resulting in higher pad temperatures.

4.3.4 Effect of oxygen diffusion on methane conversion

4.3.4.1 Effect of fan on methane conversion

It is recognized that the diffusion of oxygen in the pad could be the limiting step in catalytic combustion since the heat of reaction accelerates the rate, leading to high temperature on the catalyst surface and mass transfer limitation (Ryoo et al. 2003, Kolaczkowski 1999). However, it is equally possible that the mass transfer through the boundary layer is the rate limiting step. To examine the role of external mass transfer of oxygen on the observed behavior, a fan was installed on top of the hood to induce the forced convection in front of the catalyst pad. Methane conversion at different flow rates and fan speed are shown in Figure 4.16-4.18. It is evident from Figure 4.16 that, the methane conversion did not improve at low fan speed (5 V). However at high speed, complete methane conversion was achieved. It seems that there is a critical speed that is required for complete methane conversion.

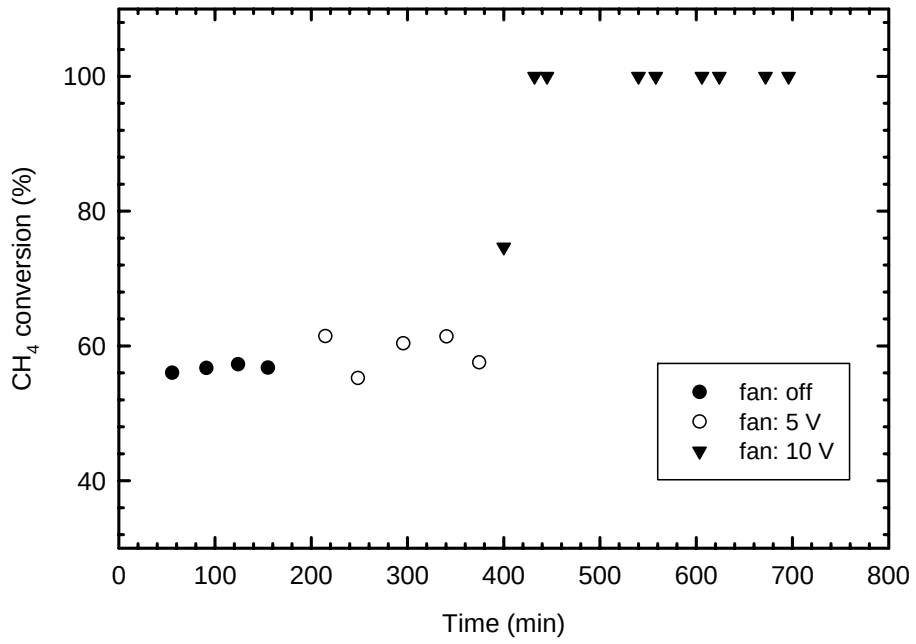

Figure 4.16. Effect of oxygen supply on conversion of 1.79 g/min methane

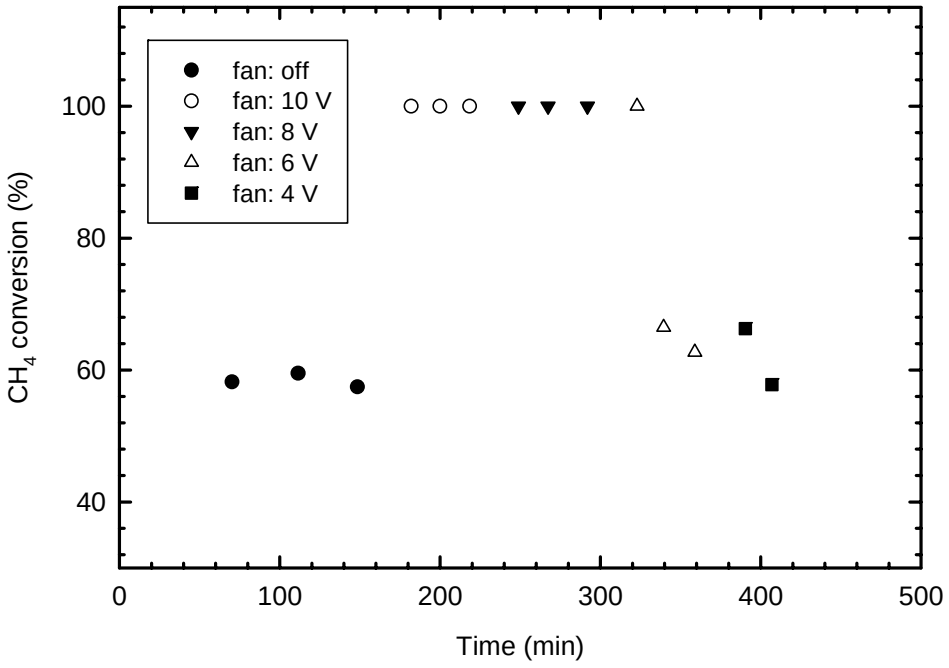

Figure 4.17. Effect of oxygen supply on conversion of 1.43 g/min methane

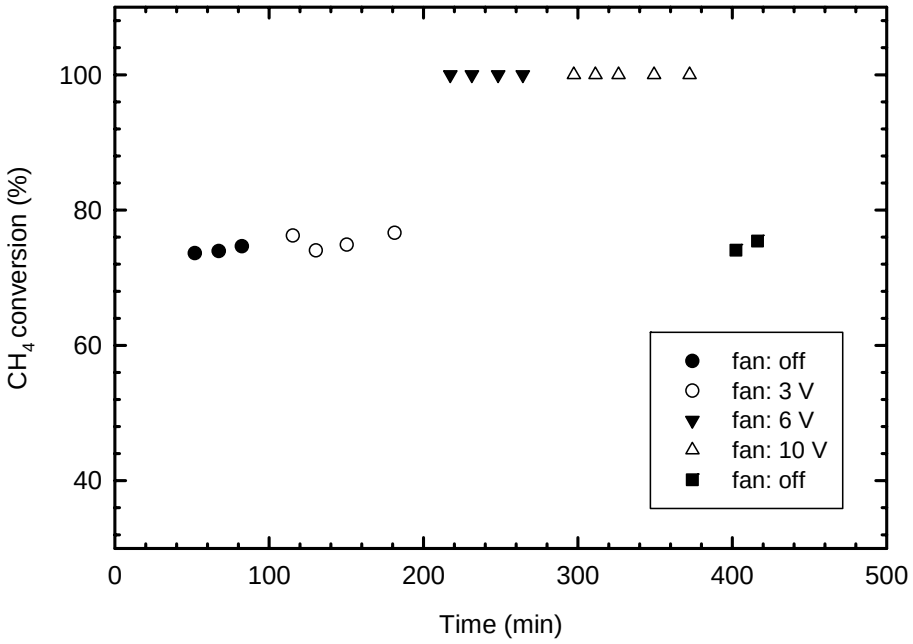

Figure 4.18. Effect of oxygen supply on conversion of 0.71 g/min methane

In fact, at higher methane flow rate, oxygen demand for combustion is greater and with lower fan speed, complete methane conversion cannot be observed. These results indicate that oxygen diffusion is likely to be the controlling step in methane conversion. Monitoring the temperature revealed that there was no change in temperature distribution across the pad while the fan was on.

The effect of presence of fan can be observed from the GC peak areas for CH_4 and CO_2. Operating the fan leads to dilution of the combustion products and smaller peak area reading from GC. The peak areas and concentrations of CH_4 and CO_2 corresponding to Fig. 4.18 is shown in Table 4.1. By increasing the fan speed, peak areas and concentrations of CH_4 and CO_2 are decreasing.

Table 4.1. Effect of fan operation on GC peak area and concentration of CH_4 and CO_2

Fan status	CH_4 peak area	CO_2 peak area	CH_4 concentration	CO_2 concentration
fan: off	12913	60385	0.909	1.353
	12753	60637	0.904	1.359
	12061	59487	0.881	1.332
fan: 3 V	7378	39617	0.731	0.862
	6847	32706	0.714	0.698
	7520	37560	0.736	0.813
	6742	37056	0.711	0.801
fan: 6 V	0	3086	0.495	0.000
	0	2664	0.495	0.000
	0	3101	0.495	0.000
	0	2439	0.495	0.000
fan: 10 V	0	2960	0.495	0.000
	0	2594	0.495	0.000
	0	2625	0.495	0.000
	0	2564	0.495	0.000
	0	2760	0.495	0.000
fan: off	12798	61250	0.905	1.374
	12713	65385	0.902	1.472

4.3.4.2 Effect of metal plate on methane conversion

One way of improving the combustion is to place a metal plate at a close distance from the catalyst pad. Using the metal sheet induce the convective air flux between two surface leading to more oxygen availability for combustion. It was found that after placing the metal plate at 8 cm and 2 cm distance from the pad, all the temperatures increased; however, only a samll increase in methane

conversion was observed. The temperature distribution and methane conversion are shown in Figure 4.19 and 4.20, respectively. In fact, the thermal energy is transferred to the plate by radiation and it radiates the energy back to the pad. This leads to increase in pad temperature that could causes the rapid circulation of air in front of the heater.

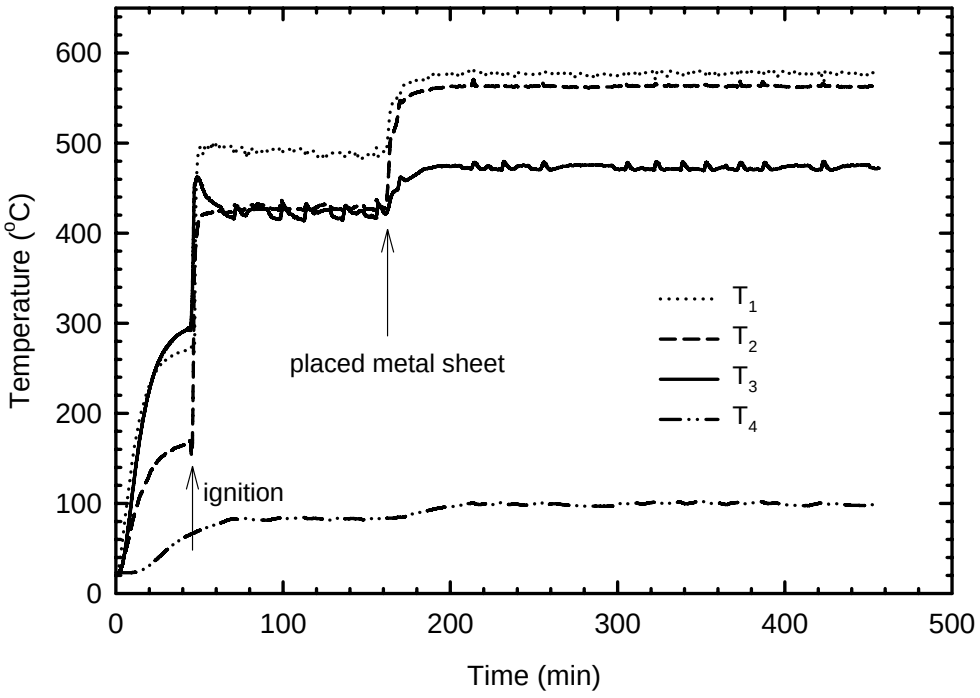

Figure 4.19. Effect of presence of metal sheet at 2 cm distance from the catalyst pad on temperature distribution at methane flow rate of 1.79 g/min

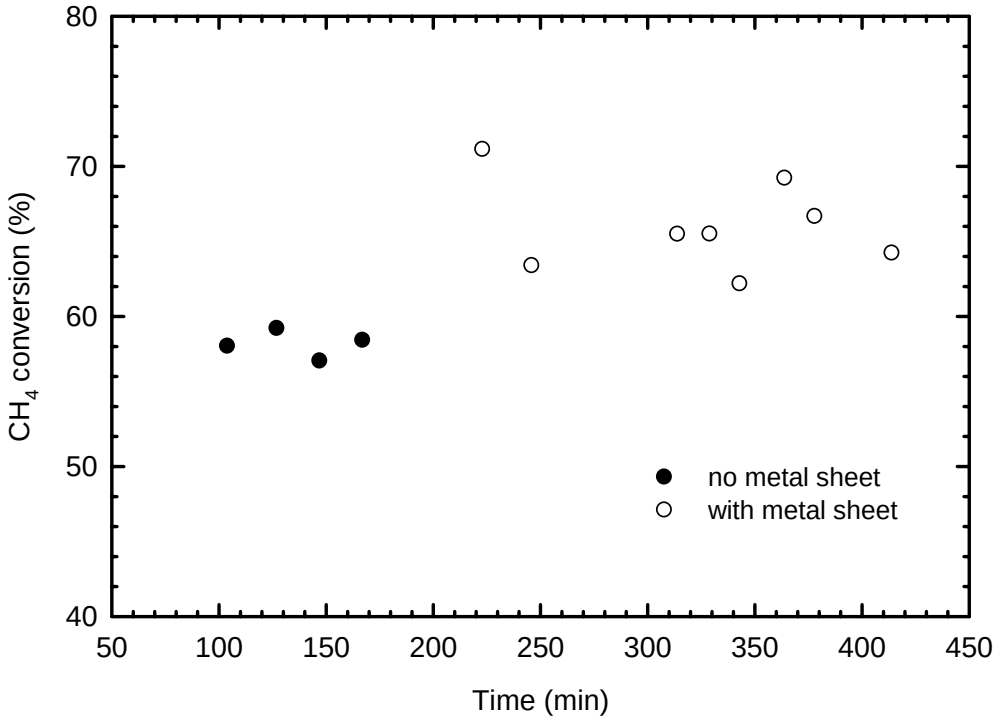

Figure 4.20. Effect of presence of metal sheet at 2 cm distance from the catalyst pad on conversion of 1.79 g/min methane

4.3.5 Effect of a thinner fiber cloth on methane conversion

There was a fiber cloth in front of the catalyst pad to protect the active catalytic material. The presence of this cloth could have negative impact on the oxygen diffusion into the pad and consequently reduce the methane conversion. The old fiber cloth was removed and a new, thinner cloth was placed on the pad surface. The methane conversion is shown in Figure 4.21. Comparing these results with the conversion data in the unit with thicker cloth (Figure 4.13) reveals no significant improvement on methane conversion by covering the catalyst pad with a thinner cloth. Therefore, it would appear that no limitation is imposed by diffusion of O_2 into the pad.

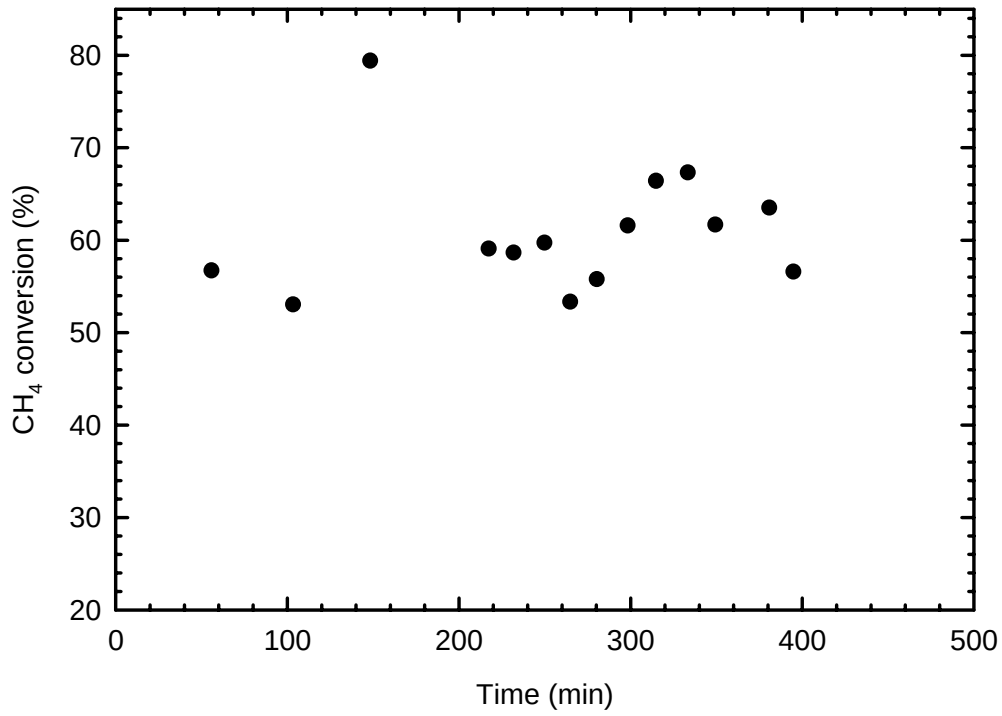

Figure 4.21. Conversion of 1.79 g/min methane with a thin fiber cloth

4.3.6 Effect of removing the fiber cloth on methane conversion

To rule out any effect induced by the fiber cloth on methane conversion, the fiber cloth was completely removed from the unit. Conversion of methane in the unit without fiber cloth is shown in Figure 4.22. Comparing Figure 4.22 and 4.13 reveals that there is no significant change in methane conversion after removing the cloth. Therefore, it is concluded that the fiber cloth is not acting as a barrier for oxygen diffusion into the catalyst pad.

Note that in both Figure 4.21 and 4.22, there is one data point showing high conversion at 148 min and 128 min, respectively. The common feature of these two points is that the samples at these two points were taken after a relatively long time passed from taking the previous sample. To confirm this fact,

an experiment was conducted in which a few exhaust gas injections were made without any delay between two injections.

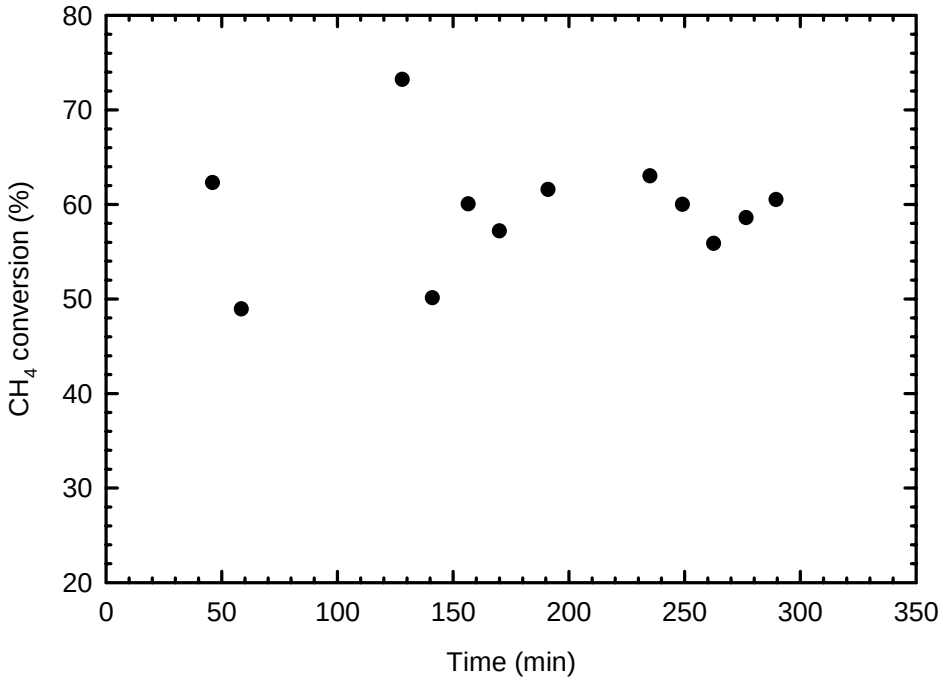

Figure 4.22. Conversion of 1.79 g/min methane with fiber cloth removed

Then next few injections were 60 min apart. The results are shown in Figure 4.23. It is obvious that the conversion is higher when there is longer time gap between each sample injection into the GC. The possible reasons are the accumulation of H_2O either in the sampling line or in GC lines that leads to high reading for the CO_2 peak and higher conversion. To investigate this observation, after taking the sample and injection into the GC, the sampling tube was moved far from the radiant heater and its opening was blocked. When it was time for sample injection, the tube was placed on top of the hood for a few minutes and

then sample was injected. The results are shown in Figure 4.24. The same trend can be seen in both Figure 4.23 and 4.24. Therefore it is concluded that high conversion is not due to accumulation of H_2O in the sampling tube and high CO_2 reading is because of the accumulation of H_2O in the GC lines.

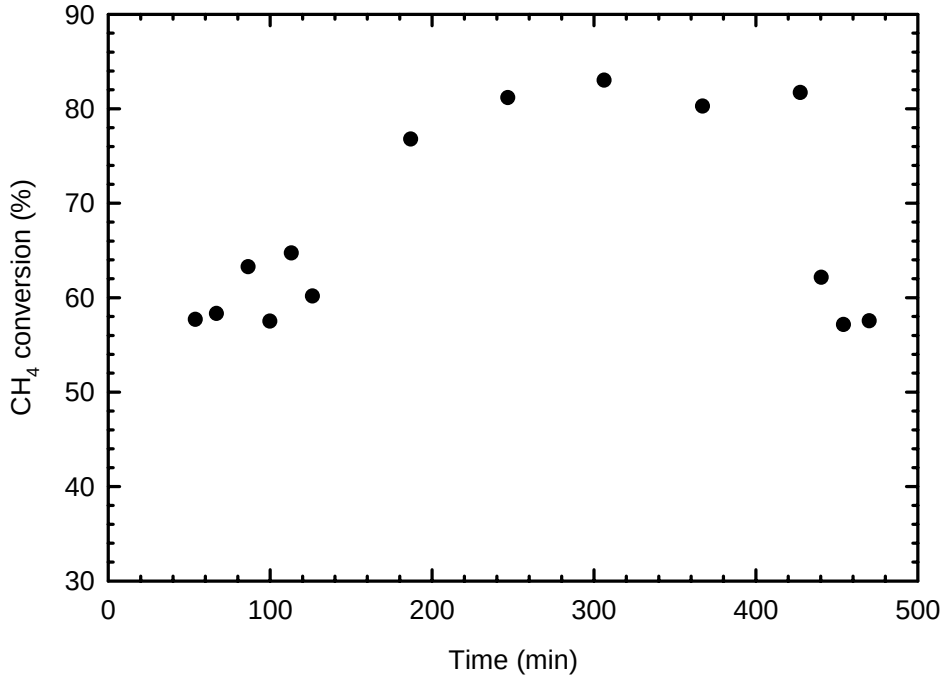

Figure 4.23. Conversion of 1.43 g/min methane with thin cloth with longer time delay between each sampling

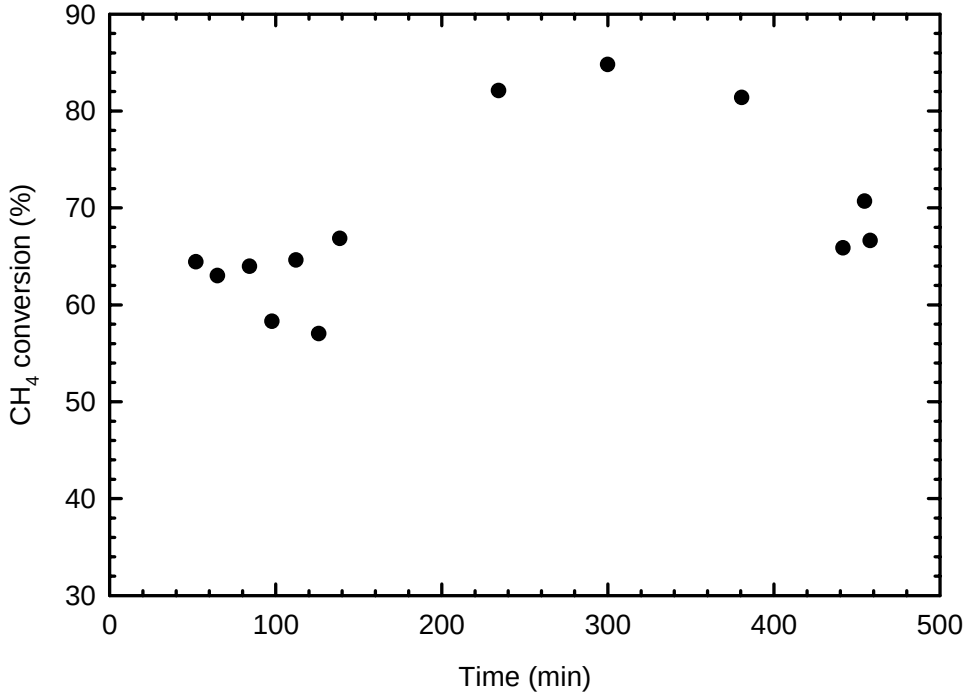

Figure 4.24. Conversion of 1.43 g/min methane with thin cloth and blockage of tube after sampling

Looking at the GC peaks revealed that, when longer time is allowed before taking the sample, the GC base line drifts and the slope is steadily rising before the CO_2 peak come out, therefore the integrated area for CO_2 peak is higher. The reason for the change in base line is the accumulation of the water in the GC column. Therefore the closer the sample injections, the more reliable the conversion data are.

4.3.7 Addition of liquid water to the radiant heater

One of the potential applications of radiant heaters is treatment of natural gas dehydration process effluent. This effluent contains almost 40 vol% water along with methane, BTEX and other VOC. In a series of experiments, liquid

water was added to the radiant heater feed. Based on the effluent composition that contain the same amount of water and methane, and considering 1.79 g/min CH_4 in the feed, the amount of liquid water to be introduced to the system was:

$$Q_{H_2O} = 2500 \frac{mL\ H_2O}{\text{min}} \times \frac{18\ g\ H_2O}{22400\ mL\ H_2O} \times \frac{1\ mL\ H_2O}{1\ g\ H_2O} = 2 \frac{mL\ H_2O}{\text{min}} \qquad (4.12)$$

Water was injected to the system starting from 0.2 g/min up to the maximum flow rate of 2 g/min, which is equivalent to 40 vol% of water. Temperature distribution and methane conversion are shown in Figure 4.25 and 4.26, respectively and the summary of methane conversion at different water flow rates is shown in Figure 4.27. In most of the runs the starting flow rate of water was 0.2 g/min that enables us to check for reproducibility of the results.

Plots of temperature distribution show that at low water flow rate, the temperature across the catalyst pad was not affected by the added water. However, by increasing water flow to 0.4 g/min and higher, T_1 is significantly affected. In fact, water was dripping down in the back of the heater, causing the cooling of the heater at the bottom. Lower part of the pad was damp at high water flow rates.

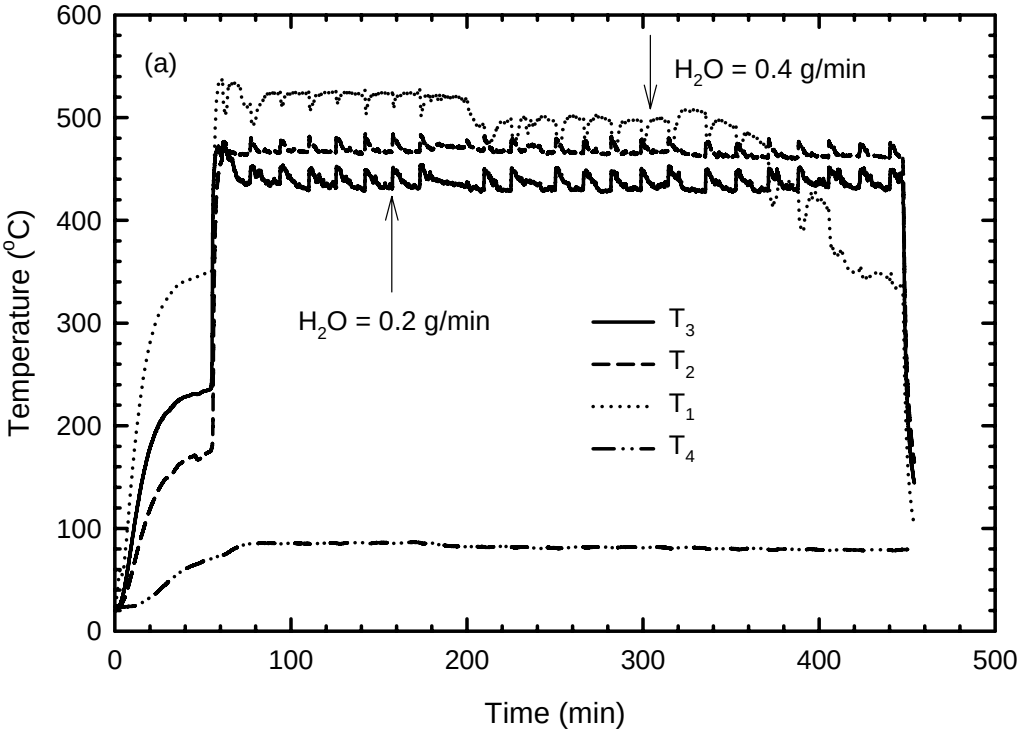
(a)
H2O = 0.4 g/min
H2O = 0.2 g/min
T3
T2
T1
T4
Temperature (°C)
Time (min)
0
100
200
300
400
500
600

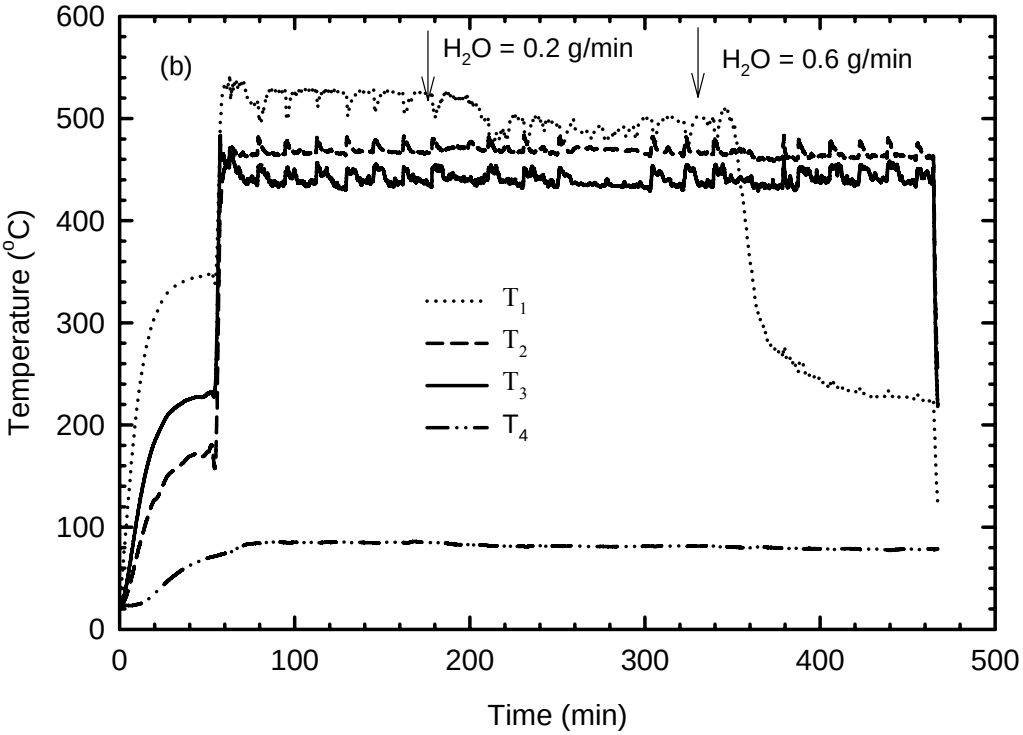
(b)
H2O = 0.2 g/min
H2O = 0.6 g/min
T1
T2
T3
T4
Temperature (°C)
Time (min)
0
100
200
300
400
500
600

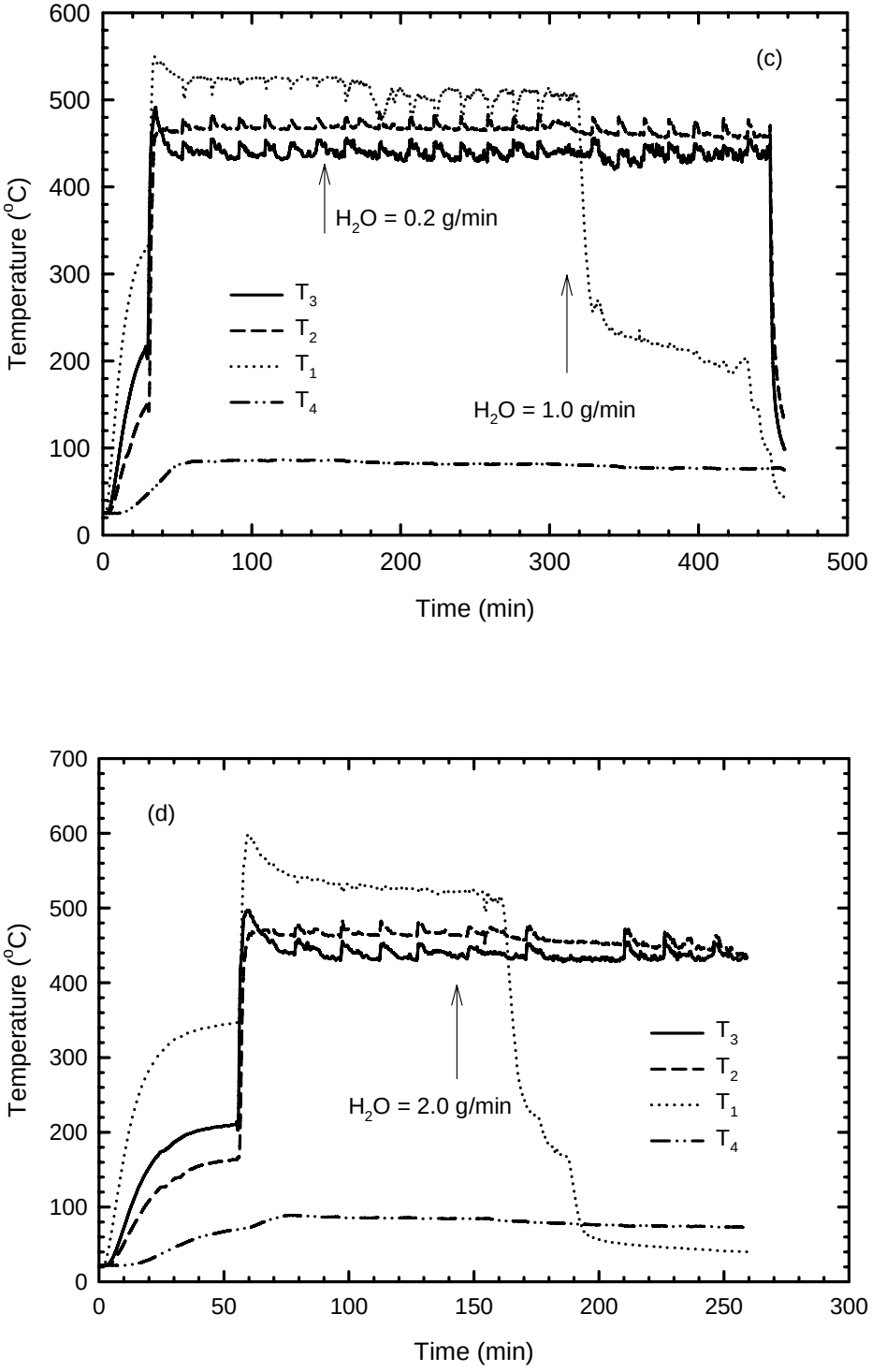

Figure 4.25. Temperature distribution in the radiant heater at methane flow rate of 1.79 g/min with addition of a) 0.2 and 0.4 g/min, b) 0.2 and 0.6 g/min, c) 0.2 and 1.0 g/min, and d) 2.0 g/min liquid water

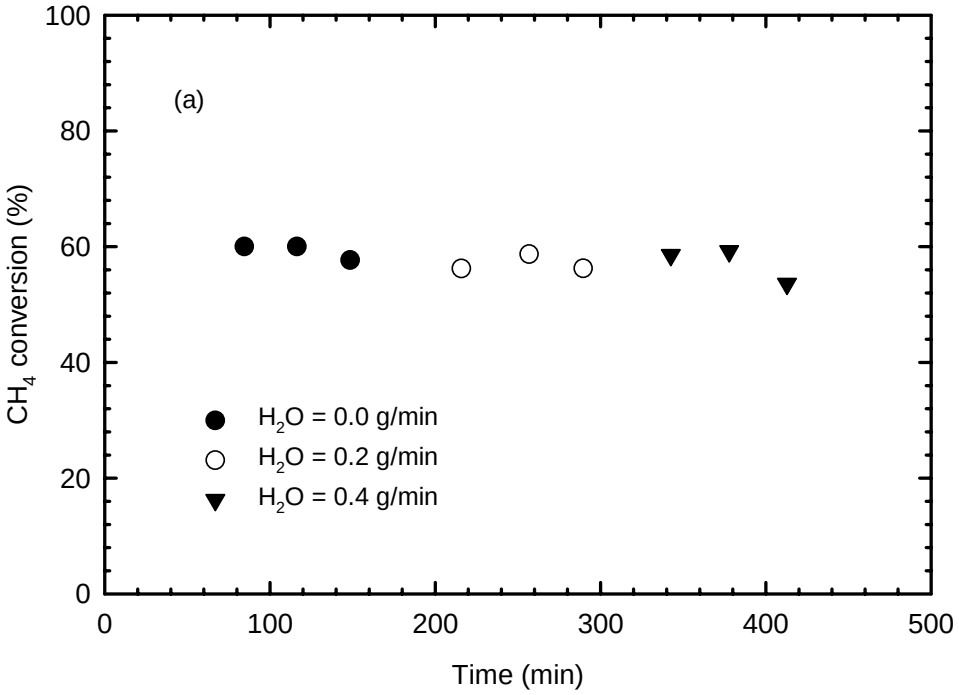
(a)
CH_4 conversion (%)
Time (min)
H_2O = 0.0 g/min
H_2O = 0.2 g/min
H_2O = 0.4 g/min
0
20
40
60
80
100
0
100
200
300
400
500

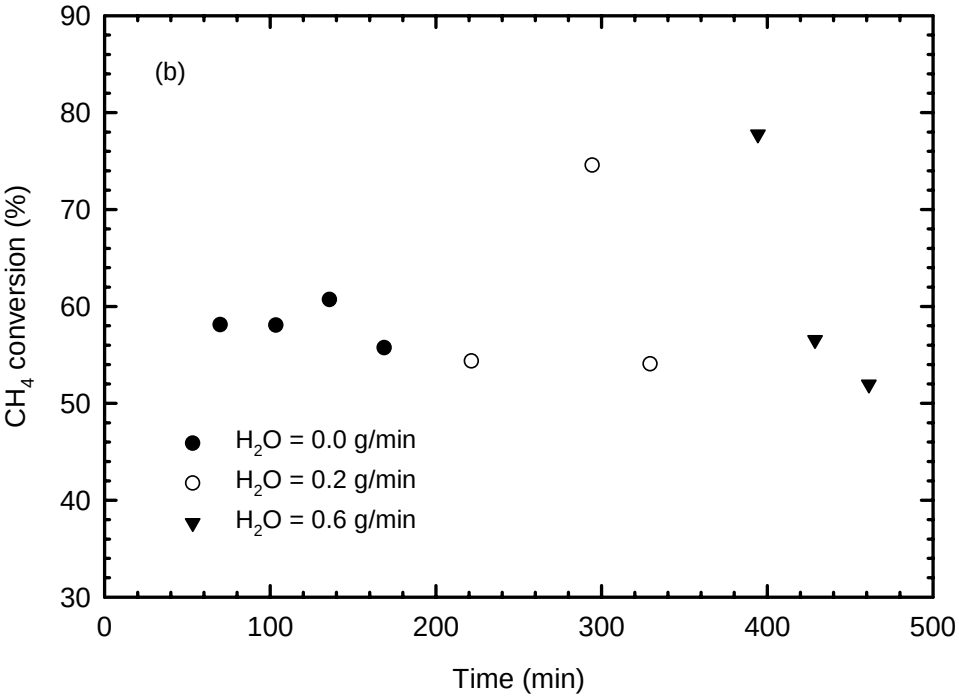
(b)
CH_4 conversion (%)
Time (min)
H_2O = 0.0 g/min
H_2O = 0.2 g/min
H_2O = 0.6 g/min
30
40
50
60
70
80
90
0
100
200
300
400
500

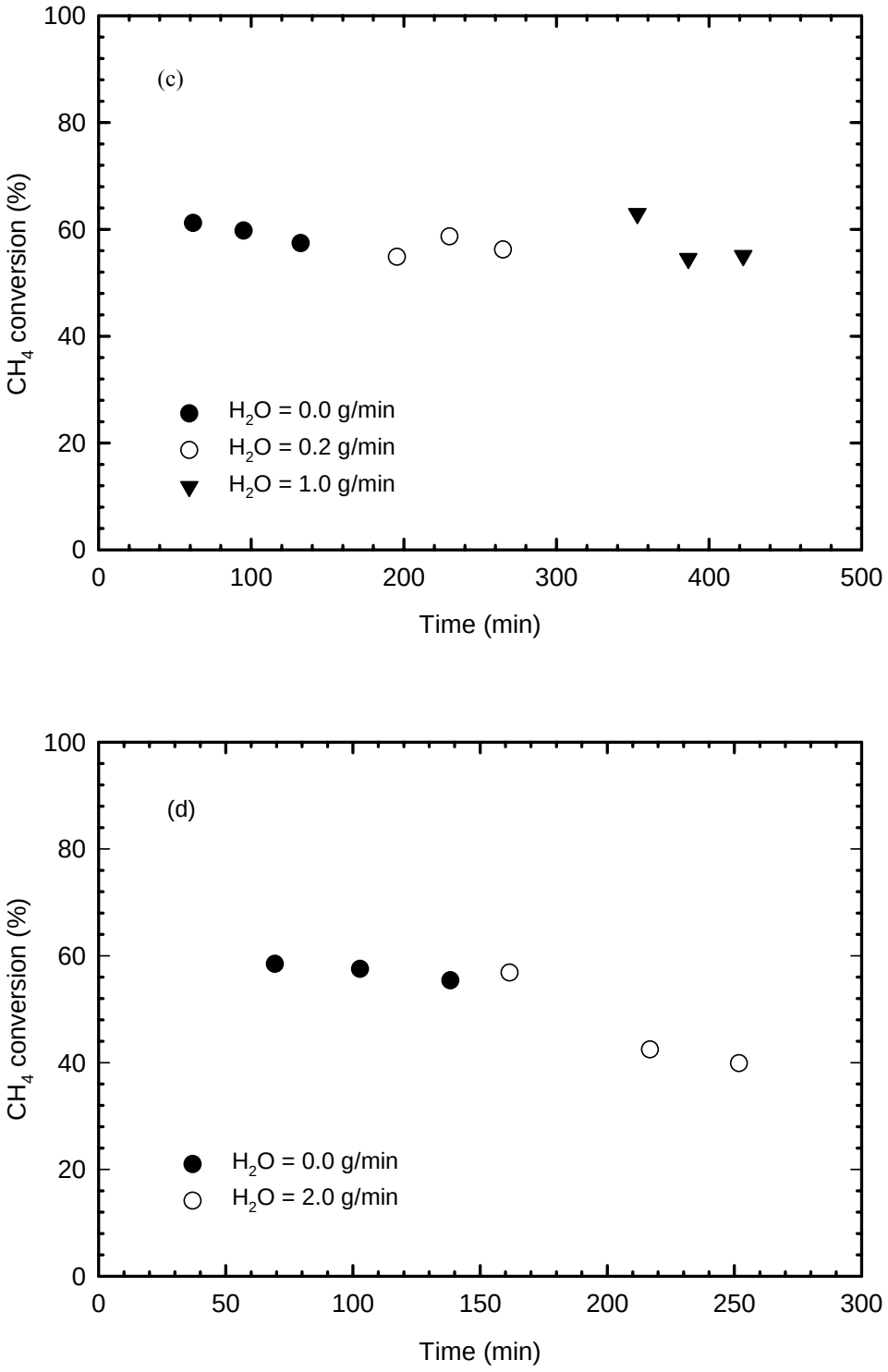

Figure 4.26. Conversion of 1.79 g/min methane with addition of a) 0.2 and 0.4 g/min, b) 0.2 and 0.6 g/min, c) 0.2 and 1.0 g/min, and d) 2.0 g/min liquid water

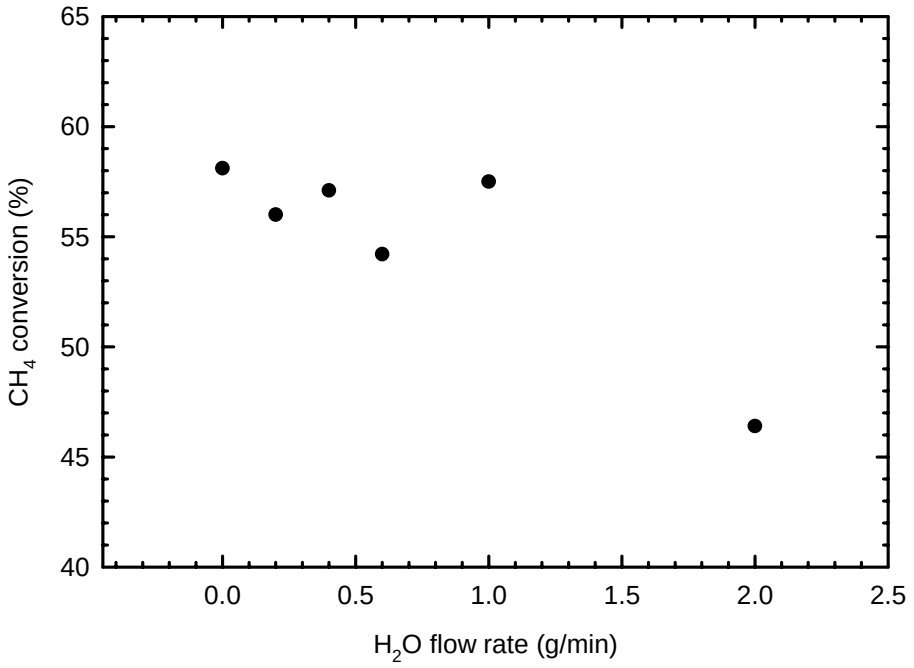

Figure 4.27. Conversion of 1.79 g/min methane in presence of different liquid water flow rates

Although presence of water in the system leads to considerable changes in the temperature distribution, it had no effect on methane conversion except at 2.0 g/min. In fact, at low water flows, the amount of water produced during the reaction was more than the added water, which does not influence the methane combustion, while high water flow results in wetting the catalyst pad, preventing the methane combustion. Based on the stoichiometry of the reaction, one mole of methane produces two moles of water in case of complete combustion. At 1.79 g/min methane, which is equivalent to 0.11 moles/min, conversion is about 57%, therefore the amount of water produced would be:

$$H_2O\ produced = 0.22\ \frac{moles}{min} \times 0.57 = 0.125\ \frac{moles}{min} \times \frac{18\ g}{1\ mole} = 2.26\ g/min \qquad (4.13)$$

which is still higher than the maximum amount of water added to the system (2 g/min). Therefore only large amounts of added water influence the radiant heater performance in terms of fuel combustion. Cullis and Willat (1984) also reported that the addition of water in comparable amount to that formed during methane combustion, has no effect on the catalyst activity (Cullis, Willatt 1984).

It is suspected that when the pad becomes wet, there is no combustion happening in that part of the pad and methane will come out at high concentrations. To verify that, the exhaust gas was sniffed from the wet part of the pad by placing the sampling tube in front of the pad in close distance. The GC peak area of methane was compared with that for dry pad without added water at the same location. Figure 4.28 shows the relative peak areas of methane. It was found that the methane peak area in case of wet pad was higher confirming the slippage of methane at wet parts of the pad.

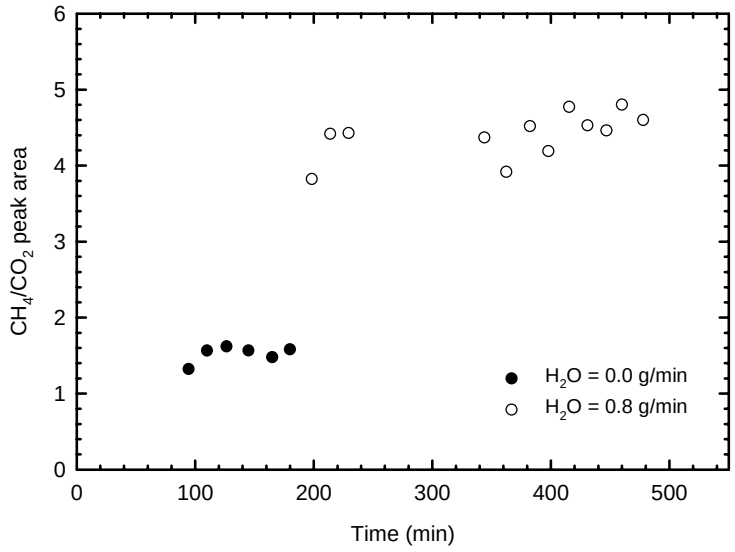

Figure 4.28. Comparison of methane peak area by sniffing from the lower right corner of the pad with and without added liquid water at methane flow of 0.71 g/min

4.3.8 Addition of liquid water, C_5 and C_7 to the radiant heater

Other than methane and water, all the other components in the natural gas dehydration effluent contribute to 20 vol% of the composition. To calculate the representative concentration of toluene, it was decided to include toluene, benzene, xylenes, methylcyclohexane and ethylbenzene in the calculation. The amount of toluene was calculated such that it would result in the concentration from all the included compounds:

$$C_7\ equivalent = \frac{0.762 \times M_1 + 0.541 \times M_2 + 0.435 \times M_3 + 0.399 \times M_4 + 0.197 \times M_5}{M_1} \quad (4.14)$$

where M_1, M_2, M_3, M_4 and M_5 represent, the molecular weight of toluene, benzene, xylenes, methylcyclohexane and ethylbenzene, respectively.

$$C_7\ equivalent = 2.35\ vol\% \quad (4.15)$$

for calculating the C_5 equivalent in the effluent, ethane, propane, butane, pentane and hexanes were included:

$$C_5\ equivalent = \frac{6.37 \times M_6 + 4.6 \times M_7 + 2.525 \times M_8 + 1.128 \times M_9 + 1.794 \times M_{10}}{M_9} \quad (4.16)$$

where M_6, M_7, M_8, M_9 and M_{10} represent, the molecular weight of ethane, propane, butane, pentane and hexanes, respectively.

$$C_5\ equivalent = 10.97\ vol\% \quad (4.17)$$

The numbers in the numerator are the amount of each component in the effluent in vol%. Noting that 1.79 g/min methane is equivalent to 2500 mL/min methane, the density of C_7 and C_5 are 0.865 and 0.626 g/mL, and the molecular weight of C_7 and C_5 are 92 and 72 g/mole, the flow rate of liquid C_7 and C_5 would be:

$$C_7 \ flow\ rate = 2.35\ vol\% \times \frac{2500\ mL/min}{40\ vol\%} \times \frac{1\ mole}{22400\ mL} \times \frac{92\ g}{1\ mole} \times \frac{1\ mL}{0.865\ g} \quad (4.18)$$

$$C_7 \ flow\ rate = 0.69\ mL/min$$

$$C_5 \ flow\ rate = 10.97\ vol\% \times \frac{2500\ mL/min}{40\ vol\%} \times \frac{1\ mole}{22400\ mL} \times \frac{72\ g}{1\ mole} \times \frac{1\ mL}{0.626\ g} \quad (4.19)$$

$$C_5 \ flow\ rate = 3.52\ mL/min$$

The total flow rate of C_5 and C_7 mixture into the radiant heater is:

$$C_5 + C_7 \ flow\ rate = 3.52 + 0.69 = 4.21\ mL/min \quad (4.20)$$

or

$$C_5 + C_7 \ flow\ rate = 0.6 + 2.2 = 2.8\ g/min \quad (4.21)$$

A mixture of C_5 and C_7 was fed to the radiant heater after it was ignited with methane and reached the steady state. Temperature distributions are shown in Figure 4.29. It is seen that by addition of C_5 and C_7 to the system, T_1 decreased which is similar to the behavior of the heater in case of liquid water addition. T_1 decreased sharply after C_5 and C_7 flow started, which is explained by extensive wetness of the lower corner of the catalyst pad. When the liquid hydrocarbon mixture flow stopped, T_1 started to recover.

It is of interest to study the effect of addition of both water and hydrocarbons to the radiant heater. Figure 4.30 and 4.31 show the temperature distribution and methane conversion in presence of water and hydrocarbons mixture in the radiant heater. The temperature of the lower corner, T_1, dropped rapidly when the water flow started and the lower corner of the pad became damp. Also the temperature in the middle of the pad, T_2, declined rapidly after the

hydrocarbon mixture flow started. In fact, the addition of higher quantities of liquid compounds to the reactor results in the temperature in the back of the reactor, T_4, falling below the boiling point of toluene. Increases in temperature at 380, 420 and 480 min occurred when the heavy hydrocarbon feed was stopped.

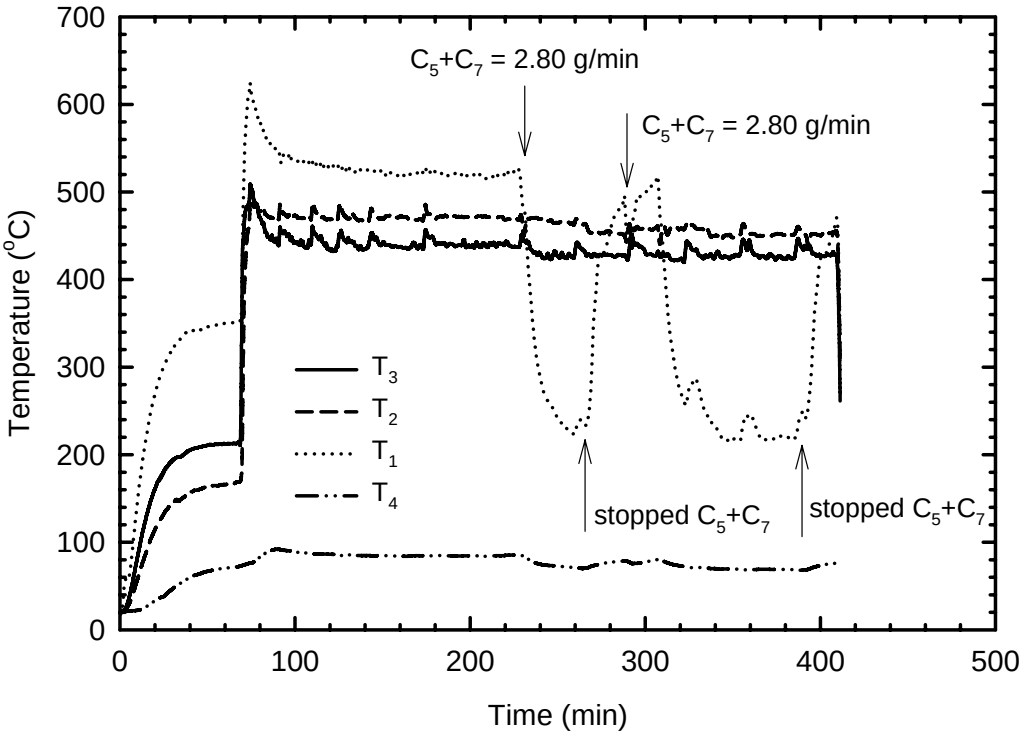

Figure 4.29. Temperature distribution in the radiant heater with addition of liquid C_5 and C_7 at 1.79 g/min methane

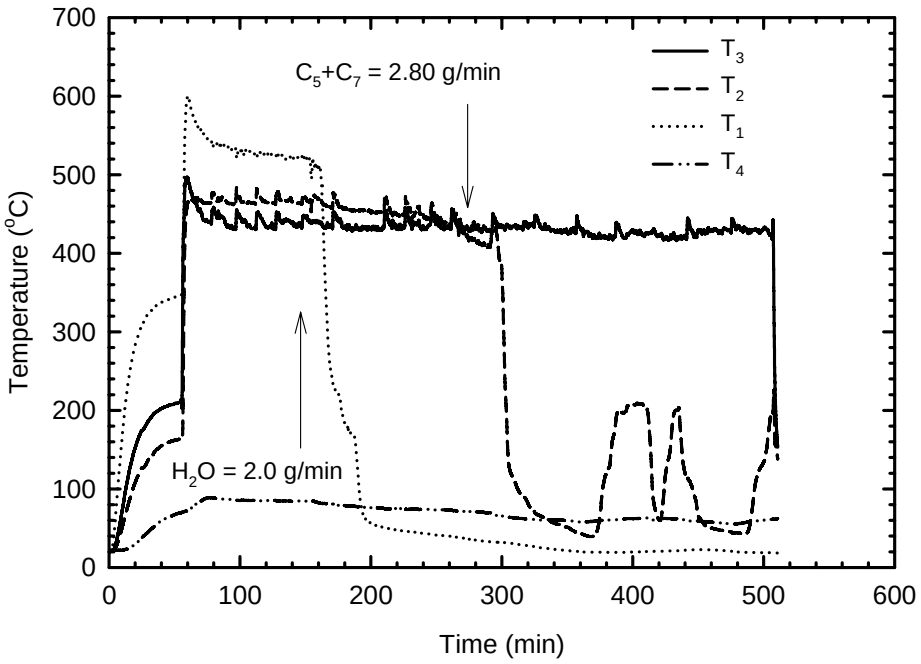

Figure 4.30. Temperature distribution in the radiant heater with addition of liquid water, C_5 and C_7 at 1.79 g/min methane

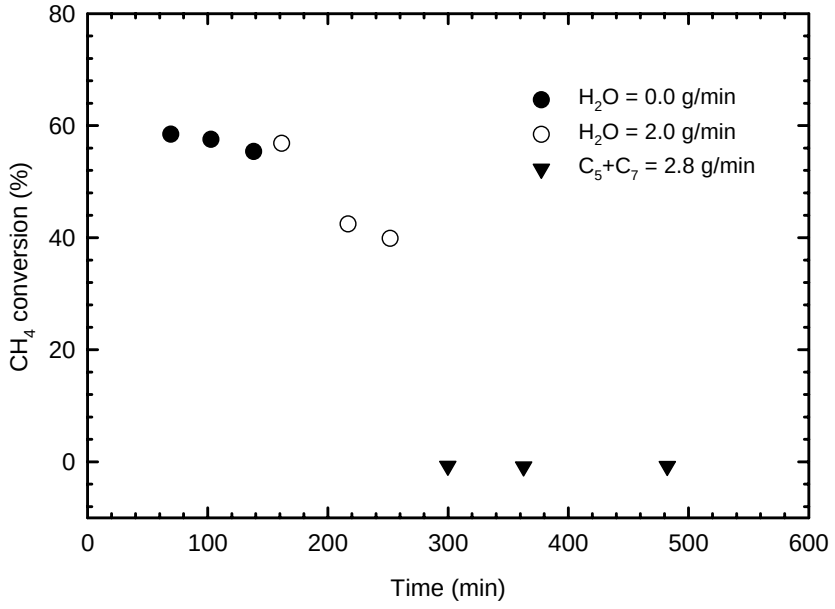

Figure 4.31. Methane conversion with addition of liquid water, C_5 and C_7 at 1.79 g/min methane

Methane conversion is affected by the addition of liquid water to the radiant heater. When C_5 and C_7 start to flow into the heater, no methane is converted. Another experiment was conducted with addition of increasing amounts of liquid C_5 to the radiant heater. The conversion is shown in Figure 4.32. It is observed that as the flow rate of C_5 increases, the conversion of methane decreases. This observation is consistent with the earlier one of decreasing methane conversion with increasing flow rate. In this experiment, by increasing the C_5, the total oxygen demand is effectively increased because the flow rate of oxygen is held constant, thus a decrease in methane conversion is expected. In fact, there is essentially no C_5 detected in the reactor effluent until the C_5 injection rate reached 1.88 g/min. At this point, the calculated methane conversion is negative, indicating that, the C_5 is not being completely combusted as assumed in Equation 4.12, which is confirmed by the presence of C_5 in the effluent. The major result of this experiment is that, C_5 is preferentially combusted, compared to methane. When at C_5 flow rate of 1.25 g/min, fan was turned on; complete conversion of methane was achieved.

It was shown previously in Figure 4.11 that, at lower methane flow rate, the heater would not remain ignited and when it was attempted to reignite the radiant heater, the same pattern was observed. However, the addition of C_5 and C_7 as supplemental fuel allowed normal operation to be maintained. The reactor temperature distribution is shown in Figure 4.33 for 0.36 g/min methane with 0.56 g/min of C_5 and C_7 mixture. Note that when the C_5 and C_7 flow stopped, the heater was extinguished.

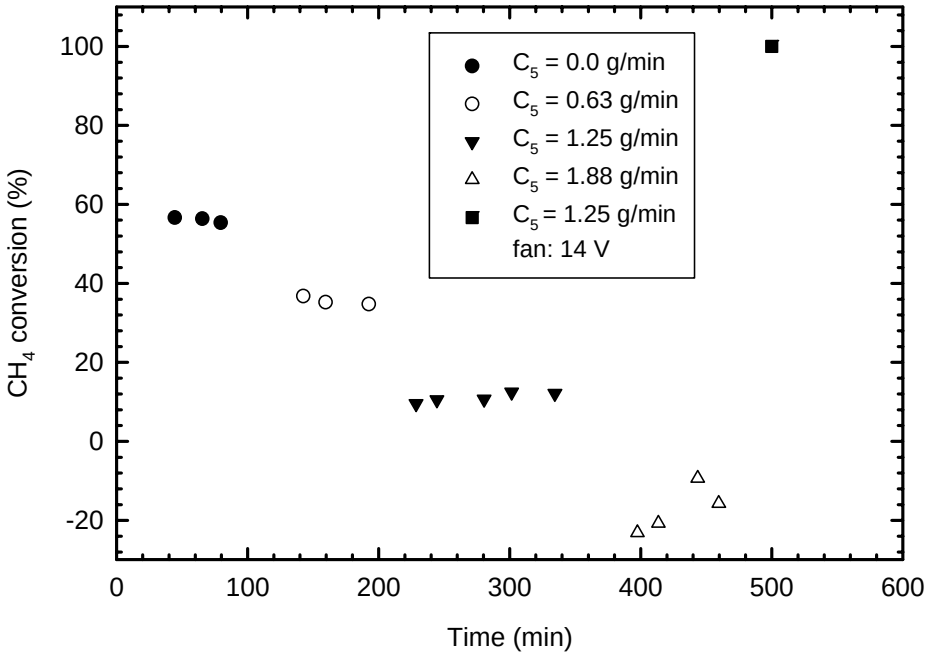

Figure 4.32. Conversion of 1.79 g/min methane with addition of C_5

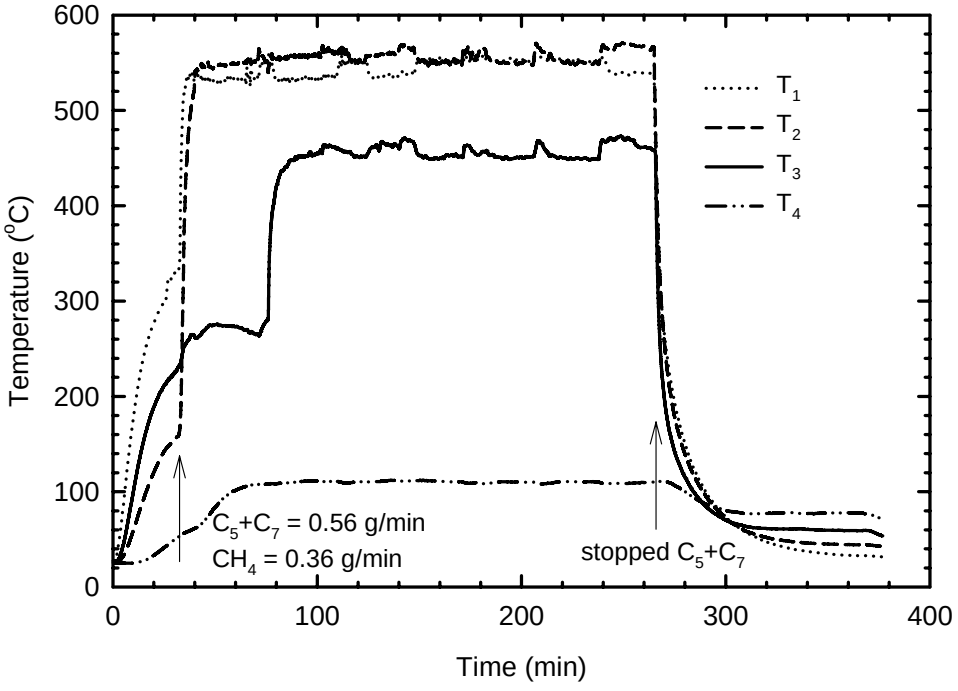

Figure 4.33. Temperature distribution with supplemental addition of C_5 and C_7 to methane feed of 0.36 g/min

4.3.9 Addition of water vapor to the radiant heater

Experiments with liquid water indicate that the presence of liquid water, cause the wetting of the catalyst pad and inhibit the methane combustion. In the real situation, water present in glycol regeneration effluent is in the vapor phase, thus a further set of experiments were undertaken, to obtain more information on the heater performance when water vapor instead of liquid water is fed to the radiant heater. The temperature distribution in the radiant heater and the conversion data are shown in Figure 4.34 and 4.35, respectively. After addition of water vapor, the temperature of the catalyst does not decrease at methane flow rate of 1.79 g/min, as was the case with liquid water feed. The methane fractional conversion remains steady at 2.0 g/min of water injected.

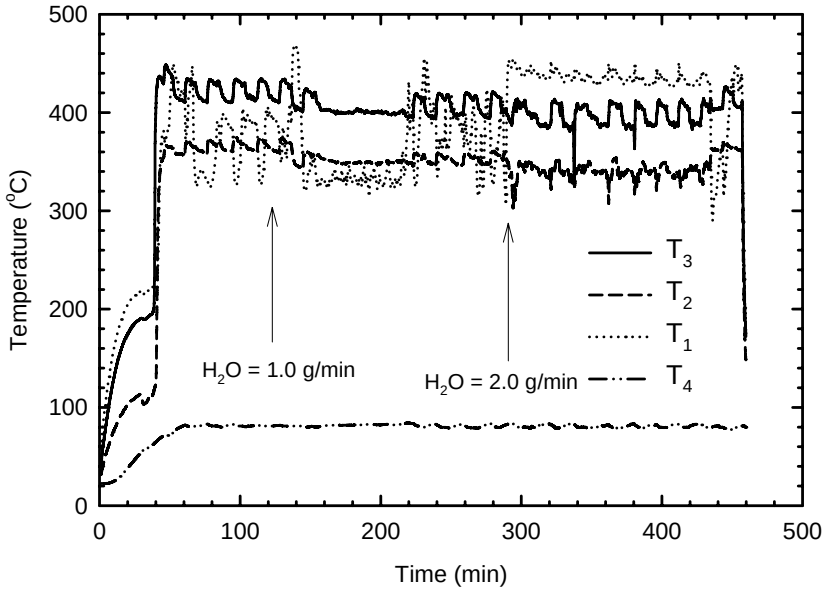

Figure 4.34. Temperature distribution in the radiant heater with addition of water vapor at 1.79 g/min methane

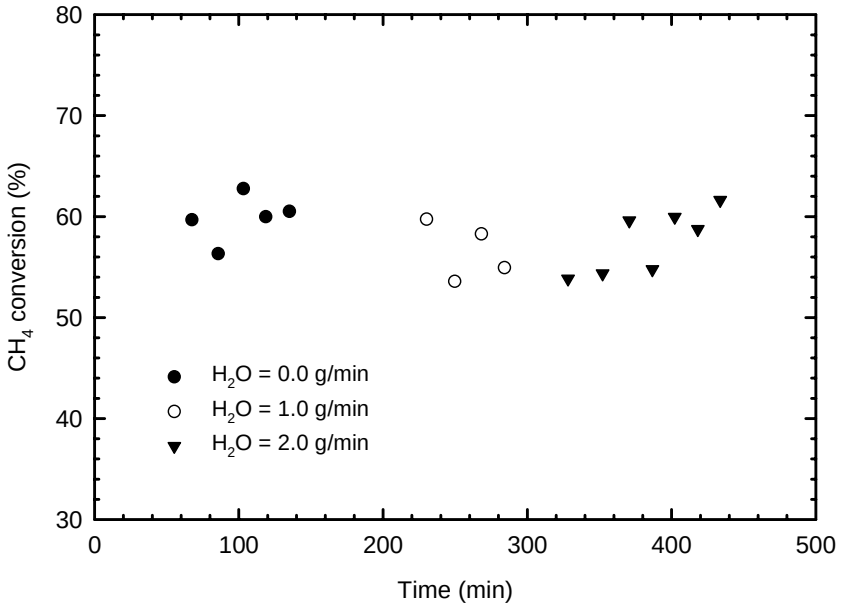

Figure 4.35. Conversion of 1.79 g/min methane with addition of water vapor

4.3.9.1 Insulation of the radiant heater

Because considerable energy is lost through the back and sides of the reactor (as evidenced by the relatively low back space temperature), the back wall and the sides of the radiant heater were insulated with fiber glass insulation blankets. The temperature profiles for the insulated reactor are shown in Figure 4.36. Insulating the radiant heater increased the temperature in the back space of the reactor to about 180^{o}C. The methane conversion in this experiment was observed to be around 60% both in the presence and absence of water.

With the observation that the water vapor does not cause a loss in methane conversion at high flow rate, it is thus safe to conclude that the conversion loss observed in the water experiments is a result of thermal effects, and not kinetic effects. It cannot be stated that water addition does not cause a reduction in the

kinetic reaction rate; since at low methane flow rate, conversion fluctuates, however, this effect is apparently not significant for the conditions used here.

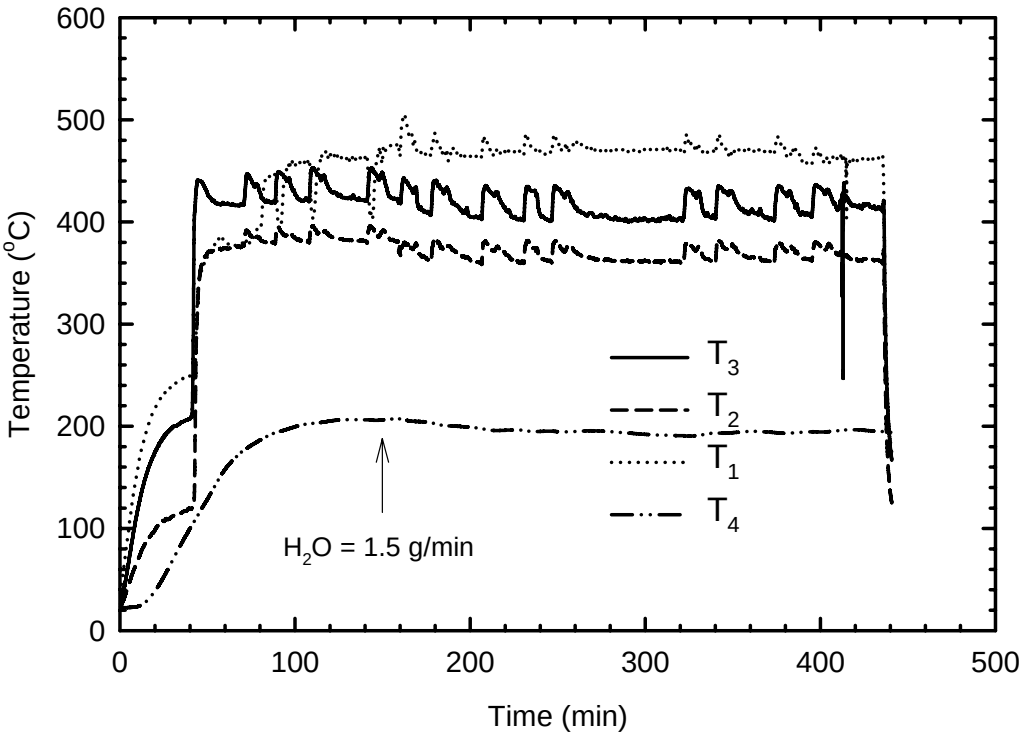

Figure 4.36. Temperature distribution in the insulated heater with addition of water vapor at 1.79 g/min methane

To summarize, the results of the experiments showed that the performance of the counter-diffusive radiant heater is limited by the external diffusion in the boundary layer which was evident from the decreasing methane conversion at higher flow rates. Although methane conversion decreased by increasing the flow rate, the amount of methane combusted showed an increasing trend. The diffusion resistance was confirmed by inducing the convective air flux in front of the catalyst pad using a small fan. It was shown that the effect of oxygen diffusion

inside the pad in not significant. Placing a metal sheet in close distance from the catalyst pad did not improve the combustion, significantly.

Addition of liquid water did not affect the system performance in terms of conversion, however at high water flows comparable to the amount produced during the reaction, methane conversion decreased and the catalyst pad appeared to be wet at the bottom. Presence of liquid water had inhibitory effect on methane combustion. Sniffing the combustion gases from the pad surface revealed higher GC peak area for methane indicating the methane slippage from the wet parts of the catalyst pad. The same inhibitory effect was observed when C_5 and C_7 mixture was added to the system. No methane was converted in presence of these compounds suggesting the competition between three hydrocarbons for oxygen.

The system performance remained unchanged when water vapor instead of liquid water was added to the radiant heater. Insulating the back wall of the heater resulted in the elevated temperature in the back space revealing that in case of liquid water addition, thermal effects play the major role in the reduced methane conversion.

Chapter 5

Computer modeling of the counter-diffusive radiant heater

5.1 Introduction

Computer modeling can be a valuable tool for obtaining an understanding of the physical phenomena happening in a system. The main advantage of computer modeling is predicting the behavior of a system or process under different set of conditions without performing expensive, time consuming or hazardous experiments (Hayes, Kolaczkowski 1997, Colannino 2006).The modeling of most chemical engineering systems of interest requires the solution of the governing conservation equations for momentum, mass and/or energy. These equations often take the form of partial differential equations that require a numerical solution. The modeling of these equations is often given the generic name, Computational Fluid Dynamics or CFD. Originally this term was used exclusively for fluid flow modeling, but lately has come to be used for a broad range of problems involving momentum, heat and mass transfer, including such applications as multiphase flow, flow in porous medium, fluid particle systems, etc. All CFD packages include three main components: a pre-processor, a solver and a post-processor. The functionality of pre-processing include constructing the system geometry, mesh generation, defining the fluid properties, selection of the physical phenomena involved and setting the appropriate boundary conditions. To visualize the solution, post-processing methods can be employed, including the display of contour and/or arrow plots of variables over the entire domain, streamline plots and display of a variable at specific boundary or sub-domain.

The two main methods used in the numerical solution of partial differential equations are the finite element and finite volume methods. Each method has advantages and disadvantages. Most commercial CFD codes (e.g. Fluent, CFX) use the finite volume method, although COMSOL Multiphysics uses the finite element method. The finite element method is a generalization of the classical variational and weighted residual methods, which are based on the idea that, the solution of a differential equation can be represented as a linear combination of unknown parameters and appropriately selected functions in the entire domain of the problem. These functions are called approximation or interpolation functions. The parameters are determined such that the differential equation is satisfied and the interpolation functions are selected such that they satisfy the boundary conditions of the problem.

The basic concept of the finite element method is that the solution domain is divided into many simple sub-domains known as finite elements, which comprise the mesh. Over each finite element, the unknown variables such as temperature, velocity, etc. are approximated using interpolation functions. These functions can be linear or higher order polynomial expansions in terms of the geometrical locations (nodes). The governing equations in the finite element method are integrated over each finite element and the contributions are assembled over the entire problem domain. As a consequence of this procedure, a set of finite linear or non-linear equations is obtained in terms of the set of unknown parameters over the elements.

Meshing is performed to discretize the geometry into smaller elements. The solution for an engineering problem can be very complex and vary unpredictably across the entire domain. By dividing (meshing) the domain into smaller elements, the solution within an element can be approximated using simple functions such as polynomials. Thus, the solution to every individual element forms the solution to the global finite element equation in the whole domain. Mesh generation is an important step in simulation such that, the quality of mesh affects the accuracy of the results. The domain has to be meshed properly into elements of specific shapes such as triangles or quadrilaterals. To minimize the degrees of freedom, the created mesh is usually of varying density. In the parts of the domain where large gradients of the variables are expected, fine mesh is needed while in the parts that are not of interest or not very critical, larger mesh size could significantly reduce the computation time (Reddy, Gartling 2000). In this work, most of the numerical simulations were performed with the commercial software package, COMSOL Multiphysics. This package uses the finite element method.

5.2 Two-dimensional modeling of the counter-diffusive radiant heater

To develop a computer model of a complex system it is reasonable to start with a simpler case and build up to the desired case. In this scenario, one is able to trace the possible problems and do the troubleshooting at the source, before moving to more complex situations. The computer model for the counter-

diffusive reactor was thus built step wise. In the first instance, natural convection over a vertical heated flat plate was studied, which was then extended to flow over a porous medium, without and with imposed inlet flow, and then to the reactor with chemical reactions. The software package used in the modeling was COMSOL Multiphysics, which is based on the finite element method.

5.2.1 Natural convection over heated plate

The first step in the modeling process was to model the natural convection over a vertical heated flat plate. Consider a vertical flat surface at constant temperature, T, immersed in quiescent air at ambient temperature, T_∞, such that $T > T_\infty$. Due to the temperature gradients, the air adjacent to the surface will get warmer and rise, while the colder air will replace it. This is called free or natural convection. Warm air has lower density and the change in the density will initiate the buoyancy effects leading to thermal and velocity boundary layer development.

To model this scenario, a plate with 0.3 m height and a domain of 0.08 m width in front of the plate was considered. The entire domain was meshed using triangular elements. The mesh size near the surface was finer than the rest of the domain, since large gradients of temperature and velocity exists at the close vicinity of the plate. Figure 5.1 shows the mesh structure of the solution domain, which is basically the area in front of the flat plate.

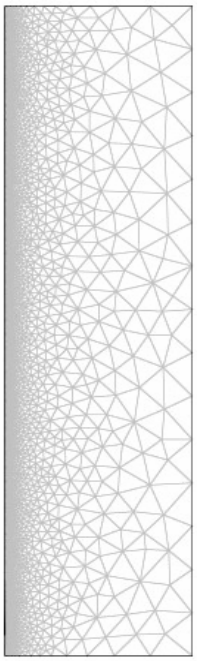

Figure 5.1. Mesh structure of the modeling domain of vertical flat plate

5.2.1.1 Governing equations and boundary conditions

The equations governing this system include continuity (Equation 5.1), Navier-Stokes for momentum balance (Equation 5.2) and general energy balance (Equation 5.3):

$$\frac{D\rho}{Dt} = -\rho(\nabla . u) \tag{5.1}$$

$$\rho\frac{Du}{Dt} = -\nabla P + \mu\nabla^2 u + \rho g \tag{5.2}$$

$$\rho C_p \frac{DT}{Dt} = \nabla .(k\nabla T) + R_{rxn}\Delta H_{rxn} \tag{5.3}$$

Where $\rho, u, P, \mu, C_p, k, T, R_{rxn}, \Delta H_{rxn}$ and g represent, fluid density, velocity, pressure, dynamic viscosity, heat capacity, thermal conductivity, temperature, reaction rate, enthalpy change due to reaction and gravitational acceleration, respectively.

The physical properties of the fluid were taken as constant, except for the density, which was evaluated using the ideal gas law. In setting the boundary conditions for momentum balance, the surface was set as wall type boundary with no slip condition. The type of boundary for three remaining boundaries is open and the boundary condition is normal stress meaning that at these boundaries:

$$P \approx f_0 \tag{5.4}$$

Where f_0 is the normal stress.

In the energy balance, the surface boundary was set to constant temperature. The boundary at the bottom and in front of surface was set to ambient temperature. Since the air in front of the plate rises upward through the upper horizontal boundary, the transport of thermal energy is dominated by convection. Therefore the top horizontal boundary was selected as convective flux which is outlet boundary condition:

$$-n(-k\nabla T) = 0 \tag{5.5}$$

5.2.1.2 Temperature and velocity profiles in the boundary layer

Figure 5.2 and 5.3 show the velocity and temperature profiles through the boundary layer at a height of 0.25 m at surface temperatures of 623, 823 and 1023 K. The contour plots of velocity and temperature are shown in Figure 5.4 and 5.5. Arrows in Figure 5.4 indicate the magnitude of velocity in the boundary layer. According to the velocity boundary condition, selected at the surface (no slip), the velocity is zero at this boundary and reaches the maximum at about 0.003 m away from the surface. Three temperatures were assigned for the surface boundary in separate runs. From Figure 5.3 it is evident that, the surface and the fluid in close vicinity are at high temperature, while moving away from the surface, the fluid temperature reaches the ambient temperature of 293 K.

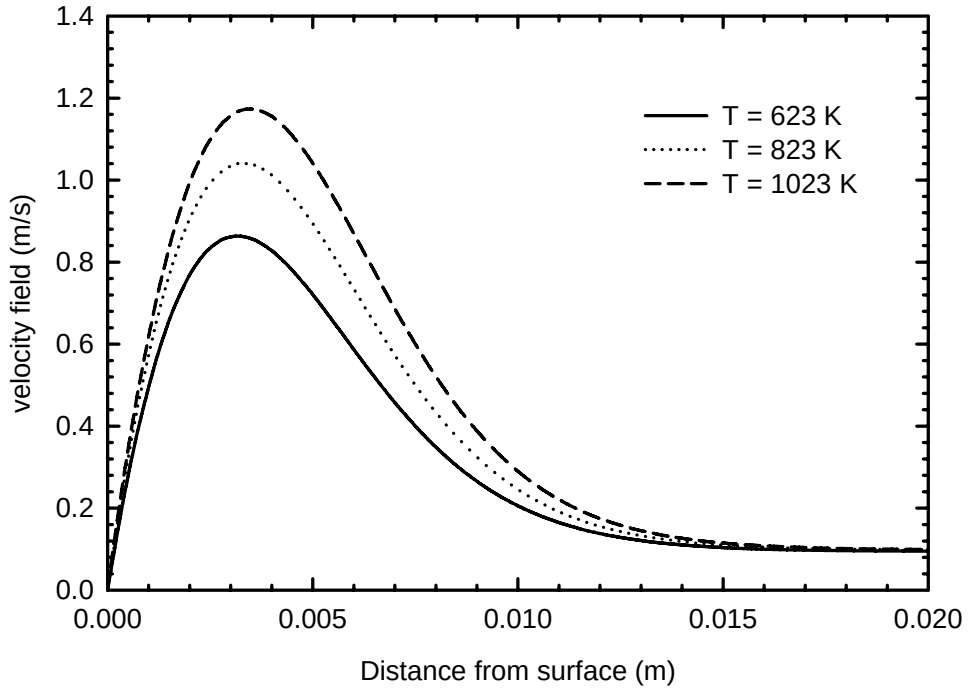

Figure 5.2. Velocity profile at a distance of 0.25 m from the leading edge

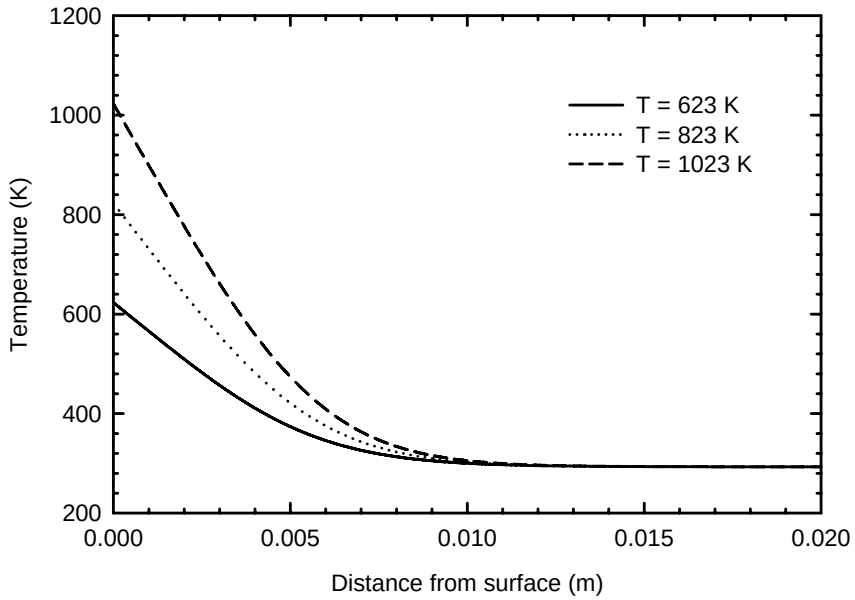

Figure 5.3. Temperature distribution at a distance of 0.25 m from the leading edge

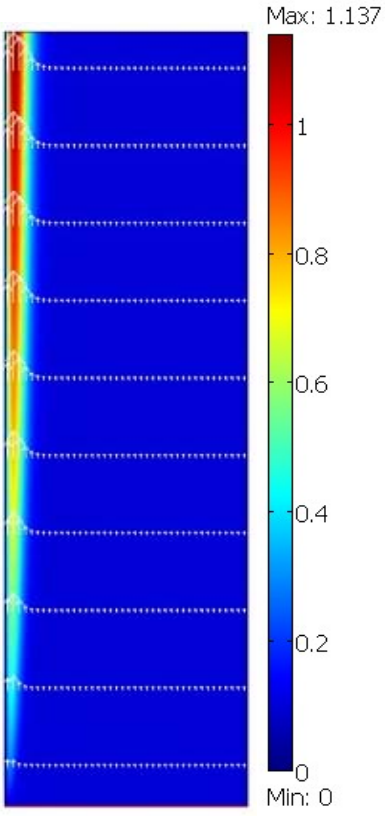

Figure 5.4. Contour plot of velocity distribution in the modeling domain

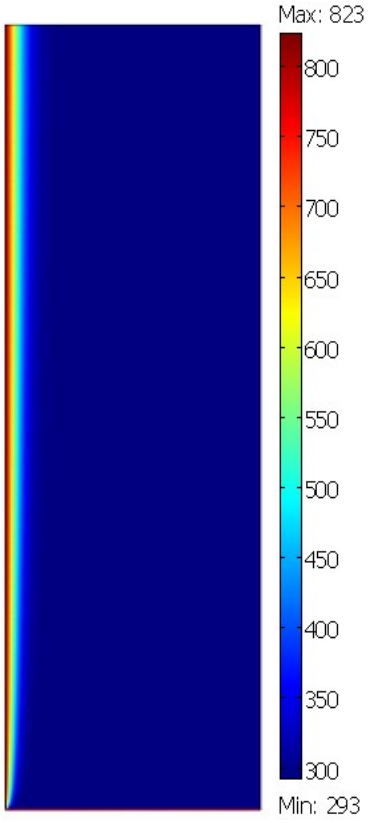

Figure 5.5. Contour plot of temperature distribution in the modeling domain

The resulting heat flux from the surface into the fluid is shown in Figure 5.6. From the heat flux plot it can be seen that, the flux is highest at the leading edge, and decreases along the surface. The heat flux is sharply higher at the leading edge, and falls rapidly in the first 5 cm, and then more gradually. The decreasing heat flux results from the increasing boundary layer thickness.

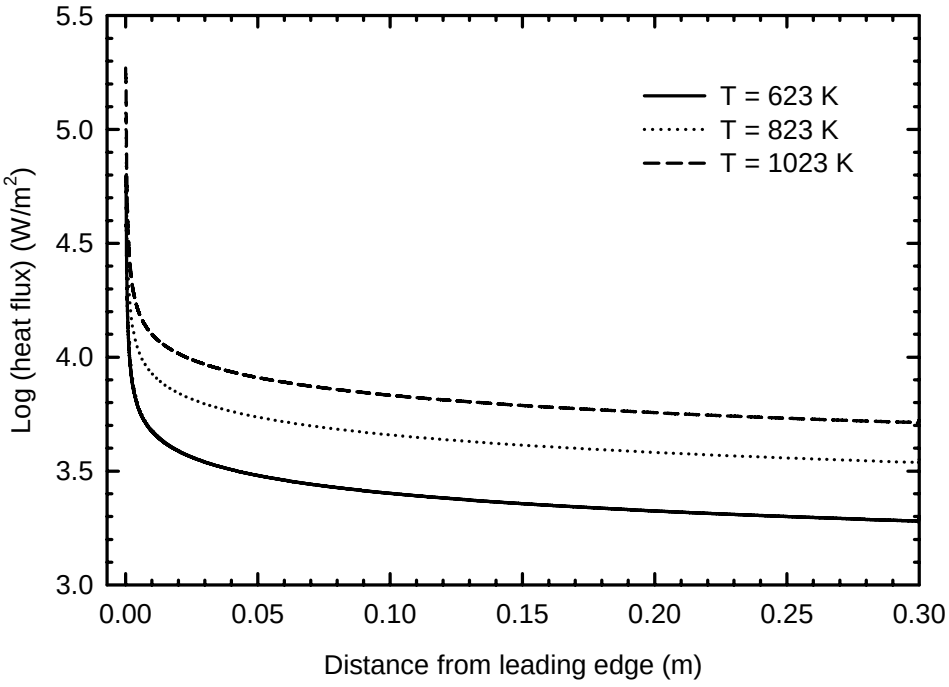

Figure 5.6. Total heat flux from the surface along the hot surface

5.2.1.3 Model prediction of the *Nu* number

The main purpose of this part of the work was to evaluate the heat transfer coefficient at the surface. The predicted *Nu* number was compared with two classical correlations in the literature for isothermal vertical flat plates. Two

correlations for the local Nu number along the surface were compared (Bejan 1993, F. Kreith, M.S. Bohn 1993):

$$Nu_y = 0.508\,\mathrm{Pr}^{0.5}(0.952+\mathrm{Pr})^{-0.25}\,Gr_y{}^{0.25} \tag{5.6}$$

$$Nu_y = 0.503\left[\frac{\mathrm{Pr}}{\mathrm{Pr}+0.986\,\mathrm{Pr}^{0.5}+0.492}\right]^{0.25} Ra_y{}^{0.25} \tag{5.7}$$

Where, Pr, Ra_y and Gr_y are the Prandtl, Rayleigh and Grashof numbers, respectively. These numbers are defined as:

$$\mathrm{Pr} = \frac{\mu C_p}{k} \tag{5.8}$$

$$Ra_y = \frac{g\beta}{\nu\alpha}(T_s\text{-}T_\infty)y^3 \tag{5.9}$$

$$Gr_y = \frac{Ra_y}{\mathrm{Pr}} \tag{5.10}$$

Where β, ν, α, T_s, T_∞ and y, represent the thermal expansion coefficient, kinematic viscosity, thermal diffusivity, surface and ambient temperatures and the location from the leading edge of the plate, respectively. To calculate the Nu_y from the above correlations, all the properties of air were calculated based on the mean temperature T':

$$T' = \frac{T_s + T_\infty}{2} \tag{5.11}$$

For an ideal gas, the coefficient of thermal expansion is given by:

$$\beta = \frac{1}{T} \tag{5.12}$$

The Nu_y at each temperature as a function of y was obtained, which was supplied to the COMSOL to plot the Nu_y along the plate. In the next step, the model predicted Nu_y was obtained. The local heat transfer coefficient is:

$$h_y = \frac{kNu_y}{y} \tag{5.13}$$

The local heat flux from the surface is evaluated by:

$$q_y = \frac{kNu_y}{y}(T_s - T_\infty) \tag{5.14}$$

The local Nu_y number from the results of the simulations can be calculated, by extracting the q_y from COMSOL, and substituting in Equation (5.14). The results were compared to the Nu_y obtained from the empirical correlations. The Nu_y at three temperatures, using the two correlations and the model data are shown in Figure 5.7-5.9.

These plots show that, the Nu_y evaluated using Equation (5.7), gives closer results to the model generated data. The deviation of the predicted modeling results from the correlation becomes larger at higher temperatures. Because the highest temperatures encountered in the radiant heater are less than 623 K, Equation 5.7 was selected for use in the subsequent reactor modeling.

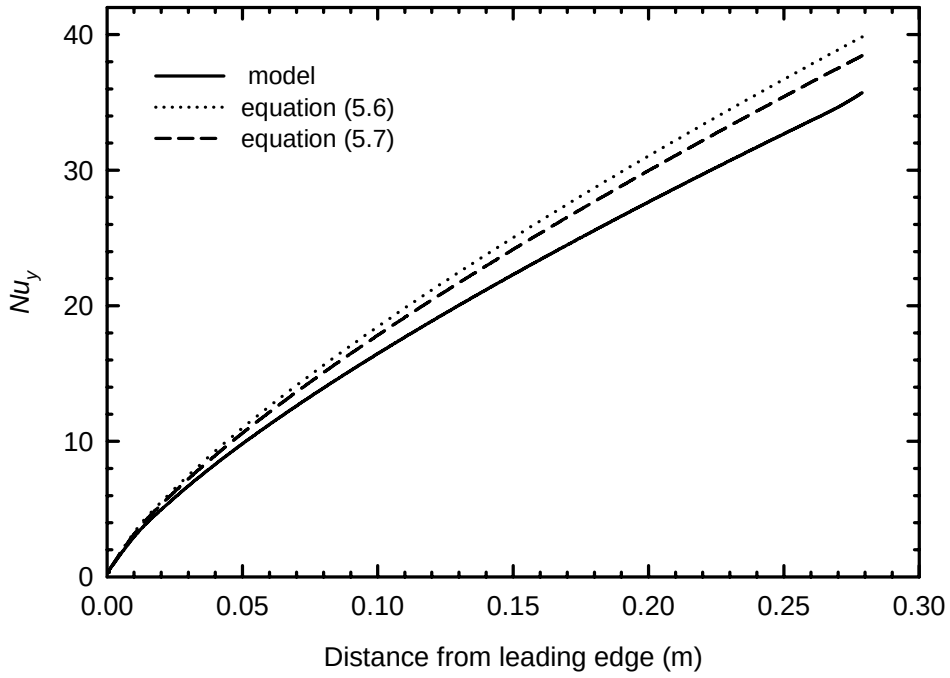

Figure 5.7. Nu_y along the surface at 623 K

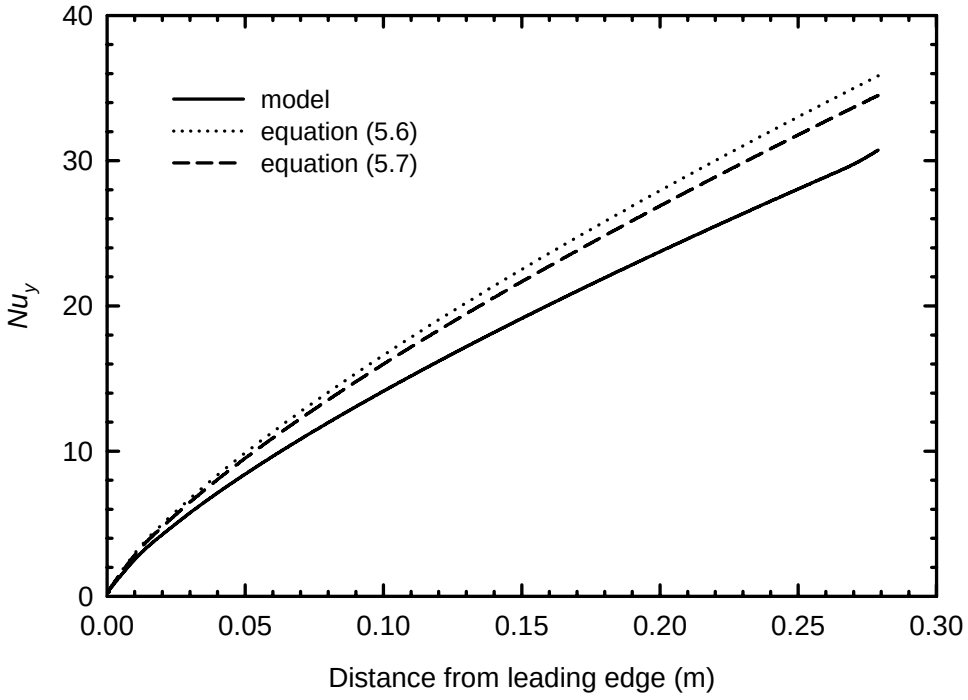

Figure 5.8. Nu_y along the surface at 823 K

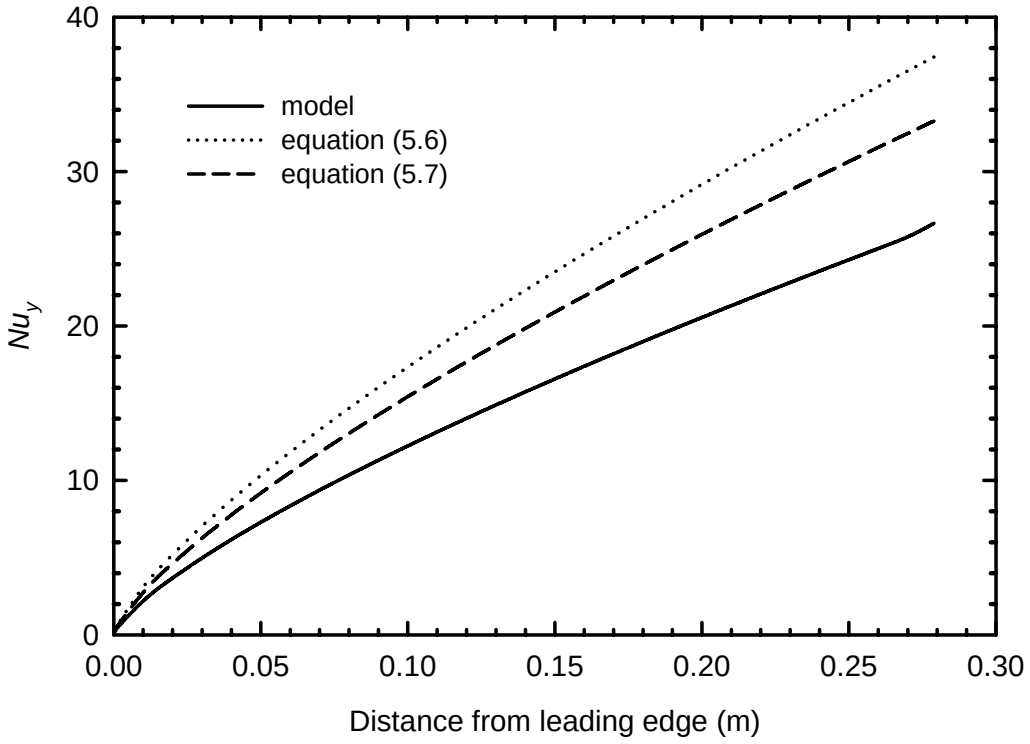

Figure 5.9. Nu_y along the surface at 1023 K

5.2.2 Natural convection in porous medium

In the counter-diffusive radiant heater, the catalyst pad is a porous medium, and moreover has normal velocity imposed, as a result of the fuel fed to the system. The next step was to determine the influence of the porous medium on the development of the natural convection boundary layer, with and without an imposed normal outflow velocity. The model domain is shown in Figure 5.10. Section B is the porous sub-domain representing the catalyst pad, and section A is the sub-domain in front of the hot surface where boundary layers develop. The total number of triangular mesh elements was 52700 and the number of degrees of

freedom was 345137. Brinkman equations were used to model the flow in porous medium.

$$\nabla P = \mu \nabla^2 u - \frac{\mu}{k_p} u \tag{5.15}$$

Where k_p is the Darcy permeability of the porous medium toward the fluid. The Brinkman equation is the extension of Darcy's law accounting for boundary effects between porous medium and free fluid (Vafai 2005). It is valid for a porous medium with porosity greater than 0.6.

5.2.2.1 Effect of porous medium and imposed inlet velocity on boundary layer development

The temperature of the domain representing the porous medium was set to a constant value. The imposed velocity was temperature-corrected, so that a constant mass flow rate was used when comparing different temperatures. Figure 5.11 and 5.12 show the velocity profiles at the height of 0.25 m without and with imposed inlet velocity, and the contour plots of velocity and temperature are shown in Figure 5.13 and 5.14, respectively.

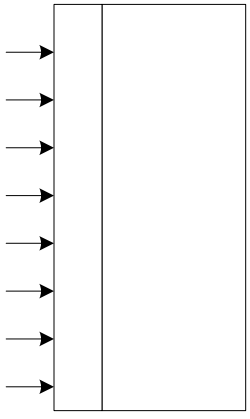

Figure 5.10. The modeling domain with porous medium

Comparing Figure 5.11 and 5.2, it is seen that the two profiles are very similar. The velocity profile developed in front of the heated surface does not appear to be greatly disturbed by the presence of a porous domain. Also, it appears from the comparison of Figure 5.11 and 5.12 that, imposing the velocity at the inlet of the porous section does not influence significantly, the velocity distribution in front of the domain. It should be emphasized that, the velocity in porous domain is orders of magnitude smaller than the velocity in front of that domain, and therefore this result is not surprising. Because of the similarity of the velocity profiles, it is expected that the temperature profiles would also be similar, and this effect can indeed be seen in Figure 5.15 and 5.16. The two temperature profiles are almost identical. As expected, the temperature is constant in the porous sub-domain and decrease to ambient temperature by moving away from the porous sub-domain.

Note that the interface of the porous domain and the fluid occurs at x = 0.0127 m, and thus the temperature and velocity at lower values of x, correspond to locations within the porous domain. The main conclusion from this set of modeling work is that, the front surface of the counter-diffusive radiant heater acts in a very similar manner to a simple flat plate, and thus, it is reasonable in the first instance to use the same correlations, to model the heat and mass transfer effects.

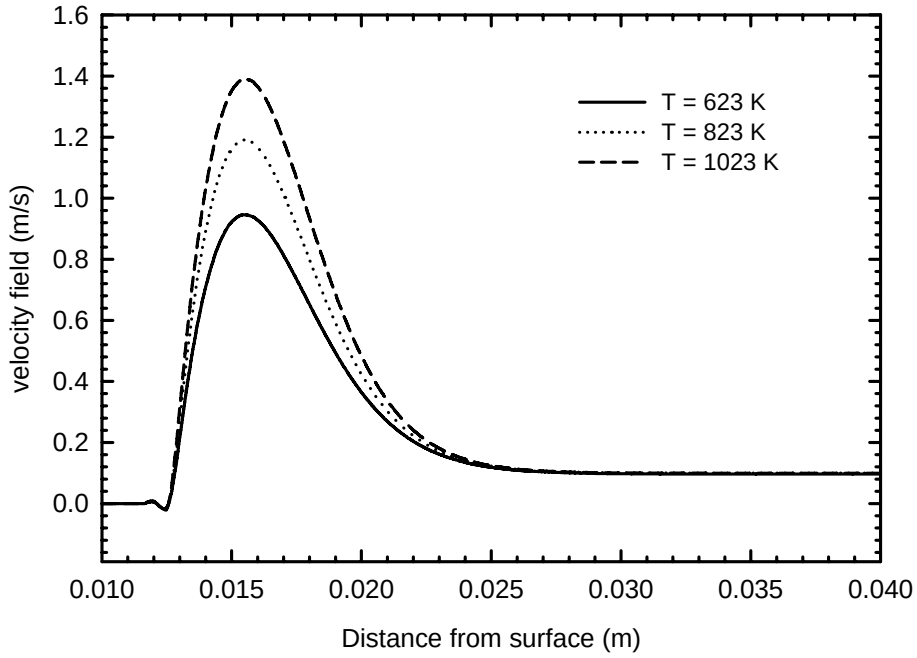

Figure 5.11. Velocity profile at 0.25 m for the flow over porous surface without imposed inlet velocity

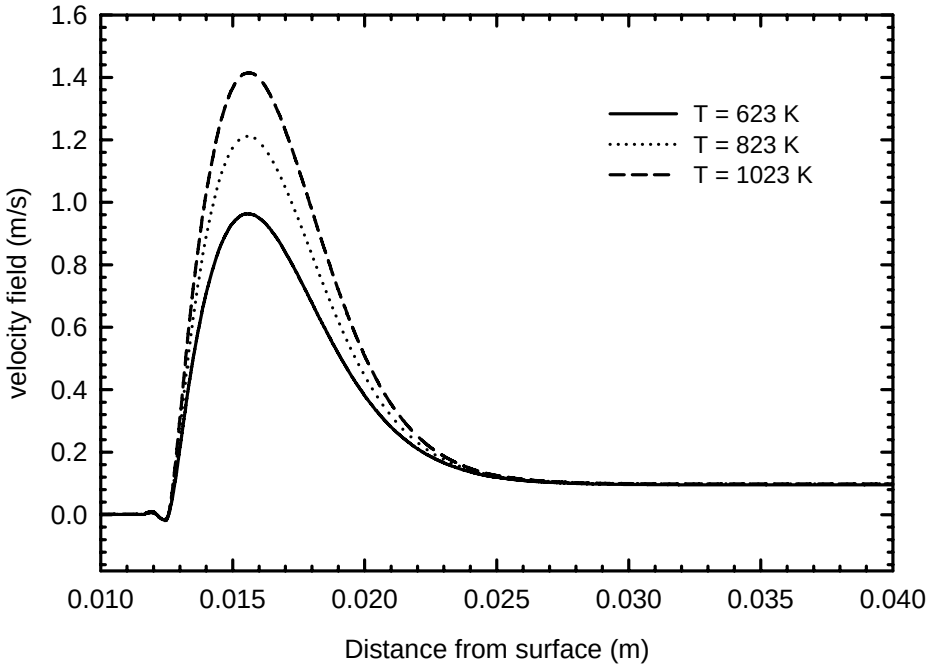

Figure 5.12. Velocity profile at 0.25 m for the flow over porous surface with imposed inlet velocity

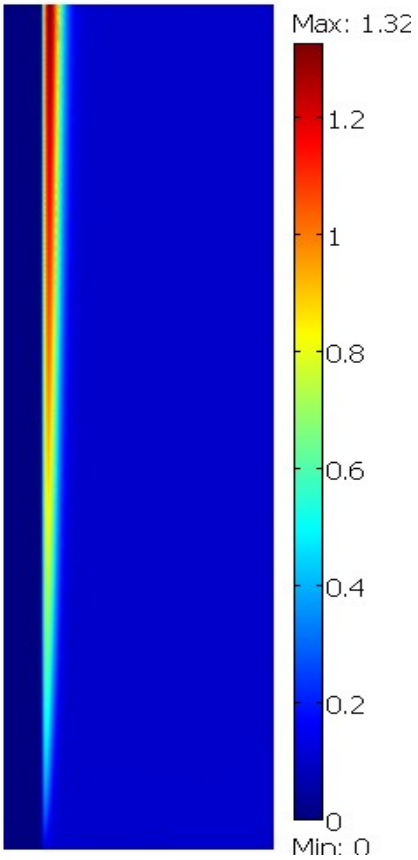

Figure 5.13. Contour plot of velocity distribution in the modeling domain with porous medium

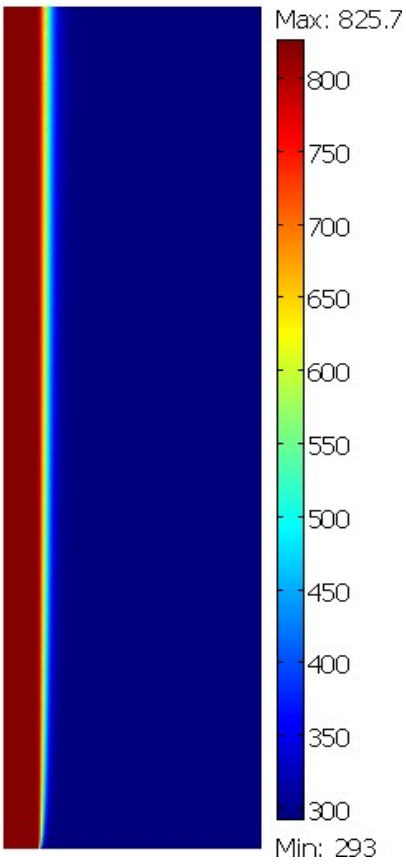

Figure 5.14. Contour plot of temperature distribution in the modeling domain with porous medium

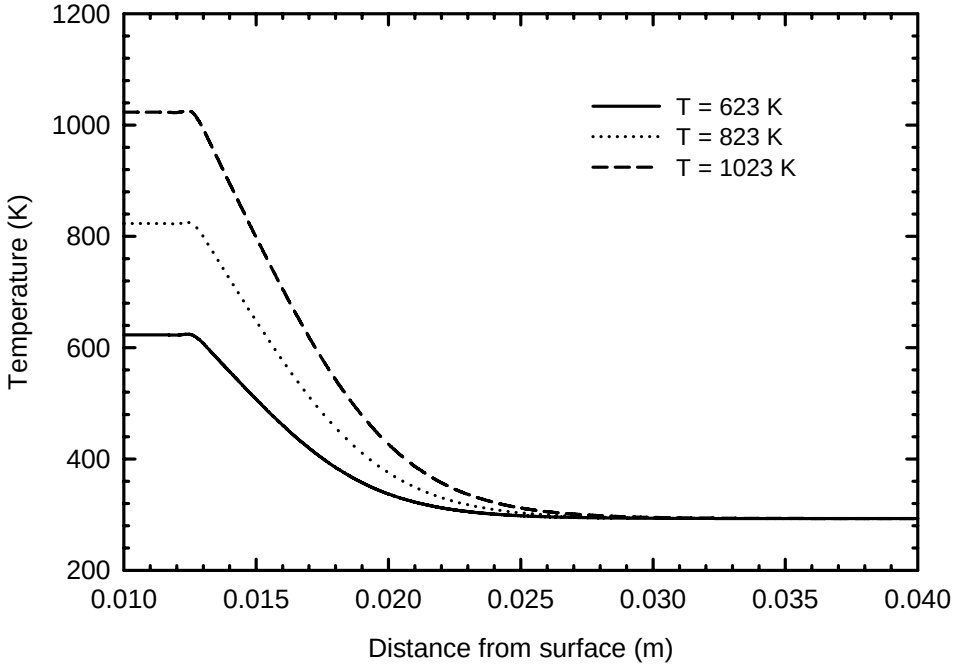

Figure 5.15. Temperature profile at 0.25 m for the flow over porous surface without imposed inlet velocity

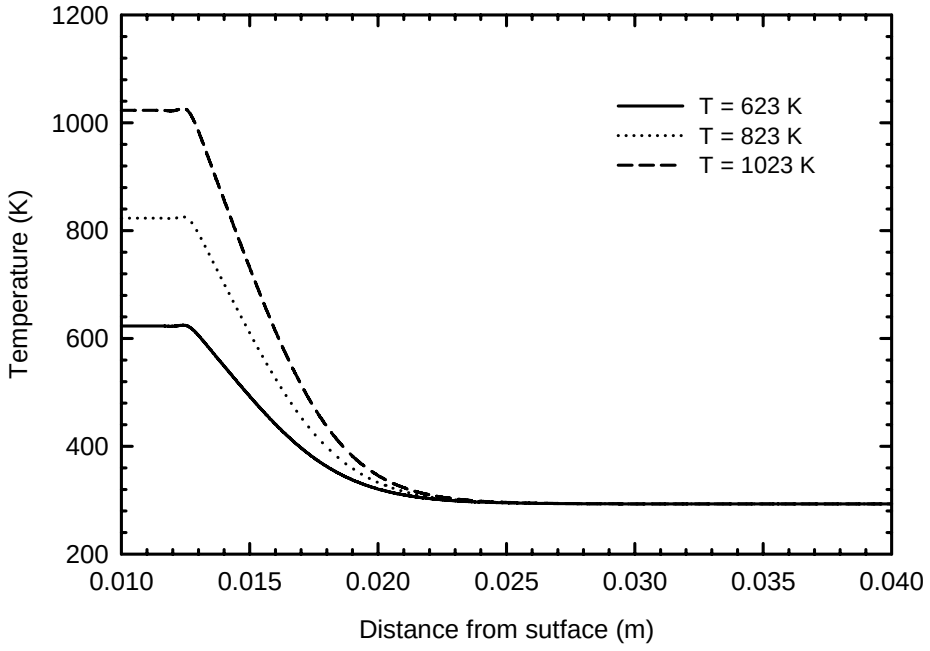

Figure 5.16. Temperature profile at 0.25 m for the flow over porous surface with imposed inlet velocity

5.2.3 Counter-diffusive radiant heater

In addition to the catalyst pad, the counter-diffusive radiant heater system consists of an insulation layer and an empty space where fuel is introduced. To model the fuel inlet, five nozzles were added to the geometry which is shown in Figure 5.17. The nozzles are considered long enough to ensure that the gas inlet temperature is 298 K and velocity has fully developed in the nozzles.

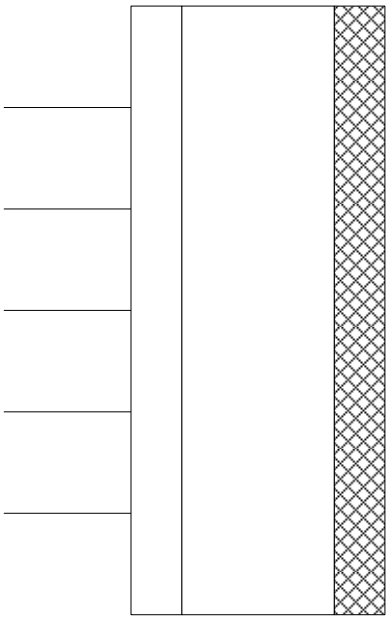

Figure 5.17. Geometry of the counter-diffusive reactor

5.2.3.1 Governing equations and boundary conditions

Governing equations of the system include continuity, Navier-Stokes for momentum balance, convection and diffusion for species balance and convection and conduction for energy balance. In momentum balance equation, the boundary condition for nozzle inlets is constant velocity. All the other boundaries including nozzle walls are considered no slip, except the outlet boundary (catalyst surface), which is set to no viscous stress.

CH_4

CH_4

CH_4

The convection-diffusion equation used in the model is:

$$\frac{Dw}{Dt} + \nabla.(-D\nabla w) = R_{rxn} \tag{5.16}$$

Where w, R_{rxn} and D are the species mass fraction, reaction rate and molecular diffusivity, respectively. In this equation, which was set up for each species in the system (CH_4, O_2, CO_2, H_2O and N_2), constant mass fraction of species was considered at the nozzle inlets. Methane is the only species at the nozzle inlet, therefore:

$$w_{CH_4} = 1 \tag{5.17}$$

For O_2, CO_2, H_2O and N_2, the mass fraction at the nozzle inlet was zero.

All the other boundaries including the nozzle walls are set to zero flux:

$$N = -D\nabla w + wu \tag{5.18}$$

Where

$$n.N = 0 \tag{5.19}$$

N is the inward flux at the boundaries.

The boundary condition at the outlet is:

$$N = -D\nabla w + wu \tag{5.20}$$

Where

$$-n.N = N_0 \tag{5.21}$$

$$N_0 = -k_m(w - w_\infty) \tag{5.22}$$

k_m is the mass transfer coefficient and w_∞ is the mass fraction of the species at a distance far from the outlet boundary, which is zero for CH_4, CO_2 and H_2O, and 0.233 and 0.767 for O_2 and N_2, respectively. For species *i*, the mass transfer coefficient is:

$$k_{m,i} = \frac{D_{i\_m} \times Sh}{y} \tag{5.23}$$

D_{i_m} represents the diffusion coefficient of species *i* in the mixture. The Sherwood number was set equal to Nu number. For *i = 1* we have

$$D_{i\_m} = \frac{1}{\sum_{j=2}^{n} \frac{y_j}{D_{i\_j}}} \tag{5.24}$$

D_{i_j} is the binary diffusion coefficient evaluated using the Fuller equation (Hayes, Kolaczkowski 1997):

$$D_{i\_j} = \frac{1.013 \times 10^{-2} T^{1.75} \left(\frac{1}{M_i} + \frac{1}{M_j} \right)^{0.5}}{P\left[\left(\sum v'_i \right)^{1/3} + \left(\sum v'_j \right)^{1/3} \right]^2} \tag{5.25}$$

Where v' represent the atomic diffusion volume. In energy balance equation, the nozzle inlet boundaries are set to ambient temperature of 298 K. The nozzle walls are set to thermal insulation (zero flux):

$$-n.(-k\nabla T) = 0 \tag{5.26}$$

All the other boundaries are set to have the heat flux:

$$-n.(-k\nabla T) = q_0 \tag{5.27}$$

To find q_0, Nu number needs to be calculated. Note, that since temperature is not constant across the catalyst surface, using constant Nu number at this boundary produces false results. Therefore local Nu number based on the catalyst pad height was calculated. For vertical boundaries including catalyst surface (outlet), Nu number was calculated using Equation 5.7. For horizontal boundaries, two different correlations were used, depending on the orientation of that boundary (Bejan 1993). For the hot surfaces facing upwards (top of the radiant heater):

$$\overline{Nu_L} = 0.15 Ra_L^{1/3} \tag{5.28}$$

For the hot surfaces facing downward (bottom of the reactor):

$$\overline{Nu}_L = 0.27\, Ra_L^{0.25} \tag{5.29}$$

Therefore, for all these boundaries:

$$q_0 = \frac{Nu.k}{L}(T_s - T_\infty) \tag{5.30}$$

However, the correlation for evaluating Nu number depends on the orientation of that boundary. The heat flux at the catalyst surface consists of bulk fluid motion (advection), convection and radiative flux. At the outlet boundary, q_0 is evaluated by:

$$q_0 = -\rho C_p u T_0 - h(T_s - T_\infty) - \varepsilon\sigma(T_s^4 - T_\infty^4) \tag{5.31}$$

Where ρ and C_p are the fluid density and heat capacity and ε (0.45) and σ (5.67×10^{-8} W/m^{2}K^4) are the emissivity and Stefan-Boltzmann constant. Fluid density, ρ, is evaluated based on the molecular weight of all species:

$$\rho = \frac{PM_{ave}}{RT} \tag{5.32}$$

$$M_{ave} = \frac{1}{\sum_{i=1}^{5} \frac{w_i}{M_i}} \tag{5.33}$$

w_i and M_i, represent the mass fraction and molecular weight of each species and subscript *i*, denote each species involved in the system. Heat capacity of the fluid is calculated by:

$$C_p = 5\times10^{-8}T^2 + 1\times10^{-4}T + 0.954 \tag{5.34}$$

Thermal conductivity and dynamic viscosity were calculated for the mixture. Thermal conductivity of the multi-component mixture was calculated using the Wassiljewa equation (Ried R.C., Prausnitz J.M. and Sherwood T.K. 1977):

$$k_{mix} = \sum_{i=1}^{n} \frac{y_i k_i}{\sum_{j=1}^{n} y_i A_{ij}} \tag{5.35}$$

Mason and Saxena suggested A_{ij} to be defined as:

$$A_{ij} = \kappa \frac{\left[1 + (k_{tri}/k_{trj})^{0.5}(M_i/M_j)^{0.25}\right]^2}{\left[8\left(1 + M_i/M_j\right)\right]^{0.5}} \tag{5.36}$$

$$\frac{k_{tri}}{k_{trj}} = \frac{\Gamma_j}{\Gamma_i} \frac{\exp(0.0464T_{ri}) - \exp(-0.2412T_{ri})}{\exp(0.0464T_{rj}) - \exp(-0.2412T_{rj})} \tag{5.37}$$

$$\Gamma_i = \frac{T_{ci}^{1/6} M_i^{1/2}}{P_{ci}^{2/3}} \tag{5.38}$$

$$T_{ri} = \frac{T}{T_{ci}} \tag{5.39}$$

T_r, T_c and P_c are reduced and critical temperatures and critical pressure, respectively and k_i is the thermal conductivity of individual species which is a function of temperature. K_{tr} is the monoatomic value of thermal conductivity and κ is a numerical constant close to unity. It was assumed to be one. For mixture viscosity, the simplified Chapman-Enskog equation was used which can be found in Ried et al. (1977) (Ried R.C., Prausnitz J.M. and Sherwood T.K. 1977).

5.2.3.2 Reaction kinetics

Power law reaction rate from a previous study was used at two temperature ranges and kinetic parameters obtained in this study were used (Trimm, Lam 1980a):

$$\begin{aligned} R_{\mathrm{CH_4}} &= R_{LT} \quad (T \le 817) \\ R_{\mathrm{CH_4}} &= R_{HT} \quad (T \ge 817) \end{aligned} \tag{5.40}$$

where:

$$R_{LT} = k_{0LT}\left[\exp(-\frac{E_{LT}}{RT})\right] w_{CH_4} w_{O_2}{}^{0.25} \qquad (T \le 817\ K) \tag{5.41}$$

$$R_{HT} = k_{0HT}\left[\exp(-\frac{E_{HT}}{RT})\right] w_{CH_4} w_{O_2} \qquad (T \ge 817\ K) \tag{5.42}$$

The activation energy at low temperature (E_{LT}) and high temperature (E_{HT}) are 1.87×10^5 J/mol and 8.61×10^4 J/mol, respectively. Effective diffusivity and effective thermal conductivity in catalyst pad and insulation layer were evaluated based on the porosity of 0.97.

Figure 5.18-5.20 show the contour plots of temperature, and methane and oxygen mass fraction at methane flow rate of 1.79 g/min. From temperature plot it is obvious that the reaction is taking place within the catalyst pad. Also the temperature at the bottom of the pad is higher, which is in good agreement with experimental observation.

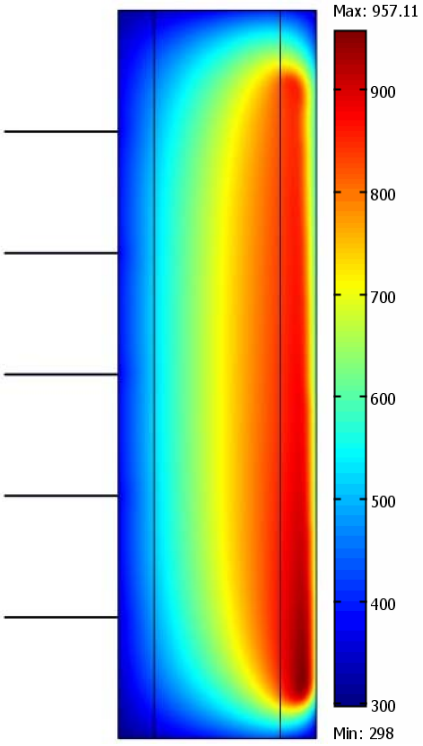

Figure 5.18. Temperature contour plot at 1.79 g/min methane flow

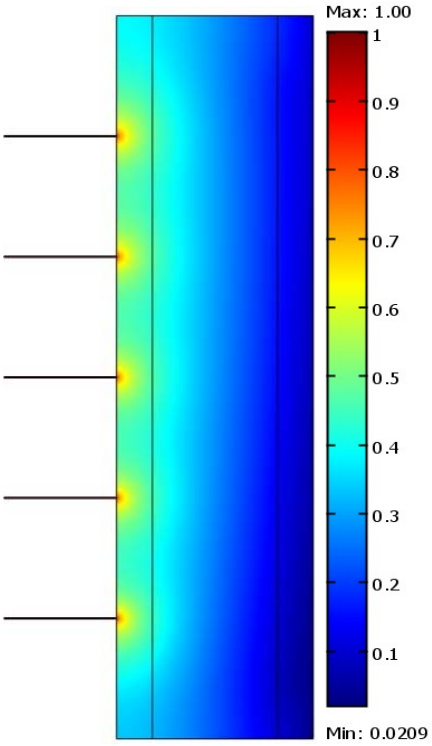

Figure 5.19. Methane mass fraction contour plot at 1.79 g/min methane flow

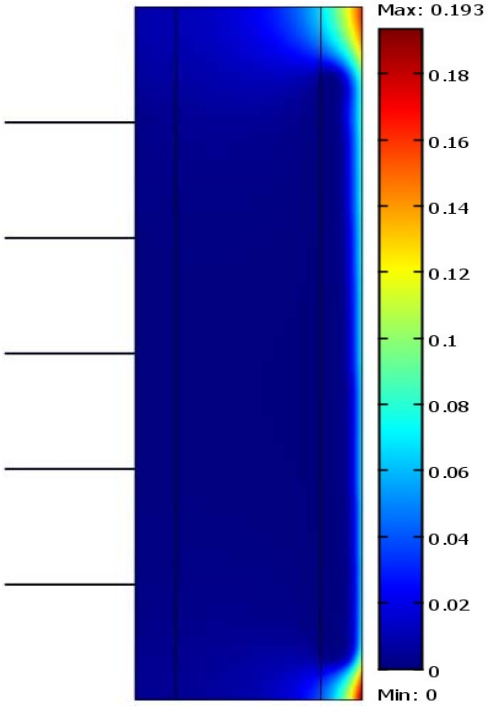

Figure 5.20. Oxygen mass fraction contour plot at 1.79 g/min methane flow

Combustion reaction leads to formation of CO_2 and H_2O within the catalyst pad. Oxygen is quickly consumed and depleted from the catalyst surface during combustion and inert nitrogen is accumulated within the system. Figure 5.21 shows the oxygen mass fraction at cross section of 0.15 m along the catalyst pad at different methane flow rates.

5.2.3.3 Comparison of model and experimental data

The model was run at several methane flow rates, and the conversion data are presented in Figure 5.22. Methane conversion from the model was calculated by comparing the total CH_4 flux at outlet boundary, to that at the inlet boundary of the insulation sub-domain. Comparing the experimental data and model prediction shows the same decreasing trend in conversion with increasing flow rate. However, there is discrepancy between the two data sets. The model predicted conversion is less than the experimental data. This difference can be explained by uncontrolled experimental conditions such as moving the experimenter in front of the unit imposing convective air fluxes in front of the unit. It should also be noted that the catalyst pad surface in experimental unit is protected by a wire mesh structure which could have an effect on the conversion data. These results indicate that it may not be realistic to model the space in front of the catalyst pad as pure natural convection. Experimental results showed that by imposing convective air flux using a fan complete methane combustion can be achieved which is explained by enhanced mass transfer coefficient at catalyst surface.

To increase the conversion data from the model, reaction rate and *Sh* number was increased separately in small increments. Figure 5.23 shows the

conversion of methane at several flow rates at different *Sh* numbers. *Sh* multiplication coefficient represents the number that was multiplied by the constant (0.503) in Equation 5.7. Note that *Sh* number was assumed to be equal to *Nu* number.

It needs to be mentioned that the proper boundary condition assignment is crucial for obtaining meaningful modeling results. In this case the most important factor is the heat and mass transfer coefficient at the catalyst boundary and without reasonably accurate values, the model would produce results that are not reliable. Since this work involved both modeling and experimental procedure, the experimental data were used to validate the model results.

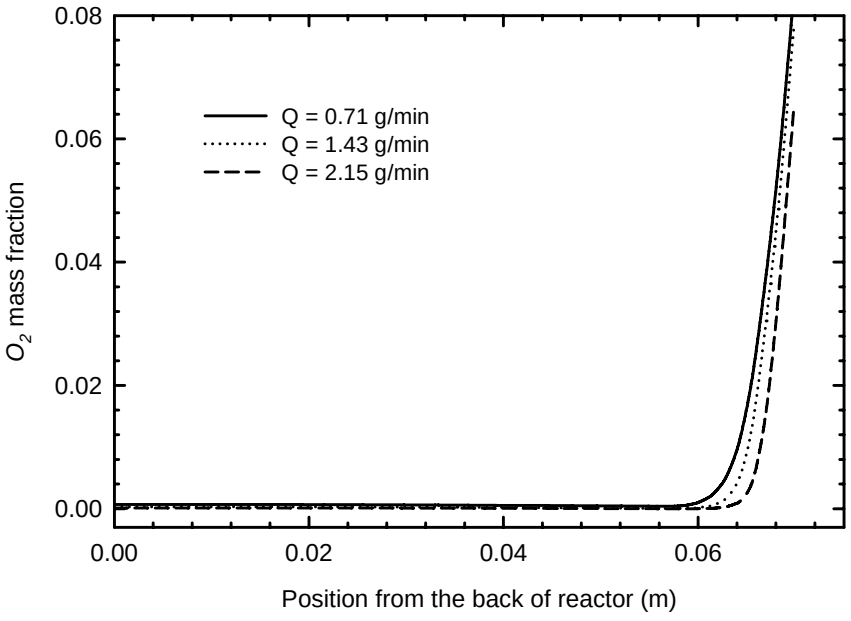

Figure 5.21. Oxygen mass fraction from the back to the front of the system at 0.15 m height

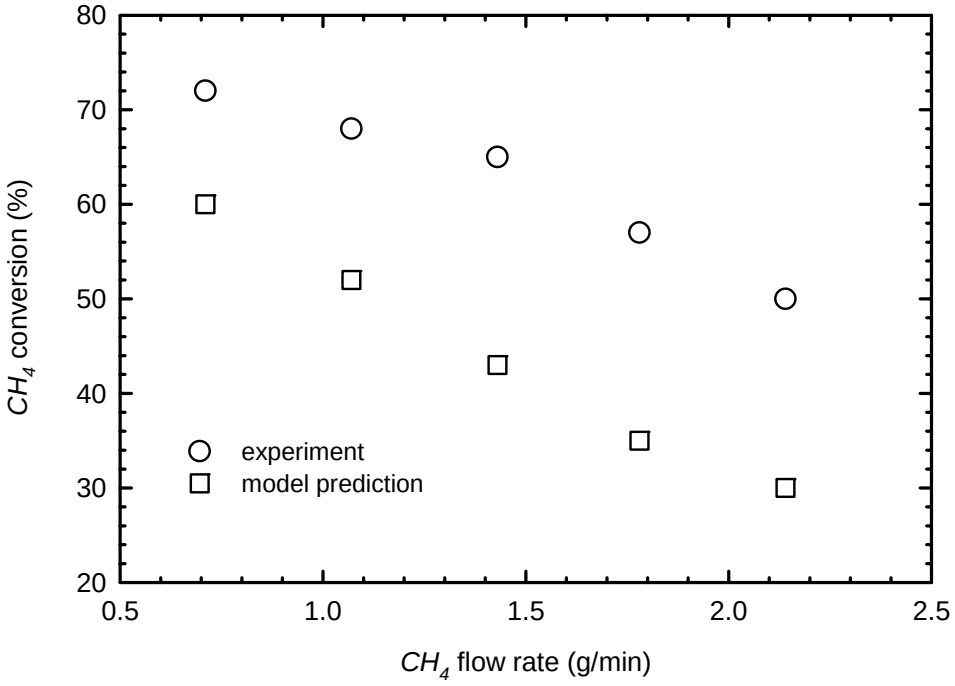

Figure 5.22. Methane conversion data from experiment and model prediction

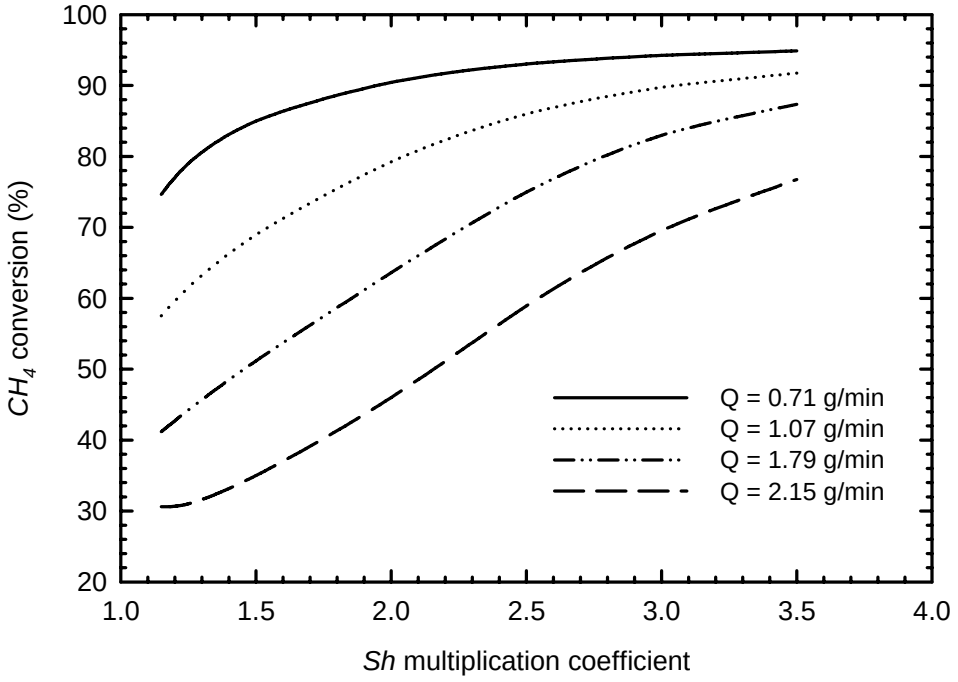

Figure 5.23. Methane conversion improvement at increasing *Sh* numbers

5.2.3.4 Effect of kinetic parameters on methane conversion

The effect of increasing the reaction rate at methane flow rate of 1.79 g/min is shown in Figure 5.24. This plot clearly indicates that changing the reaction kinetics does not have significant effect on methane conversion confirming that, there is oxygen diffusion limitation in the system. In fact oxygen transfer through boundary layer is the dominating parameter affecting the system performance in terms of fuel conversion. The role of oxygen diffusion in counter-diffusive systems has been suggested previously by other researchers (Specchia, Sicardi & Gianetto 1981, Dongworth, Melvin 1977).

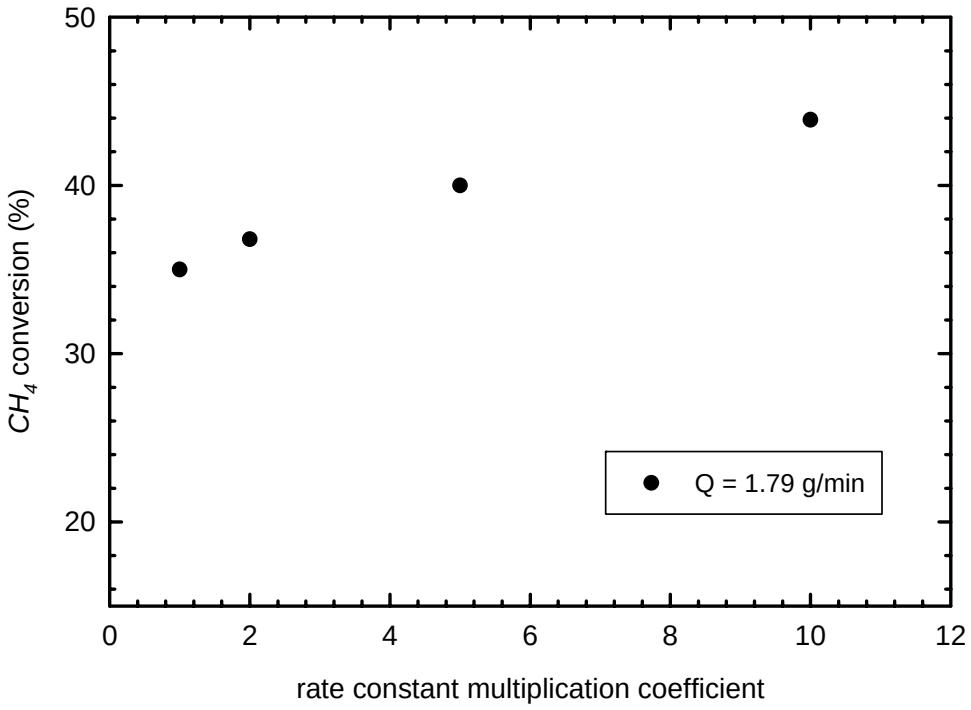

Figure 5.24. Effect of changing the reaction kinetics on methane conversion

5.3 Three-dimensional modeling

Modeling the counter-diffusive reactor was attempted in three dimensions. At first, sofware package COMSOL Multiphysics was used. It was found that this package was not very useful for three-dimensional modeling due to the instability and difficulty in obtaining the converged solution of all the physics involved. Another disadvantage of the COMSOL was the long computation time, making it expensive for three-dimensional modeling. Therefore, the Fluent package was used for the rest of the modeling work which is based on the finite volume method. In the finite volume approach, the integral form of the conservation equations are applied to the control volume defined by a cell to get the discrete equations for the cell. The domain structure and mesh was generated in GAMBIT preprocessor. The mesh structure of the domain and the mesh statistics are shown in Figure 5.25 and Table 5.1.

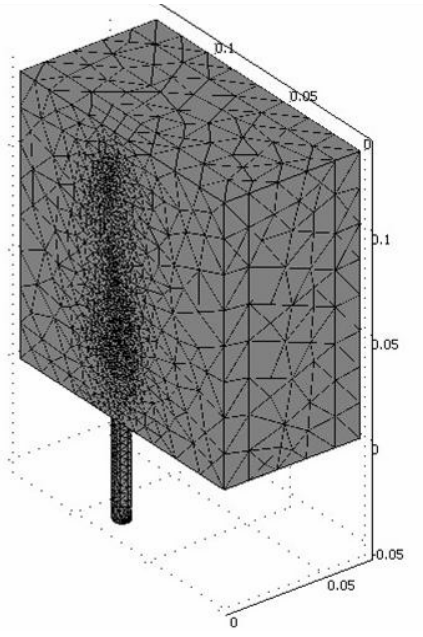

Figure 5.25. Mesh structure of the three-dimensional model

Table 5.1. Mesh statistics of the three-dimensional model

Number of dof	1300131
Number of elements	116711
Number of boundary elements	13282
Number of edge elements	1344

The governing equations and boundary conditions are similar to the two-dimensional model. Fuel is introduced into the reactor through the tube which has openings along its length for fuel distribution. To study the flow pattern in the system, momentum equations were solved without considering the reaction in the catalyst layer. It was found that most of the fuel enters through the first holes and having several holes along the tube is not necessary. Therefore the fuel distribution was not very sensitive to the design of the inlet tube. The same result was obtained from the experiments indicating that changing the orientation of the system did not have an effect on the temperature distribution in the catalyst pad. Fig. 5.26 shows the velocity vector plot in the system. The large amount of fuel coming out of the first holes is evident by the large magnitude of the velocity vectors.

To summarize, two-dimensional model predication of the methane conversion was lower compared to the experimental results although the model predicted the decreasing trend with increasing methane flow rate, successfully. It indicates that the mass transfer coefficient used in the model is smaller than the

real one. Adjusting the mass transfer coefficient led to the improved conversion data. In fact, the reaction kinetics did not have an important role in the performance of the system which was evident from Figure 5.24. First stages of the three-dimensional model development showed that the fuel distribution in the back space of the reactor is not very sensitive to the position of the feeding tube and the holes along the tube since most of the fuel came out of the first holes.

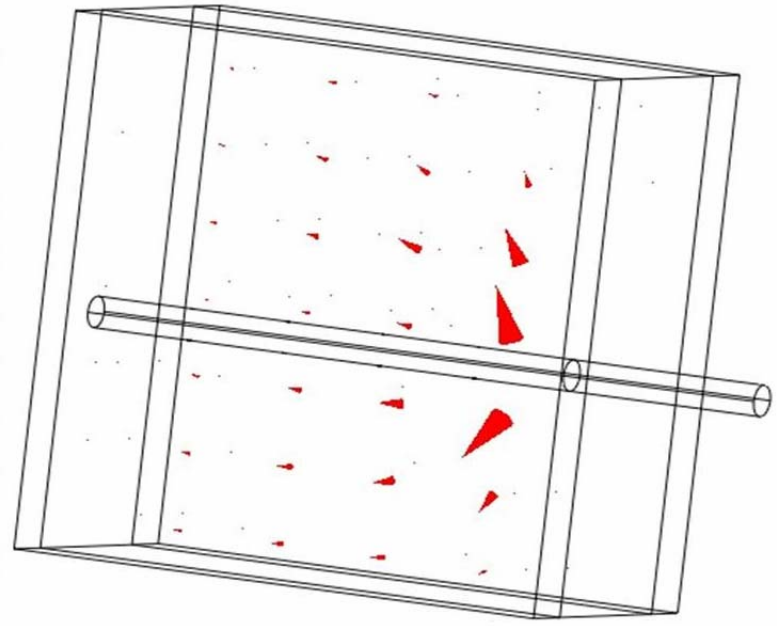

Figure 5.26. Velocity vector in three-dimensional model

Chapter 6

Conclusions and recommendation

It is well known that human activities and particularly the fossil fuel production and consumption, are mainly responsible for the environmental pollution and climate change since the pre-industrial times. Nowadays, environmental issues have become one of the major global challenges, since the harmful industrial emissions greatly influence the human health and the quality of life. With the advancement of human knowledge, effective technologies are proposed and applied for the mitigation of unwanted VOC emissions including methane and BTEX substances. The common practice for mitigation of VOC has been burning these compounds in the flare; however the disadvantages of this method motivated the initiation of this research project.

The main focus of this research was to investigate the effectiveness of the counter-diffusive radiant heater system for catalytic combustion of methane, which is known as a strong GHG, and BTEX substances that are known for their carcinogenic effects. Results of the experimental efforts indicate that, the catalytic combustion system is limited by the diffusion of oxygen through the boundary layer developed in front of the catalyst pad. In fact, oxygen diffusion limitation is responsible for the decreasing trend in hydrocarbon conversion and non-uniform temperature distribution in the catalyst pad. In spite of the decreasing trend in methane conversion with increasing the methane feed, the amount of methane combusted and the consumed oxygen increased. The presence of the pad cover or its thickness did not impose any resistance to the oxygen diffusion. The effect of oxygen limitation was verified by inducing convective air flux in the boundary layer using a fan and it was observed that complete conversion can be achieved in

presence of convective flux. The presence of metal sheet in front of the pad influenced the temperature distribution across the pad; however, no significant improvement on conversion was observed.

Experiments showed that there is competition for oxygen when more than one hydrocarbon is used as fuel in the system. Methane is the most difficult hydrocarbon to oxidize, therefore when pentane is present, oxygen is consumed by pentane first and depending on the oxygen availability, methane will be oxidized next. In fact, methane combustion is inhibited by the presence of other hydrocarbons in the system.

Presence of small volumes of liquid water in the system did not affect the hydrocarbon combustion although the temperature distribution across the pad was affected. However if the volume of water was comparable to that produced during the reaction, combustion was inhibited and the combustion efficiency decreased. Addition of water vapor into the system did not influence the combustion efficiency and the temperature distribution. Insulation of the back and side walls of the radiant heater resulted in elevated temperature in the fuel-containing space and stable conversion leading to the conclusion that the decrease in methane conversion in presence of liquid water is due to the high heat of vaporization of water and kinetics is not the major role player.

Developing the two-dimensional model of the counter-diffusive radiant heater revealed that, the model-predicted temperature distribution is in agreement with experimental data. The model also confirmed that the system is indeed mass transfer controlled. Changing the kinetic parameters did not have significant

effect on combustions while increasing the mass and heat transfer coefficients, led to improved combustion efficiency in terms of methane conversion. Methane conversion data predicted by the model had the same decreasing pattern compared to experimental results; however, the model under-predicts the methane conversion. This result indicates that the *Sh* number used in the model is lower than the real value. In fact when higher *Sh* numbers were used in the model, methane conversion was improved indicating the key role of the mass transfer coefficient on the system performance. It was found that for different methane flow rates, the real *Sh* number was 1.5-2 times higher than the values used in the model. Three-dimensional modeling of the system revealed that fuel distribution is not sensitive to feeding tube design which was in agreement with experimental results. Model can be validated using the real experimental data and can be a useful tool for prediction of the system performance at different conditions. It should be noted that the choice of boundary condition is important in order to obtain reasonable answer from the model. Having a wrong condition for a single boundary could result in completely different results.

According to the results of this study, it can be concluded that the counter-diffusive radiant heater system is a better alternative for mitigation of methane and other VOC from natural gas dehydrator emissions. If the oxygen diffusion limitation is overcome, this system can be used in the industry for environmental applications. Since these systems are already in use for other purposes, workers are familiar with their operation. In addition, these units offer higher safety levels compared to the flares. As an example, these units can be used in oil well sites

that contain methane. If the released methane from the well is captured and fed to the radiant heater, not only methane emissions from this source can be minimized, the generated thermal energy can be used for space heating. Especially during the winter and in remote locations, the cost of the fuel and its transportation can be minimized by utilizing these emissions as fuel and using the thermal energy for space heating or protection of pipes and other equipments.

In this study one type of catalyst was used during the experiments. Although it was found that this system in not controlled by the kinetics; however, it is recommended to investigate the role of different catalyst types on the radiant heater performance. Also it would be beneficial to complete the three-dimensional model of the system to able to capture the system characteristics in three dimensions.

References

Ablow, C.M. & Sadamori, H. 1987, "Analytic model of combustion in a catalytic fiber-mat burner", *Combustion Science and Technology,* vol. 55, pp. 1-22.

Aryafar, M. & Zaera, F. 1997, "Kinetic study of the catalytic oxidation of alkanes over nickel, palladium, and platinum foils", *Catalysis Letters,* vol. 48, pp. 173-183.

Baldwin, T.R. & Burch, R. 1990, "Catalytic combustion of methane over supported palladium catalysts: I. Alumina supported catalysts", *Applied Catalysis,* vol. 66, pp. 337-358.

Barresi, A.A. & Baldi, G. 1997, "Deep catalytic oxidation of aromatic hydrocarbon mixtures: reciprocal inhibition effects and kinetics", *Industrial and Engineering Chemistry Research,* vol. 33, pp. 2964-2974.

Bejan, A. 1993, *Heat Transfer,* John Wiley & Sons.

Bernstein, L., Bosch, P., Canziani, O., Chen, Z., Christ, R., Davidson, O., Hare, W., Huq, S., Karoly, D., Kattsov, V., Kundzewicz, Z., Liu, J., Lohmann, U., Manning, M., Matsuno, T., Menne, B., Metz, B., Mirza, M., Nicholls, N., Nurse, L., Pachauri, R., Palutikof, J., Parry, M., Qin, D., Ravindranath, N., Reisinger, A., Ren, J., Riahi, K., Rosenzweig, C., Rusticucci, M., Schneider, S., Sokona, Y., Solomon, S., Stott, P., Stouffer, R., Sugiyama, T., Swart, R., Tirpak, D., Vogel, C. & Yohe, G. 2007, *Climate Change 2007: Synthesis Report, Contribution of Working Groups I, II and III to the Fourth Assessment Report of the Intergovernmental Panel on Climate Change*, IPCC, Geneva, Switzerland.

Bond, G.C. (ed) 1987, *Heterogeneous catalysis: principles and applications*, 2nd edn, Clarendon Press, Oxford.

Braek, A.M., Almehaideb, R.A., Darwish, N. & Hughes, R. 2001, "Optimization of process parameters for glycol unit to mitigate the emission of BTEX/VOCs", *Process Safety and Environmental Protection,* vol. 79, pp. 218-232.

Briot, P., Auroux, A., Jones, D. & Primet, M. 1990, "Effect of particle size on the reactivity of oxygen-adsorbed platinum supported on alumina", *Applied Catalysis,* vol. 59, pp. 141-152.

Brühl, C. 1993, "The impact of the future scenarios for methane and other chemically active gases on the GWP of methane", *Chemosphere,* vol. 26, pp. 731-738.

Burch, R. 1997, "Low NOx options in catalytic combustion and emission control", *Catalysis Today,* vol. 35, pp. 27-36.

Burch, R. & Loader, P.K. 1994, "Investigation of Pt/Al_2O_3 and Pd/Al_2O_3 catalysts for the combustion of methane at low concentrations", *Applied Catalysis B: Environmental,* vol. 5, pp. 149-164.

Burch, R., Loader, P.K. & Urbano, F.J. 1996, "Some aspects of hydrocarbon activation on platinum group metal combustion catalysts", *Catalysis Today,* vol. 27, pp. 243-248.

Burch, R., Urbano, F.J. & Loader, P.K. 1995, "Methane combustion over palladium catalysts: The effect of carbon dioxide and water on activity", *Applied Catalysis A: General,* vol. 123, pp. 173-184.

Canadian Association of Petroleum Producers June 2006, *Control of benzene emissions from glycol dehydrators*, Canadian Association of Petroleum Producers, Canada.

Canadian Environmental Protection Act 1993, *Benzene (Priority substances list assessment report)*, Government of Canada, Environment Canada, Health Canada, Canada.

Carroll, J. 2003, *Natural gas hydrates: a guide for engineers,* Elsevier Science Publications, United States of America.

Chorkendrorff, I. & Niemantsverdriet, J.W. 2003, *Concepts of modern catalysis and kinetics,* Wiley-VCH, Germany.

Chou, C., Chen, J., Evans, G.H. & Winters, W.S. 2000, "Numerical studies of methane catalytic combustion inside a monolith honeycomb reactor using multi-step surface reactions", *Combustion Science and Technology,* vol. 150, pp. 27.

Choudhary, T.V., Banerjee, S. & Choudhary, V.R. 2002, "Catalysts for combustion of methane and lower alkanes", *Applied Catalysis A: General,* vol. 234, pp. 1-23.

Cimino, S., Pirone, R. & Lisi, L. 2002, "Zirconia supported $LaMnO_3$ monoliths for the catalytic combustion of methane", *Applied Catalysis B: Environmental,* vol. 35, pp. 243-254.

Ciuparu, D., Lyubovsky, M.R., Altman, E., Pfefferle, L.D. & Datye, A. 2002, "Catalytic combustion of methane over palladium-based catalysts", *Catalysis Reviews: Science and Engineering,* vol. 44, pp. 593.

Colannino, J. 2006, *Modeling of combustion systems: a practical approach,* Taylor & Francis, Boca Raton, United States of America.

Cullis, C.F., Nevell, T.G. & Trimm, D.L. 1972, "Role of catalyst support in oxidation of methane over palladium", *Journal of Chemical Ssociety, Faraday Transactions I,* vol. 68, pp. 1406.

Cullis, C.F. & Willatt, B.M. 1984, "The inhibition of hydrocarbon oxidation over supported precious metal catalysts", *Journal of Catalysis,* vol. 86, pp. 187-200.

Cullis, C.F. & Willatt, B.M. 1983, "Oxidation of methane over supported precious metal catalysts", *Journal of Catalysis,* vol. 83, pp. 267-285.

Danny Harvey, L.D. 1993, "A guide to global warming potentials (GWPs)", *Energy Policy,* vol. 21, pp. 24-34.

Darwish, N.A., Al-Mehaideb, R.A. & Break, A.M. 2004, "Computer simulation of natural gas dehydration processes: the use of mixed solvents and its role in mitigating BTEX emissions", *Proceedings of the IASTED International Conference: applied simulation and modeling* ACTA Press, Anaheim, pp. 143.

Demoulin, O., Le Clef, B., Navez, M. & Ruiz, P. 2008, "Combustion of methane, ethane and propane and of mixtures of methane with ethane or propane on Pd/γ-Al_2O_3 catalysts", *Applied Catalysis A: General,* vol. 344, pp. 1-9.

Deshmukh, S.R. & Vlachos, D.G. 2007, "A reduced mechanism for methane and one-step rate expressions for fuel-lean catalytic combustion of small alkanes on noble metals", *Combustion and Flame,* vol. 149, pp. 366-383.

Deutschmann, O., Maier, L.I., Riedel, U., Stroemman, A.H. & Dibble, R.W. 2000, "Hydrogen assisted catalytic combustion of methane on platinum", *Catalysis Today,* vol. 59, pp. 141-150.

Dincer, I. & Rosen, M.A. 1999, "Energy, environment and sustainable development", *Applied Energy,* vol. 64, pp. 427-440.

Dongworth, M.R. & Melvin, A. 1977, "Diffusive catalytic combustion", *Symposium (International) on Combustion,* vol. 16, pp. 255.

Dupont, V., Zhang, S., Bentley, R. & Williams, A. 2002, "Experimental and modelling studies of the catalytic combustion of methane", *Fuel,* vol. 81, pp. 799-810.

Environment Canada 1990, *National inventory of sources and emissions of benzene(1985)*.

Escandón, L.S., Ordóñez, S., Vega, A. & Díez, F.V. 2005, "Oxidation of methane over palladium catalysts: effect of the support", *Chemosphere,* vol. 58, pp. 9-17.

Etiope, G. & Favali, P. 2004, "Geologic emissions of methane from lands and seafloor: mud volcanoes and observing systems", *Environmental Geology,* vol. 46, pp. 987-987.

Etiope, G., Fridriksson, T., Italiano, F., Winiwarter, W. & Theloke, J. 2007, "Natural emissions of methane from geothermal and volcanic sources in Europe", *Journal of Volcanology and Geothermal Research,* vol. 165, pp. 76.

F. Kreith & M.S. Bohn 1993, *Principles of Heat Transfer,* 5th edn, West Publishing Company, United States of America.

Firth, J.G. & Holland, H.B. 1969, "Catalytic oxidation of methane over noble metals", *Transactions of the Faraday Society,* vol. 65, pp. 1121-1127.

Fisher, K.S., Rueter, C., Lyon, M. & Gamez, J. 1995, "Glycol dehydrator emission control improved", *Oil and Gas Journal,* vol. 93, pp. 40.

Florides, G.A. & Christodoulides, P. 2009, "Global warming and carbon dioxide through sciences", *Environment international,* vol. 35, pp. 390-401.

Foreign Affairs and International Trade Canada 2010, 2010/11/04-last update, *Canadian energy facts* [Homepage of Foreign Affairs and International Trade Canada], [Online]. Available: http://www.international.gc.ca/enviro/energy-energie/facts-faits.aspx?lang=eng [2010, 12/06].

Forster, P., Ramaswamy, V., Artaxo, P., Berntsen, T., Betts, R., Fahey, D.W., Haywood, J., Lean, J., Lowe, D.C., Myhre, G., Nganga, J., Prinn, R., Raga, G., Schulz, M. & Van Dorland, R. 2007, *Changes in atmospheric constituents and in radiative forcing. in: Climate Change 2007: The Physical Science Basis. Contribution of Working Group I to the Fourth Assessment Report of the Intergovernmental Panel on Climate Change,* Cambridge University Press, Cambridge, United Kingdom.

Forzatti, P. & Groppi, G. 1999, "Catalytic combustion for the production of energy", *Catalysis Today,* vol. 54, pp. 165-180.

Gangwal, S.K., Mullins, M.E., Spivey, J.J., Caffrey, P.R. & Tichenor, B.A. 1988, "Kinetics and selectivity of deep catalytic oxidation of n-hexane and benzene", *Applied Catalysis,* vol. 36, pp. 231-247.

Gao, D., Zhang, C., Wang, S., Yuan, Z. & Wang, S. 2008, "Catalytic activity of Pd/Al_2O_3 toward the combustion of methane", *Catalysis Communications,* vol. 9, pp. 2583-2587.

Garetto, T.F. & Apesteguía, C.R. 2001, "Structure sensitivity and in situ activation of benzene combustion on Pt/Al_2O_3 catalysts", *Applied Catalysis B: Environmental,* vol. 32, pp. 83-94.

Gearhart, L.E. 1998, "New glycol-unit design achieves VOC, BTEX reductions", *The Oil and Gas Journal,* vol. 96, pp. 61-63.

Ghigier, N. 1981, *Energy, combustion and environment,* McGraw-Hill Inc., New York, United States of America.

Goralski, C.T. & Schmidt, L.D. 1999, "Modeling heterogeneous and homogeneous reactions in the high-temperature catalytic combustion of methane", *Chemical Engineering Science,* vol. 54, pp. 5791-5807.

Government of Canada, Environment Canada 2010, *National inventory report 1990-2008, Greenhouse gas sources and sinks in Canada, The Canadian government's submission to the UN Framework Convention on Climate Chang*e, Environment Canada.

Grbic, B., Radic, N. & Terlecki-Baricevic, A. 2004, "Kinetics of deep oxidation of n-hexane and toluene over Pt/Al_2O_3 catalysts: oxidation of mixture", *Applied Catalysis B: Environmental,* vol. 50, pp. 161-166.

Greenhouse Gas Technology Center, Southern Research Institute 2003, *Environmental technology verification report, Engineered concepts, LLC quantum leap dehydrator*, U.S. Environmental Protection Agency.

Groppi, G., Tronconi, E. & Forzatti, P. 1999, "Mathematical models of catalytic combustors", *Catalysis Reviews: Science and Engineering,* vol. 41, pp. 227.

Guan, G., Kusakabe, K., Taneda, M., Uehara, M. & Maeda, H. 2008, "Catalytic combustion of methane over Pd-based catalyst supported on a macroporous alumina layer in a microchannel reactor", *Chemical Engineering Journal,* vol. 144, pp. 270-276.

Hartley, F.R. 1985, *Supported metal complexes,* D.Reidel publishing company, Holland.

Hayes, R.E. 2004, "Catalytic solutions for fugitive methane emissions in the oil and gas sector", *Chemical Engineering Science,* vol. 59, pp. 4073-4080.

Hayes, R.E. & Kolaczkowski, S.T. 1997, *Introduction to catalytic combustion,* Gordon and Breach Science Publishers.

Hayes, R.E., Kolaczkowski, S.T., Thomas, W.J. & Titiloye, J. 1996, "Transient experiments and modeling of the catalytic combustion of methane in a monolith reactor", *Industrial & Engineering Chemistry Research,* vol. 35, pp. 406-414.

Hicks, R.F., Qi, H., Young, M.L. & Lee, R.G. 1990, "Structure sensitivity of methane oxidation over platinum and palladium", *Journal of Catalysis,* vol. 122, pp. 280-294.

Hong, S., Lee, G. & Lee, G. 2003, "Catalytic combustion of benzene over supported metal oxides catalysts", *Korean Journal of Chemical Engineering,* vol. 20, pp. 440-444.

Hunter, P. & Oyama, S.T. 2000, *Control of volatile organic compound emissions,* John Wiley & Sons, Inc., United States of America.

International Energy Agency 2004, *energy policies of IEA countries, Canada 2004 review,* IEA Publications, Paris, France.

Jaccard M., R.N. 2007, *Canadian policies for deep greenhouse gas reduction,* Institute for Research on Public Policy.

Jahn, R., Snita, D., Kubícek, M. & Marek, M. 1997, "3-D modeling of monolith reactors", *Catalysis Today,* vol. 38, pp. 39-46.

Jodeiri, N., Wu, L., Mmbaga, J., Hayes, R.E. & Wanke, S.E. 2010, "Catalytic combustion of VOC in a counter-diffusive reactor", *Catalysis Today,* vol. 155, pp. 147-153.

Khilyuk, L.F. & Chilingar, G.V. 2004, "Global warming and long-term climatic changes: a progress report", *Environmental Geology,* vol. 46, pp. 970-979.

Kirchgessner, D.A., Richards, R.G., Heath, F. & Smith, R.D. 2004, "Advanced dehydrator design recovers gas, reduces emissions", *Oil and Gas Journal,* vol. 102, pp. 52.

Kirchgessner, D.A., Lott, R.A., Michael Cowgill, R., Harrison, M.R. & Shires, T.M. 1997, "Estimate of methane emissions from the U.S. natural gas industry", *Chemosphere,* vol. 35, pp. 1365-1390.

Kirk, R.E., Othmer, D.F., Grayson, M. & Eckroth, D. 1983, *Kirck-Othmer encyclopedia of chemical technology,* John Wiley & Sons, Inc., New York.

Kiwi-Minsker, L., Yuranov, I., Slavinskaia, E., Zaikovskii, V. & Renken, A. 2000, "Pt and Pd supported on glass fibers as effective combustion catalysts", *Catalysis Today,* vol. 59, pp. 61-68.

Kolaczkowski, S.T. 1999, "Modelling catalytic combustion in monolith reactors – challenges faced", *Catalysis Today,* vol. 47, pp. 209-218.

Lee, J.H. & Trimm, D.L. 1995, "Catalytic combustion of methane", *Fuel Processing Technology,* vol. 42, pp. 339-359.

Lelieveld, J., Crutzen, P.J. & Brühl, C. 1993, "Climate effects of atmospheric methane", *Chemosphere,* vol. 26, pp. 739-768.

Litto, R.M. 2008, *Catalytic combustion for mitigation of lean methane emission*, PhD thesis in chemical engineering, University of Alberta, Edmonton, Canada.

Lyubovsky, M., Karim, H., Menacherry, P., Boorse, S., LaPierre, R., Pfefferle, W.C. & Roychoudhury, S. 2003, "Complete and partial catalytic oxidation of methane over substrates with enhanced transport properties", *Catalysis Today,* vol. 83, pp. 183-197.

Ma, L., Trimm, D.L. & Jiang, C. 1996, "The design and testing of an autothermal reactor for the conversion of light hydrocarbons to hydrogen I. The kinetics

of the catalytic oxidation of light hydrocarbons", *Applied Catalysis A: General,* vol. 138, pp. 275-283.

MacDonald, G.J. 1990, "The future of methane as an energy resource", *Annual Review of Energy,* vol. 15, pp. 53-83.

Mazumder, S. & Sengupta, D. 2002, "Sub-grid scale modeling of heterogeneous chemical reactions and transport in full-scale catalytic converters", *Combustion and Flame,* vol. 131, pp. 85-97.

Metz, B. 2010, *controlling climate change,* 1st edn, Cambridge university press, United Kingdom.

Moulijn, J.A. van Leeuwen, P.W.N.M. & van Santen, R.A. (eds) 1993, *Catalysis- An integrated approach to homogeneous, heterogeneous and industrial catalysis*, 1st edn, Elsevier Science Publications, Amsterdam.

Niwa, M., Awano, K. & Murakami, Y. 1983, "Activity of supported platinum catalysts for methane oxidation", *Applied Catalysis,* vol. 7, pp. 317-325.

Ordóñez, S., Bello, L., Sastre, H., Rosal, R. & Díez, F.V. 2002, "Kinetics of the deep oxidation of benzene, toluene, n-hexane and their binary mixtures over a platinum on γ-alumina catalyst", *Applied Catalysis B: Environmental,* vol. 38, pp. 139-149.

Persson, K., Pfefferle, L.D., Schwartz, W., Ersson, A. & Järås, S.G. 2007, "Stability of palladium-based catalysts during catalytic combustion of methane: The influence of water", *Applied Catalysis B: Environmental,* vol. 74, pp. 242-250.

Pfefferle, L.D. & Pfefferle, W.C. 1987, "Catalysis in Combustion", *Catalysis Reviews: Science and Engineering,* vol. 29, pp. 219-267.

Radcliffe, S.W. & Hickman, R.G. 1975, "Diffusive catalytic combustors", vol. 48, pp. 208.

Reddy, J.N. & Gartling, D.K. (eds) 2000, *The finite element method in heat transfer and fluid dynamics*, 2nd edn, CRC Press, Boca Raton, FL.

Ribeiro, F.H., Chow, M. & Dallabetta, R.A. 1994, "Kinetics of the complete oxidation of methane over supported palladium catalysts", *Journal of Catalysis,* vol. 146, pp. 537-544.

Ried R.C., Prausnitz J.M. and Sherwood T.K. 1977, *The properties of gases and liquids,* Mc-Graw Hill.

Ryoo, M., Chung, S., Kim, J., Song, Y.S. & Seo, G. 2003, "The effect of mass transfer on the catalytic combustion of benzene and methane over palladium catalysts supported on porous materials", *Catalysis Today,* vol. 83, pp. 131-139.

Sadamori, H. 1999, "Application concepts and evaluation of small-scale catalytic combustors for natural gas", *Catalysis Today,* vol. 47, pp. 325-338.

Saint-Just, J. & der Kinderen, J. 1996, "Catalytic combustion: from reaction mechanism to commercial applications", *Catalysis Today,* vol. 29, pp. 387-395.

Salomons, S., Hayes, R.E., Poirier, M. & Sapoundjiev, H. 2003, "Flow reversal reactor for the catalytic combustion of lean methane mixtures", *Catalysis Today,* vol. 83, pp. 59-69.

Sarbak, Z. & Andersson, S. 2007, "Effect of support and loading on oxidation of methane over platinum catalysts", *Reaction Kinetics and Catalysis Letters,* vol. 92, pp. 231-238.

Satterfield, C.N. (ed) 1991, *Heterogeneous catalysis in industrial practice*, 2nd edn, McGraw-Hill Inc., New York.

Seo, Y.S., Kang, S.K. & Shin, H.D. 1999, "A catalytic burner using propane and toluene alternatively for the drying of textile coatings", *International Journal of Energy Research,* vol. 23, pp. 543.

Seo, Y.S., Cho, S.J., Song, K.S. & Kang, S.K. 2002, "A fibre-mat catalytic burner for the heating system of PVC tiles", *International Journal of Energy Research,* vol. 26, pp. 921-934.

Silverstein, A., Silverstein, V. & Nunn, L.S. 2009, *Global warming,* Twenty-First Century Books, Minneapolis, USA.

Specchia, V., Sicardi, S. & Gianetto, A. 1981, "Methane combustion with catalytic panels: interpretation of the internal profiles of a longitudinal dispersion model", *Chemical Engineering Communications,* vol. 10, pp. 189.

Stone, D.K., Lynch, S.K., Pandullo, R.F., Evans, L.B. & Vatavuk, W.M. 1991, "Flares" in *OAQPS control cost manual*, 5th edn, US EPA, Research Triangle Park, North Carolina, chapter 7.

Su, S. & Agnew, J. 2006, "Catalytic combustion of coal mine ventilation air methane", *Fuel,* vol. 85, pp. 1201-1210.

Takeguchi, T., Aoyama, S., Ueda, J., Kikuchi, R. & Eguchi, K. 2003, "Catalytic combustion of volatile organic compounds on supported precious metal catalysts", *Topics in Catalysis,* vol. 23, pp. 159-162.

Thevenin, P.O., Menon, P.G. & Jaras, S.G. 2003, "Catalytic processes to convert methane: partial or total oxidation-part 11-catalytic total oxidation of methane", *CATTECH,* vol. 7, pp. 10-22.

Thomas, J.M. & Thomas, W.J. 1967, *Introduction to the principles of heterogeneous catalysis,* Academic Press Inc., London.

Thomson, S.J. & Webb, G. (eds) 1968, *Heterogeneous catalysis*, John Wiley & Sons, Inc., New York.

Trimm, D. 1983, "Catalytic combustion (review)", *Applied Catalysis,* vol. 7, pp. 249-282.

Trimm, D.L. & Lam, C. 1980a, "The combustion of methane on platinum-alumina fibre catalysts_I_ Kinetics and mechanism", *Chemical Engineering Science,* vol. 35, pp. 1405.

Trimm, D.L. & Lam, C. 1980b, "The combustion of methane on platinum—alumina fibre catalysts—II design and testing of a convective-diffusive type catalytic combustor", *Chemical Engineering Science,* vol. 35, pp. 1731-1739.

True, W.R. 1995, "EPA backs model for estimating HAPs, VOCs from glycol dehydrators", *Oil and Gas Journal,* vol. 93, pp. 60.

Tyler, J.M. 1995, "Combustion systems" in *Handbook of air pollution control engineering and technology*, eds. J.C. Mycock, J.D. McKenna & L. Theodore, Lewis Publishers, New York, Chapter 11.

U.S.EPA 2002, *EPA air pollution control cost manual*, United States Environmental Protection Agency, Office of Air Quality Planning and Standards, United States of America.

United Nations Framework Convention on Climate Change (UNFCC) 2010, *feeling the heat* [Homepage of UNFCC], [Online]. Available: http://unfccc.int/essential_background/feeling_the_heat/items/2917.php [2010, 08/30] .

Vafai, K. (ed) 2005, *Handbook of porous media*, 2nd edn, CRC Press.

van Giezen, J.C., van den Berg, F.R., Kleinen, J.L., van Dillen, A.J. & Geus, J.W. 1999, "The effect of water on the activity of supported palladium catalysts in the catalytic combustion of methane", *Catalysis Today,* vol. 47, pp. 287-293.

Vatavuk, W.M. 1991, *Estimating costs of air pollution control,* 2nd edn, Lewis Publishers, Michigan.

Veser, G. & Frauhammer, J. 2000, "Modelling steady state and ignition during catalytic methane oxidation in a monolith reactor", *Chemical Engineering Science,* vol. 55, pp. 2271-2286.

Wahlen, M. 1993, "The global methane cycle", *Annual Review of Earth and Planetary Sciences,* vol. 21, pp. 407-426.

Weinberg, F.J. (ed) 1986, *Advanced combustion methods*, 1st edn, Academic Press Inc., London.

Wuebbles, D.J. & Hayhoe, K. 2002, "Atmospheric methane and global change", *Earth-Science Reviews,* vol. 57, pp. 177.

Xia, Q., Hidajat, K. & Kawi, S. 2001, "Adsorption and catalytic combustion of aromatics on platinum-supported MCM-41 materials", *Catalysis Today,* vol. 68, pp. 255-262.

Yao, Y.Y. 1980, "Oxidation of alkanes over noble metal catalysts", *Industrial & Engineering Chemistry Product Research and Development,* vol. 19, pp. 293-298.

Zhdanov, V.P. 2002, "Impact of surface science on the understanding of kinetics of heterogeneous catalytic reactions", *Surface Science,* vol. 500, pp. 966-985.